INVESTIGATION OF DYNAMIC NOISE AFFECTING GEODYNAMICS INFORMATION IN A TETHERED SUBSATELLITE

NASA GRANT NAG5-325

FINAL REPORT

For the period 1 June 1983 through 31 May 1984

Principal Investigator

Dr. Gordon E. Gullahorn

May 1984

Prepared for
National Aeronautics and Space Administration
Greenbelt, Maryland 20771

Smithsonian Institution
Astrophysical Observatory
Cambridge, Massachusetts 02138

The Smithsonian Astrophysical Observatory
is a member of the
Harvard-Smithsonian Center for Astrophysics

The NASA Technical Officer for this Grant is Mr. Jean E. Welker, Code 921 Earth Survey Applications Division, Goddard Space Flight Center, Greenbelt, Maryland 20771.

INVESTIGATION OF DYNAMIC NOISE AFFECTING GEODYNAMICS INFORMATION IN A TETHERED SUBSATELLITE

NASA GRANT NAG5-325

FINAL REPORT

For the period 1 June 1983 through 31 May 1984

Principal Investigator

Dr. Gordon E. Gullahorn

May 1984

Prepared for
National Aeronautics and Space Administration
Greenbelt, Maryland 20771

Smithsonian Institution
Astrophysical Observatory
Cambridge, Massachusetts 02138

The Smithsonian Astrophysical Observatory
is a member of the
Harvard-Smithsonian Center for Astrophysics

The NASA Technical Officer for this Grant is Mr. Jean E. Welker, Code 921 Earth Survey Applications Division, Goddard Space Flight Center, Greenbelt, Maryland 20771.

TABLE OF CONTENTS

1.0 INTRODUCTION

This is the Final Report for Grant NAG 5-325 entitled "Investigation of Dynamic Noise Affecting Geodynamic Instrumentation in a Tethered Subsatellite." The author of this report, and the primary analyst, is Dr. Gordon Gullahorn. Contributions were also made, and appendices written, by Dr. Mario Grossi and Dr. Enrico Lorenzini. The Principal Investigator at the inception of the Grant was Dr. Giuseppe Colombo. After Dr. Colombo's untimely death, Dr. Gullahorn was made P.I.

As summarized in the body and appendices of this report, SAO has, under this Grant:

- Formulated a research plan for dynamic noise studies under the Grant and a portion of the proposed follow-on.
- Investigated, in the literature, the current knowledge of irregularities in the atmospheric density in the thermosphere. Unfortunately, little appears to be known about irregularities at the altitudes of interest (120-220 km), the best information being available for altitudes around 250-300 km.
- Calculated effects of the tethered satellite system's internal dynamics on the subsatellite in the frequency range of interest. This includes both overall motions (libration and attitude oscillations) and internal tether oscillations.
- Modified the SKYHOOK tether simulation program to operate with atmospheric density variations and to output quantities of interest.
- Developed techniques and software for analyzing the results, including noise spectral analysis.
- Begun development of a program for computing a stable configuration of a tether system subject to air drag. These configurations will be of use as initial conditions for SKYHOOK and, through linearized analysis, directly for stability and dynamical studies.
- Performed a simple case study in which the subsatellite traverses an atmospheric density enhancement. This has confirmed some theoretical calculations, and pointed out some aspects of the interaction with the tether system dynamics.

- Presented, at the first meeting of the Tethered Satellite Core Equipment Definition Team at NASA/MSFC in Huntsville, Alabama, February 9-10, Some of these results for the purpose of defining a core equipment package for the measurement of expected acceleration variations in the subsatellite. A copy of the presentation by Dr. Grossi is given here as Appendix A.

- Presented, at the NASA Geodynamics Conference (a special session of the American Geophysical Union 1984 Spring Meeting) in Cincinnati, Ohio, May 14-17, a paper "Feasibility of Gravity Gradient Measurements from a Tethered Subsatellite Platform." A copy of the presentation by Dr. Gullahorn is included here as Appendix C.

2.0 RESEARCH PLAN FOR DYNAMICAL ANALYSIS

Considering the uncertainties in current knowledge of the fine structure of the thermosphere, the effort involved in model development and program modification, and the time available for the study, the following research plan for the dynamical noise analysis portion of the effort was developed. Part of this analysis has been completed under the current grant, and part must wait for the proposed follow-on effort.

Initially, we will consider the subsatellite dynamically as a point mass, though it will be subject to appropriate air drag; this is a not unreasonable first approximation since the subsatellite is nearly spherical. SKYHOOK runs will be made with a deployed tether and subsatellite moving through a perturbed atmosphere, and the accelerations experienced by the subsatellite determined. The subsatellite attitude is not explicitly included in SKYHOOK. If deemed appropriate, a simple model of the interaction of the subsatellite attitude dynamics and the tether may be developed to check for rotational effects.

It may be of interest to disentangle the direct and indirect effects of the atmospheric perturbations. E.g., we might:

- compute the perturbed accelerations of the subsatellite, without actually applying them to the dynamical simulation,
- apply the perturbed drag only to the subsatellite, but this time allow the resultant accelerations of the subsatellite to interact with the tether, generating waves, etc., which will react back on the subsatellite,
- apply the perturbed drag only to the tether, to see if the indirect effect on the subsatellite is significant.

These computations should involve only minor program changes; the major effort would be in the analysis of results. This analysis might be useful

in developing noise reduction methods.

The applied atmospheric perturbations will be developed in a stepwise fashion:

- First, a number of simple "units" will be used, such as
  - a localized density variation, e.g., a turbule, cell, etc.
  - an extended wave, e.g. a gravity wave
  - a "damped" wave, to simulate those found by Gross and Huang (1984; see Section 3.0 below);
  - a step function variation, e.g. a terminator effect.

Results from these simple models should enhance our understanding of the response of the system and the relative importance of different density variations.

- Then, using the best knowledge of the density fluctuations of the lower thermosphere, we will generate a sample perturbed atmosphere. This will be done by superposing a variety of localized enhancements of different scales and strengths. Perhaps several such models may be needed to adequately span the possibilities allowed by current theory and observation.

Further modifications that might be desirable in SKYHOOK are:

- include the subsatellite attitudinal dynamics, including torques around the tether attachment point due to air drag;
- include a model of the gradiometer and its suspension.

It may also be possible to estimate these effects analytically with less effort than modifying and running SKYHOOK.

Unfortunately, SKYHOOK may not allow fine enough discretization of the tether to provide valid results for tether vibrations over the whole frequency range of interest. To provide realistic results for periods as low as 2 to 3 seconds with SKYHOOK will require so many masses (at least twenty) that running simulations will not only be very expensive but have inconveniently long turn around. This problem would be aggravated by the fact that we will need simulations for long periods of (physical) time in

order to get good spectra and to allow the perturbations to fully develop; and the fact that the perturbations are constantly varying, even turning on and off, which would lead to inefficiency in the SKYHOOK integration routine. Resolution of tether effects with 1 to 2 second periods is totally infeasible. (This problem is discussed further in Section 8.0.)

To study system response in this short period regime, we may be able to apply the techniques of random structural vibrations (Nigam, 1983) or of statistical energy analysis (Lyon, 1975). The structure, in this case, would consist of an equilibrium configuration created by the stable configuration generator discussed in Section 9.0. This structure is subject to random forces, in this case due to the atmospheric density fluctuations; the statistics of the induced vibrations are derived from those of the forcing function.

3.0 ATMOSPHERIC VARIABILITY

The region in which the subsatellite and tether will be deployed (120 to 220 km. altitude) is in the lower thermosphere, a region about which our direct knowledge appears to be limited. G. Carignan (U. Michigan), J. Slowey (SAO), S. Gross (NY Poly) and F. Marcos (AFGL) have generously shared their experience and knowledge with us and allowed us to develop a brief bibliography. Professor Gross, in particular, sent us copies of papers before publication. The relevant papers we have acquired are listed in the references.

There are two forms of possibly relevant data available. The data directly on our region of interest appear to come only from perigee passages of satellites with elliptical orbits: SPADES (Marcos and Champion, 1972), and Atmosphere Explorer-C (Reber, et al. 1975; Potter, Kayser and Mauersberger, 1976). This form of data, brief samples at constantly varying altitude, has several disadvantages for our purposes: it is difficult to disentangle the horizontal variations from the vertical; thus, the wave vs. random nature of the variations is not convincingly demonstrated; and (probably for these reasons) no sophisticated analysis has been published. The reason for this form of data is, of course, that the atmospheric density is high enough that a satellite would soon decay from these altitudes.

At higher altitudes, still in the thermosphere but substantially above the altitudes of interest to us, it is possible to maintain an orbit constant for many revolutions. More sophisticated analyses have been made of this higher altitude data: for Atmosphere Explorer-E at altitudes near 300 km (Hoegy, et al., 1979) and for Atmosphere Explorer-C near 250 km

(Gross and Huang, 1984; Gross, Reber and Huang, 1984).

The lower altitude data allow little to be said firmly and quantitatively for our purposes (although there are a number of intriguing features relating to, for instance, the relative phase of variations in different atmospheric components). Roughly, the variations experienced along-trajectory appear to be in the range of a few percent, up to about 20%, with distance scales in the range of tens to hundreds of kilometers (this is most clearly shown in Figure 3 of Reber, et al.).

The higher altitude data are more complete and better analyzed; although their relevance to our purpose may be debated, in some sense it is the best we can do. At 250 km altitude, Gross and Huang observe a power law spectrum for general variations in the density, and notice some discrete waves of finite extent in the horizontal direction: e.g., a wave of 250 or 300 km wavelength that extends for only 1250 or 1500 km of a total path of 4100 km. They obtain variability over the entire range of tens to hundreds of kilometers (about seconds to tens of seconds at a velocity of 7.8 km/sec). Gross, Reber and Huang find variability extending to thousands of km with an overall power law spectrum but also some very distinct, persistent wave structures, possibly global standing waves.

One form of information which does not seem to be available is the <u>vertical</u> correlation of density fluctuations. Although the primary influence of density fluctuations is certainly the direct drag fluctuation on the subsatellite, the effect on the full tether system will depend on whether the tether as a whole experiences the fluctuations simultaneously, or whether the different regions are perturbed independently. One model which could be used to derive the correlation would be to assume that

density fluctuations are essentially due to vertical displacement: an enhancement, say, seen as the satellite moves horizontally at a given altitude would really be due to its seeing air which has been moved up the appropriate distance; thus, a higher tether segment would see the nominal density from the same distance below its true altitude. This corresponds to a gravity wave model, and there is some observational evidence corroborating it, at least for wave-like motions. Whether it should apply to random (turbulent-like) variations is less clear.

4.0 UNFORCED SYSTEM DYNAMICS

It is instructive to look at the dynamics of the system when it is not subject to the random drag forcing; we do, however, include the long period librations induced by winds in a non-equatorial orbit, as they have an indirect effect on attitude dynamics. Several aspects of the problem have been decoupled and analyzed separately; the results are in the subsections below. A full self-consistent treatment would be lengthy to carry out, though perhaps worth-while; some of the complications are discussed in Section 4.2.1.

4.1 Subsatellite Rotation Dynamics:

The overall librational motion of the tether system is long period (orbital or some fraction thereof) and of no direct concern. However, the subsatellite also oscillates as a free pendulum with the tether's end as an attachment point. Dr. E. Lorenzini has estimated the librational and attitudinal oscillations; his calculations are in Appendix B. The period of attitudinal oscillation is about 5 seconds, and the associated acceleration about 10^{-5} g. (This latter value was computed assuming the amplitude of the subsatellite oscillation was the same, in degrees angle, as the librational motion.)

4.2 Tether Elasticity Effects:

The tether elasticity leads to three sets of vibrational modes in the tethered satellite system:

- spring-mass mode, the subsatellite oscillating as if on the end of a massless spring;

- longitudinal (stretching) oscillations of the tether;
- latitudinal ("plucked string") oscillations of the tether.

The latter two are here calculated as if for a tether with fixed ends ("infinite mass" satellites). The frequencies of the modes are fixed for any expected amplitude (so long as the forces are linear), but the amplitudes will depend on the specific excitation experienced. The modal frequencies are calculated in Section 4.2.1, and a specific excitation mechanism is considered in Section 4.2.2.

4.2.1 Calculation of the Modes:

Spring/Mass Mode:

Here we consider the system composed of a large (infinite mass) Shuttle, a massless tether with spring constant $k = EA/L$, and a subsatellite of mass m; E = elasticity = 0.7×10^{12} for Kevlar, A is the tether cross-sectional area, and L the tether length. Then the period of oscillation is

$$P_{ms} = 2\pi \sqrt{mL/EA}$$

which evaluates to $P_{ms} = 95$ s for our specific mission.

Tether Oscillation Modes, Longitudinal and Latitudinal:

Both modes of oscillation are governed by the wave equation with fixed ends:

$$\begin{cases} W[u] = u_{tt} - c^2 u_{xx} = 0 \\ \\ u(0,t) = u(L,t) = 0 \end{cases}$$

where u(x,t) represents the displacement at time t of a physical point on the tether whose position at equilibrium would be x. The only difference is in the value of c (the speed of propagation) and the interpretation of "displacement" (along the tether for longitudinal waves, perpendicular for latitudinal waves). The solution of this equation is a simple exercise in separation of variables (see Kaplan, 1981, or almost any applied mathematics text). Any solution will be a linear combination of the eigenfunctions:

$$u\ (x,t) = \sin(n\pi\ x/L)\ \exp\ (\pm\ i\ \omega_n t)$$

$$\omega_n = n\pi c/L$$

and these represent the normal modes of the system. Here we are interested only in the eigenfrequencies ω_n, or the associated periods

$$P_n = 2\pi/\omega_n$$

The propagation speeds are given by

$c = \sqrt{T/\mu}$ latitudinal oscillations

$c = \sqrt{E/\rho}$ longitudinal oscillations

where T = the equilibrium tension,

ρ = the volume density

μ = the linear tether density, = ρA.

For Kevlar ($E = 0.7 \times 10^{12}$ dyne cm^{-2}, $\rho = 1.5$ g cm^{-3}) and at an altitude of 250 km (assuming the equilibrium tension is due solely to linear gravity gradient force), these evaluate to

$c = 0.22$ km/sec latitudinal

$c = 6.8$ km/sec longitudinal,

leading to oscillation periods of

$P_n = 910/n$ seconds latitudinal

$P_n = 29/n$ seconds longitudinal.

Note that both types of waves have modes in the regime of interest, from 5 or 10 to 200 seconds. The longitudinal vibrations will have several modes near the low period end. The latitudinal oscillations will have numerous modes throughout the range, though one may expect that the higher modes (short period) will be less strongly excited and more highly damped and thus be less distinct.

The model used in this section is an idealization. It does not include the effects of:

- damping forces in the tether and elsewhere;
- finite masses of the end masses (satellite and shuttle);
- attitudinal dynamics in the end masses;
- the three dimensional nature of the possible oscillations;
- the overall (equilibrium) curvature of the tether due to

air drag;
- external forces on the tether, such as gravity gradient or air drag (though these will possibly drop out when considering small displacements about equilibrium).

A full, self-consistent calculation including the above effects should perhaps be made. However, it promises to be a lengthy process, including coupled sets of ordinary and partial differential equations, and probably eventually requiring numerical calculation of the modes. An approximate, non-self-consistent calculation of one effect of subsatellite attitude dynamics is given in the next section.

4.2.2 Excitation of Longitudinal Modes by Subsatellite Attitude Oscillation:

To explore how one might get energy into the above modes, we performed a sample calculation using the results of sections 4.1 and 4.2.1:

- Take the subsatellite attitude oscillation period and amplitude as given in section 4.1;
- regard these as a fixed forcing oscillation of the tether's end, and calculate the response in the form of longitudinal oscillations;
- using the derived formulae, compute the tension, and hence accelerations, at the subsatellite end of the tether; this response occurs at the forcing frequency and at the tether natural mode frequencies.

We should emphasize that, complicated as the expressions derived may seem, this calculation has several limitations:

- It is not self-consistent; no attempt has been made to include the effects of tether oscillations on the subsatellite motion. The small accelerations found give some hope that this is not a significant omission except near resonances.
- Only longitudinal waves were considered. The latitudinal case should also be considered; the calculation of the tether response would be similar, although calculation of the back-reaction on the subsatellite will differ.
- Resonance effects are not considered. However, the forcing period is in the region spanned by the natural frequencies and changes in

mission parameters (or effects not in the calculation) could easily put the system close to resonance. Resonance with a high latitudinal mode will be even more likely. This clearly deserves further study.

Using the notation of section 4.1.1, the governing equations for the tether motion are:

$$\begin{cases} W[u] = 0 \\ u(0,t) = 0 \\ u(L,t) = A \sin(\omega_f t); \end{cases}$$

a complete problem also requires some form of initial conditions, typically specifying $u(x,0)$ and $u_t(x,0)$ at time $t=0$.

The calculations are straightforward but lengthy, and we shall only give the results. Following Kaplan (1981, pp. 422-423), we try a solution of the form

$$u(x,t) = \sum_{k=1}^{\infty} [h_k(t)\sin(k\pi x/L)] + (x/L)\, A \sin(\omega_f t)$$

where the $h_k(t)$ are to be determined from the equations. The resulting solutions are

$$h_k(t) = B\sin(\omega_k t+\phi) + (-1)^{k+1} \left(\frac{2A}{k\pi}\right)\left[\frac{\omega_f^2}{\omega_k^2-\omega_f^2}\right] \sin(\omega_f t)$$

where B and ϕ are constants to be determined (for each mode k) by the initial conditions imposed. To give a concrete example, we set $u = u_t = 0$ at $t=0$. Then,

$$h_k(t) = (-1)^k \left(\frac{2A}{k\pi}\right) \left[\frac{\omega_f^2}{\omega_k^2-\omega_f^2}\right] \quad [(\omega_k/\omega_f)\ \sin\omega_k t - \sin\omega_f t]$$

where $\omega_k = k\pi c/L$

ω_f = given forcing frequency

(subsatellite attitude oscillation frequency)

The tension in the tether is then

$$T = E\sigma\ u_x(x,t)$$

and evaluating this at x = L gives

$$[L/(AE\sigma)\ T = \sin(\omega_f t) \quad \left\{1 - \sum_{k=1}^{\infty} \frac{2\omega_f{}^2}{\omega_k^2-\omega_f^2}\right\} + \sum_{k=1}^{\infty}\left[\frac{2\omega_k\ \omega_f}{\omega_k^2 - \omega_f^2}\right] \sin\omega_k t$$

We may divide this into the components:

T_f at the forcing frequency

T_k at the normal mode frequencies $\omega_k = k\pi c/L$, k = 1,2...

This tension will have the following effect on the subsatellite:

- Linear acceleration in the direction along the tangent to the tether; broken into the above modes:

$a_{()} = T_{()}/M$

where M is the subsatellite mass, 0.5×10^6 grams.

From the discussion of Dr. Lorenzini (Appendix B), we know that the forcing frequency corresponds to a period of about 5 seconds. The mean angle of the subsatellite to the tether is 1^{o} and the oscillation amplitude also about 1^{o}. The amplitude of the forcing oscillations will then be about

$$A = (75 \text{ cm}) \ (1 - \cos 2^{o})/2 = .023 \text{ cm}.$$

A brief program was written to evaluate the resultant accelerations. For forcing periods near 5 seconds, we note

- one or two modes near resonance will have linear acceleration about 2 to 5 micro-g (10^{-6} gravities)
- the rest of the natural modes will have linear acceleration less than about 0.5 micro-g, decreasing as 1/k for the higher modes
- the back-reaction at the forcing frequency is roughly linear acceleration about 2 to 5 micro-g

Although these studies have given some definite numbers to use for design purposes, the connection to the actual experiment of measuring gravity gradients is not clearly defined. This will depend strongly on the instrument used and, especially, its suspension system. This connection deserves careful study.

5.0 SOFTWARE DEVELOPMENT -- SKYHOOK

SAO has developed and maintains SKYHOOK, a general tether simulation program. SKYHOOK models the tether as a series of discrete masses connected by massless tether segments. The equations of motion are integrated in Cartesian coordinates. Most known forces may be taken into account, and new versions generated for particular studies.

A version of SKYHOOK has been prepared which allows superposition of density variations on the smooth ambient atmospheric density. Output is made to the informational print file, and to a machine readable file for plotting and analysis. The non-gravitational acceleration of the subsatellite is computed at each output interval, and expressed in two orthogonal coordinate systems for output: in one, the axes are defined by the local vertical and the orbital motion; in the other, the tangent to the tether and the orbital motion are used. The print file also includes such quantities as height, ambient unperturbed density and the ratio actual/unperturbed for each mass point. This version does not include subsatellite attitude dynamics, so rotational velocities are not output.

The organization has purposely been made general enough that most specific density variation models can be accomodated with only minor reprogramming, at a limited number of points in the code. New models will be added to the old ones, incrementally generalizing the program rather than proliferating a sequence of narrowly specific program versions. We have developed a set of lexical routines which will allow input parameter specification in a "user friendly" flexible fashion, and a set of programmer protocols for addition of model enhancements to SKYHOOK. These should considerably simplify future changes.

The specific perturbation model which has been incorporated so far consists of an elliptical region in which the density is enhanced or reduced. The perturbation is two-dimensional, in the orbit plane, since the distance scales of interest (tens of kilometers or more) are much greater than anticipated out-of-plane motions. As parameters one may input: the size of the region (horizontal and vertical axes); the center placement (height, and distance "along orbit" from the start of the run); and the density ratio perturbed/ambient.

A long-standing problem leading to occasional mysterious failures was diagnosed and fixed. The atmospheric temperature routine did not always handle angle variables correctly; the resultant temperatures could be outside the domain of the lookup table used to get atmospheric density, and no checks were made to guard against this, so that the contents of some random position in memory would become the "density." This led to unpredictable results.

Results of sample simulations are given in section 7 below.

6.0 SOFTWARE DEVELOPMENT -- ANALYSIS PROGRAMS

Once a SKYHOOK run has been made and a file of accelerations has been produced, we must do something with this data. Several service routines have been written to help examine the results.

6.1 Spectral Analysis

Gradiometer, accelerometer and other instrument sensitivity are commonly quoted as functions of frequency. Thus, the spectral decomposition of a sample acceleration profile is, at the least, a useful tool for estimating instrument response.

Experiment with available packaged routines for spectral analysis (from IMSL) produced confusing results in test programs, so a routine was developed to produce simple spectral results (using, however, the FFT routine from IMSL, which performs the clearly defined task of computing a discrete Fourier transform (DFT)). We describe very briefly the capacities of the routine:

If we have N samples of some quantity at times t = 0, dt, 2dt, 3dt, ... (N-1) dt, then the DFT will produce 1+N/2 results at frequencies f = 0, df, 2df, ... (N/2)df. Here we assume N is even; a power of 2 (e.g. 256, 512, 1024, ...) makes for computational efficiency, but is not necessary. The frequencies f are in Hertz. The frequency resolution (lowest discernible frequency or longest period) depends on the total length of the observed time interval: df = 1 / (Ndt). The highest frequency (shortest period) available depends only on the sampling interval dt: (N/2)df = 1 / (2dt) (the Nyquist frequency).

Before we compute the DFT of the sample, we perform a process known as "Hanning" to reduce the effects of the finite length of the data stream. This consists of multiplying the data by a function that reduces smoothly to zero near the edges of the data span ("window"), reducing ringing or "leakage" in the Fourier transform domain (see, e.g., Brigham 1974, pp. 140-146). Some simple tests we ran confirm that this technique dramatically improves the resolution of edges and discrete frequency components not at an exact value k.df of the discrete spectral domain. Sample data created with an exact frequency k.df (e.g. a simple sine function) had their spectra slightly smeared, over the two adjacent frequency samples. This seems a small price to pay for the generally improved performance, but we should be aware of the decreased resolution; in particular, a peak two or four frequency samples wide may actually be quite sharp.

A program was written which reads the file of accelerations produced by SKYHOOK. The user may then request the spectrum (amplitude of the Fourier transform; this is the square root of the power spectral density) for any time interval of data, and the spectra of all six acceleration components (three components in each of the two coordinate systems defined in section 5.0) are output to a file for printing, plotting or analysis. Each component's spectrum is normalized to have a maximum of 1.

6.2 Other Routines:

Programs to do printer plots of the accelerations and of the spectra from the program in section 6.1 were written. Only the two acceleration components tangent to the tether ("along") and orthogonal (in the orbital plane; our runs so far have had no out-of-plane component) to this are

used. The logarithms of the spectral power are plotted.

A program was written to difference two of the acceleration files output from SKYHOOK. This allowed us to look at only the effects of atmospheric perturbations by making identical runs with and without the perturbation and subtracting the results.

7.0 A CASE STUDY

A case was run to examine the effects of a single enhanced density region. The orbit was equatorial, with all motion in the orbital plane. Ten masses were used: the shuttle, the subsatellite, and eight tether masses. Because our standard initial condition generator (DUMBEL) considers only the gravity gradient force, we put heavy damping in the tether and ran the DUMBEL produced configuration until most of the longitudinal oscillations had damped out. The result of this run was used as input to the simulations described here, with the damping removed.

We used a 100 ton shuttle, an 0.5 ton subsatellite deployed downward, and a 100 km tether of 0.2 cm diameter Kevlar ($E = 0.7 \times 10^{12}$ dyne cm^{-2}, $\rho = 1.5$ g cm^{-3}). The Shuttle was in a 220 km altitude, circular, equatorial orbit.

The atmospheric density perturbation consisted of a 20 km radius circular region enhanced by 20% over ambient density, with its center at 120 km altitude (the same height as the subsatellite) and 100 km along orbit from the start of the run.

Two runs were made, each following the tether for 700 (physical) seconds. The first run, in which the density perturbation was turned off, was for comparison purposes and took 15 minutes of computer time. The second run, with the perturbation on, took 19 minutes.

7.1 Analysis of the Results:

Since the damped SKYHOOK run which produced our initial conditions had not completely relaxed, even the run without the density perturbation exhibited substantial oscillations. To isolate the effects of the perturbation, we differenced the acceleration output of the two runs and worked with the resulting file. In the regime of small disturbances explored here, either residual oscillations from "deployment" or due to atmospheric perturbations, we expect linearity; thus this scheme should be equivalent to starting with a fully relaxed initial state.

The clearest results were seen looking at the components (1) along the tangent to the tether (nearly vertical), and (2) in the perpendicular direction (nearly horizontal, parallel to the drag force). This choice of coordinates most clearly distinguishes the various effects.

First we consider the accelerations produced by the density enhancement in the time domain; we will consider the frequency domain below.

The obvious immediate effect is an acceleration in the "across tether" (horizontal) direction of -0.084 gal (1 gal = 1 cm sec^{-2}). This is very nearly constant throughout the period when the enhancement is on. The post-enhancement response is limited to the range [-8.1 micro-gal , +49 micro-gal], i.e. down by more than three orders of magnitude. A printer plot of this post-enhancement response is given in Appendix D, Figure D-1. The overall variation is seen to be quite smooth, with little short scale oscillation. The immediate response during the enhancement is not plotted, since the post-enhancement response would not then be discernable.

The entire acceleration response in the "along-tether" direction (vertical) is shown in Figure D-2. The total range of response is [-0.086 gal, +0.096 gal]. During the enhancement, the acceleration along-tether rises gradually to 0.024 gal. This brief perturbation has excited the tether, and in the post-enhancement response we see substantially larger accelerations produced by the back-reaction of the tether rather than directly by the enhancement. Note that these post-enhancement accelerations in the along-tether direction are much larger than the across-tether accelerations. Also, the along-tether response shows much more variation on short time scales, a fact which will also be apparent from the spectral analysis below.

The spectra of both components were computed as outlined in Section 6.1. Data for 512 points (at one second intervals) immediately post-enhancement were used, giving a frequency resolution of about .002 Hz. This is actually somewhat misleading since the Hanning window used to suppress "leakage" from sharp spectral peaks also smears them by about 1 frequency resolution element on either side; thus the true resolution is closer to .006 Hz. Printer plots for the across-tether and along-tether components are given in Appendix D, Figures D-3 and D-4 respectively. These are the logarithms of the spectral amplitude. A portion of the along-tether spectral decomposition, labeled so as to be the logarithm of the power spectral density, is shown in Figure 7-1.

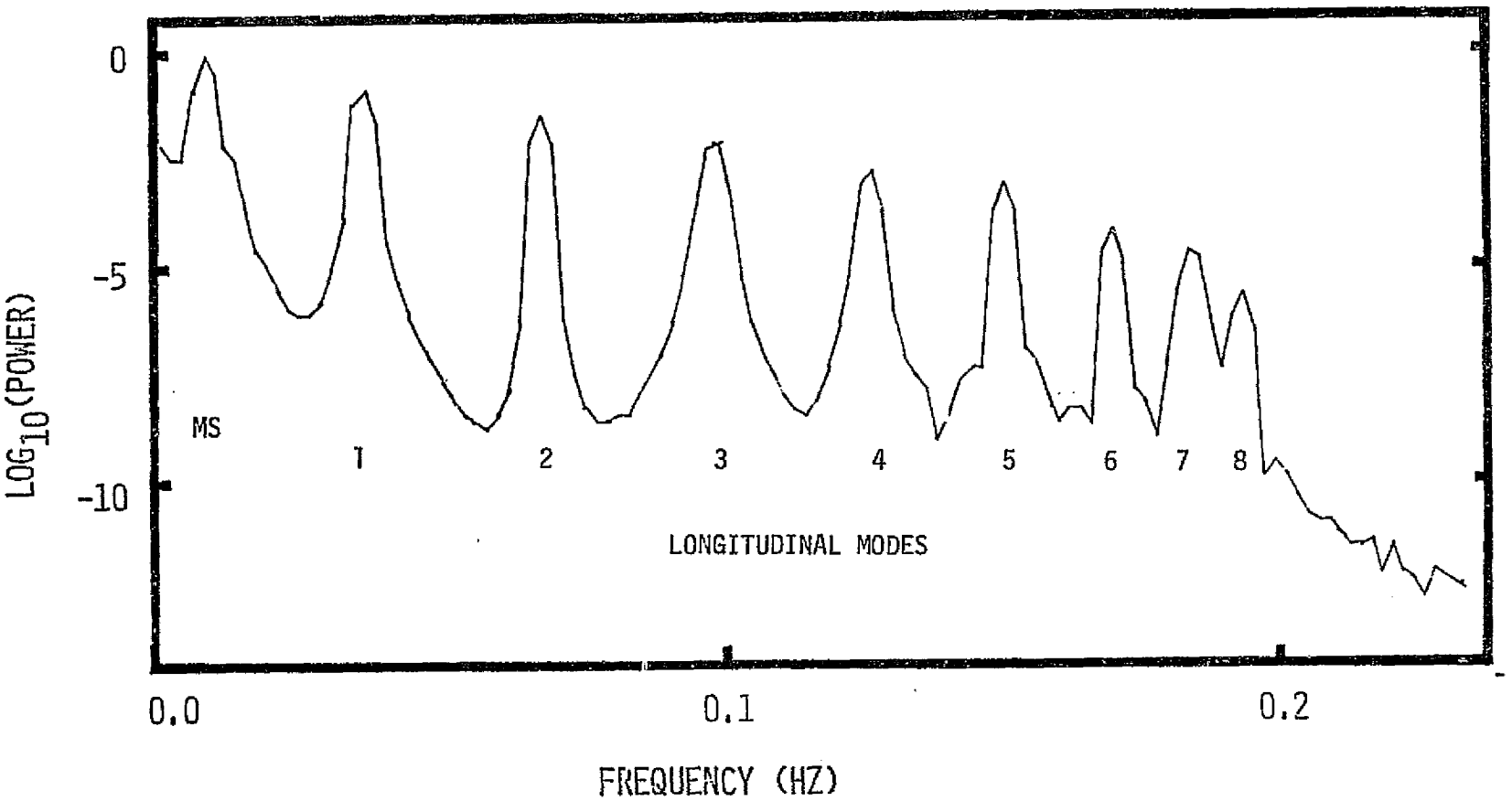

Figure 7-1. Power Spectral Densidy of the subsatellite acceleration after encountering an atmospheric density enhancement (see discussion in text). The along-tether component is plotted; for a more extensive plot and for the perpendicular component, see Appendix D. The mass-spring mode ("MS") and the expected eight longitudinal oscillation modes are marked.

Comparing Figures D-3 and D-4, we see directly that the across-tether component shows only a few indistinct peaks at low frequency (long period), while the along-tether component shows several strong peaks down to a period of about 5 seconds, before decreasing to a random tail. The physical nature of the peaks is labeled in Figure 7-1. One is seen to be the spring-mass mode discussed in Section 4.2.1, with a period of about 100 seconds, as close to the predicted value of 95 seconds as can be determined. We also see eight modes of longitudinal tether oscillation; their frequencies, and the frequencies predicted from the model of the continuous tether with fixed ends, are:

Mode	Theoretical	Simulation
1	0.034 Hz	0.037 Hz
2	0.068	0.068
3	0.102	0.100
4	0.137	0.127
5	0.171	0.148
6	0.205	0.170
7	0.239	0.184
8	0.273	0.193

We see that the agreement is quite good for the lower modes, and gradually deteriorates for the higher modes. The disagreement is probably due to the discretization (point masses and springs model) used in the simulation, although the limits of the theoretical model (primarily the assumption of fixed ends) also introduces some error in the theoretical figures. Note that precisely eight modes are expected for the simulation, as observed: ten masses were used, eight internal plus the shuttle and subsatellite, and one will expect one longitudinal mode for each internal mass. The latitudinal modes do not show up at all in the simulation results. This is probably due to their low frequency: the low order, stronger, modes will be confused with the spring-mass mode and all the modes will be so closely spaced as to be unresolved from our data.

8.0 ADEQUACY OF SKYHOOK FOR VIBRATION STUDIES

The above case study, with ten masses run for twelve minutes of simulated time, and with only one density enhancement, was a significant computational effort. But as we can see from the table given in Section 7.1, the highest frequency adequately resolved is 0.15 to 0.20 Hz.

More complete results will require accurate simulation of frequencies to 0.5 or even 1.0 Hz. We can compute two estimates of the number of masses needed: the first is based on the naive assumption that all the theoretical modes are the same as the simulated modes; and the second on the observation that about half the simulated modes adequately approximate the real (theoretical) modes. These estimates give 17 masses and 32 masses respectively to achieve 0.5 Hz resolution; and 32 and 61 masses for 1.0 Hz.

Additionally, we will wish to make runs for much longer periods to allow the full effects of the noise to build up, and to include the dynamics of the subsatellite and the gravimeter suspension. A realistic atmospheric model will include many more perturbations, each of which will cause the integrator used in SKYHOOK to have at least some difficulty in continuing and will increase the time required for solution.

Experience has shown that SKYHOOK simulations for more than ten masses become expensive very rapidly, as well as leading to inconvenient turn around time. Twenty masses is about the limit feasible even in a very smoothly evolving case, and thirty to sixty mass runs would require a large dedicated machine unless the programs efficiency can be very substantially enhanced.

One non-SKYHOOK option which is being explored is the use of statistical methods for dynamical systems, such as random vibrations (Nigam,1983) or statistical energy analysis (Lyon, 1975). In broad outline, these methods require a model of the system in an equilibrium state, and a statistical description of the perturbing forces (e.g. atmospheric density irregularities). As output, one achieves a statistical description of the system response. This is used to derive quantities of engineering interest. Some steps have already been taken, for another purpose, which would help implementation (Section 9.0 below), though significant study would be required before useful results could be obtained.

9.0 SOFTWARE DEVELOPMENT -- EQUILIBRIUM CONFIGURATION GENERATOR

We have partially developed a program to generate equilibrium deployed configurations with large numbers of masses and taking into account the non-perturbed atmospheric drag. Other forces could be easily added if deemed advisable.

The original motivation was to generate initial conditions for use with SKYHOOK. The current program used to generate initial configurations, DUMBEL, does not account for drag forces and has other limitations. Thus, the first stages of the SKYHOOK run consist of a long period spent damping vibrations before any significant analysis of the perturbed response can be made. This is expensive enough in both computer and person time, that an effort to generate usable initial configurations already in equilibrium is justified.

An additional benefit is that the equilibrium configurations thus generated could be used as the systems for the statistical perturbation analyses mentioned in Section 9.0. In addition to the configuration we would need to compute the linearized force matrix, but this would be a simple addition to the program.

The linearized system could also be used in stability analyses by simply computing the eigenvalues of the force matrix using available subroutine packages.

The program has been fully designed in such a manner that convergence to a true solution seems assured from both a physical and an algorithmic viewpoint. Schematically, the program consists of several levels of subroutines each of which solves for a given variable or set of variables

by an iterative or exact process; when iterative processes are used, the lower level subroutine may be called upon many times to solve its own sub-problem with slightly different pa meters. Some of the inner loops have been coded (a conscious departure from standard top-down programming practice), and completion should take about one week.

10.0 SUGGESTIONS FOR SYSTEM DEVELOPMENT

From the above analyses and simulations we see that the acceleration perturbations experienced by instruments in an atmospheric mission subsatellite are certain to be substantial and complex. Elimination or compensation for these perturbations will be crucial to the success of a gradiometer mission.

It is anticipated that the longitudinal tether vibrations excited by the atmospheric density variations can be damped either by physical devices (appropriately chosen spring-dashpot combinations) or by manipulation of the tether reel on the deployer as discussed in Colombo, et al. (1984, section 5.1) in a different context.

It is likely that measurements of the atmospheric density perturbations will allow removal of some effects in post-processing. This measurement could be made either with an external instrument or simply by observing the varying drag with an on board accelerometer.

Rotations, as well as linear acceleration, will be induced in the subsatellite. These effects should be more clearly understood. Rotation of the gradiometer instrument will give false readings. However, if all nine gravity gradient tensor components are measured, it is in theory possible to measure the rotation and remove its effects leaving only the actual gravity gradient.

In any event, the suspension of the gradiometer within the subsatellite is crucial. It cannot be simply attached rigidly to the instrument platform. The gradiometer itself will exercise a significant "common-mode" rejection of linear acceleration noise: that is, since all

accelerometer components of the gradiometer are perturbed by the same amount, the measured gradient (the difference of accelerations) is not, in theory, perturbed. The degree of this rejection achieved by various instruments must be determined. More difficult to circumvent are the effects of rotation. Even if the subsatellite itself does not rotate, a one-point suspension would cause gradiometer rotation in response to linear accelerations. A suspension must be designed to obviate this problem.

11.0 REFERENCES

Barlier, F. and Berger, C. 1983. "A Point of View on Semi-Empirical Thermospheric Models," Planetary and Space Science, 31, 945-966.

Brigham, E.O. 1974. The Fast Fourier Transform, Prentice-Hall, Englewood Cliffs, New Jersey.

Colombo, G., Arnold, D.A., Gullahorn, G.E. and Taylor, R.S. 1984. "Tether Dynamics Software Review; High Resolution Tether Dynamics Studies; Advanced Tether Applications," final report on Contract NAS8-35036, January 1984.

Gross, S.H. and Eun, H. 1976. "Traveling Neutral Disturbances," Geophysical Research Letters, 3, 257-260.

Gross, S.H. and Huang, F.T. 1984. "Medium Scale Gravity Waves in the Thermosphere Observed by the AE-C Satellite," preprint.

Gross, S.H., Reber, C.A. and Huang, F. 1984. "Large Scale Waves in the Thermosphere Observed by the AE-C," preprint (accepted for IEEE Trans. Geoscience).

Hoegy, W.R., Dyson, P.L., Wharton, L.E. and Spencer, N.W. 1979. "Neutral Atmospheric Waves Determined From Atmospheric Explorer Measurements," Geophysical Research Letters, 6, 187-190.

Kaplan, W. 1981. Advanced Mathematics for Engineers, Addison Wesley, Reading Massachusetts.

Lyon, R.H. 1975. Statistical Energy Analysis of Dynamical Systems, MIT Press, Cambridge Mass.

Marcos, F.A. and Champion, K.S.W. 1972. "Gravity Waves Observed in High Latitude Neutral Density Profiles," Space Research XII, 791-796.

Nigam, N.C. 1983. Introduction to Random Vibrations, MIT Press, Cambridge Mass.

Potter, W.E., Kayser, D.C. and Mauersberger, K. 1976. "Direct Measurement of Neutral Wave Characteristics in the Thermosphere," Journal of Geophysical Research, 81, 5002-5012.

Prolss, G.W. and von Zahn, U. 1976. "Large and Small Scale Changes in the Disturbed Upper Atmosphere," Journal of Atmospheric and Terrestrial Physics, 38, 655-659.

Reber, C.A., Hedin, A.E., Pelz, D.T., Potter, W.E. and Brace, L.H. 1975. "Phase and Amplitude Relationships of Wave Structure Observed in the Lower Thermosphere," Journal of Geophysical Research, 80, 4576-4580.

Trinks, H. and Mayr, H.G. 1976. "Large-Scale Neutral Composition Gravity Waves in the Thermosphere Observed by Esro 4," Journal of Geophysical Research, 81, 4023-4026.

Villain, J.-P. 1979. "Analysis of Perturbations of the Total Density Determined by the Low-G Accelerometer CACTUS," Space Research XIX, 231-234.

APPENDIX A

A Presentation Made By

Dr. Mario D. Grossi

to

Tethered Satellite Core Equipment Definition Team

NASA/MSFC Huntsville, Alabama

February 9-10, 1984

Core Equipment for TSS:

Sensor of Dynamic Noise

CORE EQUIPMENT FOR T.S.S.

SENSOR OF DYNAMIC NOISE

FEBRUARY 1984

SMITHSONIAN INSTITUTION

ASTROPHYSICAL OBSERVATORY

CAMBRIDGE, MASSACHUSETTS 02138

RECOMMENDED SENSOR SYSTEM

- THREE LINEAR ACCELEROMETERS, ONE FOR EACH OF THE THREE X, Y, Z AXES

- THREE GYROS, EACH WITH AXIS COINCIDENT WITH ONE OF THE THREE X, Y, Z AXES

- A SET OF TRANSLATIONAL AND ROTATIONAL DAMPERS TO ISOLATE TETHERED SUBSATELLITE FROM ACCELERATION NOISE CAUSED BY TETHER DYNAMICS

TYPICAL USERS' DEMANDS

EXAMPLE OF USERS : GEODYNAMICS COMMUNITY, WITH GRAVITY GRADIOMETER AS INSTRUMENT ON-BOARD TETHERED SUBSATELLITES

(A) REQUIREMENTS FOR LIMITATION IN UNCORRELATED NOISE, PROOF MASS - TO - PROOF MASS, VALUES COMPUTED FOR 1 SEC INTEGRATION TIME, GRADIOMETER BASELINE 50 CM :

$0.35\ 10^{-9}$ cm sec^{-2} = $0.35\ 10^{-12}$ g	to achieve a threshold sensitivity of	10^{-2}	Eötvös Units
$0.35\ 10^{-10}$ " = $0.35\ 10^{-13}$ g	" " "	10^{-3}	" "
$0.35\ 10^{-11}$ " = $0.35\ 10^{-14}$ g	" " "	10^{-4}	" "

(LINEAR ACCELERATION NOISE)

BECAUSE AT THE VERY BEST WE WILL HAVE A THRESHOLD SENSITIVITY OF 10^{-8} g / $\sqrt{Hz}$ (MAYBE WE CAN HAVE A THRESHLOD SENSITIVITY AS GOOD AS 10^{-10} g / $\sqrt{Hz}$, WE HAVE TO RELY IN THE COMMON-MODE REJECTION MECHANISM (MASS-TO-MASS NOISE CORRELATION) TO ACHIEVE THE FOLLOWING DEGREES OF NOISE CANCELLATION :

IF USING A 10^{-8} g / $\sqrt{Hz}$ ACCELEROMETER	IF USING A 10^{-10} g / $\sqrt{Hz}$ ACCELEROMETER	GRADIOMETER SENSITIVITY GOAL
A FACTOR OF $3\ 10^{4}$	A FACTOR OF $3\ 10^{2}$	10^{-2} EU
" $3\ 10^{5}$	" $3\ 10^{3}$	10^{-3} "
" $3\ 10^{6}$	" $3\ 10^{4}$	10^{-4} "

THESE SPECIFICATIONS ARE DIFFICULT TO MEET WITH A SIMPLE AND LOW-COST ACCELEROMETER.

TYPICAL USERS' DEMANDS (CONT.)

WE COULD CONSIDER USING SUCH HIGH-PERFORMANCE ACCELEROMETERS AS THE ONES BEING DEVELOPED IN FRANCE BY ONERA, MATRAS, ETC. (THRESHOLD SENSITIVITY 10^{-13} g/$\sqrt{\text{Hz}}$).

OUR RECOMMENDATIONS ARE, HOWEVER, THAT WE SHOULD KEEP WITHIN PRACTICAL BOUNDS ACCELEROMETER SENSITIVITY. WE SHOULD PERFORM TRADE-OFF ANALYSIS BETWEEN THIS SENSITIVITY AND ACHIEVABLE DEGREE OF COMMON-MODE REJECTION, WITH THE AIM OF ESTABLISHING A FAIR SHARE OF THE BURDEN (BASED ON FEASIBILITY, PRACTICALITY AND COST) BETWEEN ACCELEROMETER REQUIRED PERFORMANCE AND COMMON-MODE REJECTION SPECIFICATIONS.

AT THIS POINT, WE EXPECT THAT 10^{-8} g/$\sqrt{\text{Hz}}$ (POSSIBLY 10^{-10} g/$\sqrt{\text{Hz}}$) SHOULD BE THE SENSITIVITY TO BE CONSIDERED IN THE PRE-PROCUREMENT SEARCH FOR A SUITABLE ACCELEROMETER.

ANALYSIS OF PRACTICALLY ACHIEVABLE COMMON-MODE REJECTION IS, AT PRESENT, AN URGENT, OPEN REQUIREMENT.

AMOUNT OF ACHIEVABLE REJECTION: TBD

(B) REQUIREMENTS FOR LIMITATIONS IN ROTATIONAL ACCELERATION NOISE, VALUES OF GYRO ANGULAR VELOCITY STABILITY REQUIRED IN 1 SEC INTEGRATION TIME:

$\Delta\omega < 3.16\ 10^{-6}$ rad/sec to achieve a threshold sensitivity of 10^{-2} Eötvös Units

$\Delta\omega < 10^{-6}$ rad/sec to achieve a threshold sensitivity of 10^{-3} Eötvös Units

$\Delta\omega < 3.16\ 10^{-7}$ rad/sec to achieve a threshold sensitivity of 10^{-4} Eötvös Units

TYPICAL USERS' DEMANDS (CONT.)

WITH A GYRO THAT HAS A VELOCITY STABILITY OF 1 MILLIDEGREE/HOUR, WE HAVE

$$\Delta\omega = \frac{10^{-3}}{57} \times \frac{1}{3600} \simeq 5\ 10^{-9} \quad \text{rad/sec}$$

THIS AMPLY SATISFIES REQUIREMENTS SET FORTH IN PREVIOUS SLIDE.

WITH A GYRO THAT HAS A VELOCITY STABILITY OF 3 MILLIDEGREE/HOUR WE HAVE $\Delta\omega \simeq 10^{-8}$ rad/sec. THIS GYRO ALSO SATISFIES (WITH A SMALLER MARGIN, THOUGH) THE REQUIREMENTS ABOVE.

WE CONCLUDE THAT STATE-OF-THE-ART GYROS HAVE A PERFORMANCE GOOD ENOUGH TO BE USED IN T.S.S. DYNAMIC NOISE SENSING INSTRUMENTATION. NO PROBLEMS HERE.

(C) SPECTRAL SENSITIVITY OF INTEREST TO GEODYNAMICS : THE BAND BETWEEN 10^{-3} HZ AND 1 HZ (IF IT WOULD MAKE A DIFFERENCE FOR INSTRUMENT COMPLEXITY,THIS BAND COULD BE REDUCED TO 10^{-2} HZ-to-0.2 HZ).

LIST OF SOURCES OF DYNAMIC NOISE

- o ATMOSPHERIC DENSITY GRANULARITIES, AS A CAUSE OF TIME-VARIABLE DRAG
- o TETHER'S PENDULAR LIBRATIONS, IN-PLANE AND OUT-OF-PLANE
- o NATURAL MODES OF LONGITUDINAL (STRETCHING) OSCILLATIONS (TENSION WAVE MODES)
- o ACCELERATIONS IN PAYLOAD MODULE OF SUBSATELLITE DUE TO ITS ROTATIONAL DYNAMICS WITH RESPECT TO TETHER
- o LONGITUDINAL OSCILLATIONS DUE TO TETHER CONTROL
- o LATITUDINAL OSCILLATIONS
- o GROSS MOTION OF SUBSATELLITE ALONG DIRECTION OF TETHER (SPRING- MASS MODEL)
- o FLUCTUATIONS OF ARTIFICIAL GRAVITY ON-BOARD SUBSATELLITE

CHARACTERIZATION OF EXPECTED DYNAMIC NOISE

o ATMOSPHERIC DENSITY GRANULARITIES

(WE ASSUME 10 % ARIR DENSITY SPATIAL FLUCTUATIONS)

	ACCELERATION MAGNITUDE	FREQUENCY SPECTRUM
100 Km TETHER, DOWNWARDS, SHUTTLE AT 230 KM, 28° INCLINATION (CASE A)	$0.5\ 10^{-4}$ g	$4\ 10^{-3}$ HZ to 0.25 HZ
20 Km TETHER, UPWARDS, SHUTTLE AT 295 KM, 28° INCLINATION (CASE B)	$0.5\ 10^{-7}$ g	same as above

o TETHER PENDULAR LIBRATIONS

CASE A	10^{-3} g (IN PLANE)	freq. = $4\ 10^{-4}$ HZ
	10^{-5} g (OUT OF PLANE)	" $2\ 10^{-4}$ HZ
$\lvert\dot{\theta}\rvert_{max} = 4\ 10^{-5}$ rad/sec		freq. = $4\ 10^{-4}$ HZ
$\lvert\dot{\varphi}\rvert_{max} = 2\ 10^{-5}$ rad/sec		" $2\ 10^{-4}$ HZ

CHARACTERIZATION OF EXPECTED DYNAMIC NOISE (CONT.)

o TETHER PENDULAR LIBRATIONS (CONT.)

CASE B	ACCELERATION MAGNITUDE	FREQUENCY SPECTRUM
	$3\ 10^{-5}$ g (IN PLANE)	freq. = $3\ 10^{-4}$ HZ
	$2\ 10^{-5}$ g (OUT OF PLANE)	" $4\ 10^{-4}$ HZ
	$\lvert\dot{\theta}\rvert_{max} = 7\ 10^{-6}$ rad/sec	freq.= $3\ 10^{-4}$ HZ
	$\lvert\dot{\varphi}\rvert_{max} = 4\ 10^{-6}$ rad/sec	" $4\ 10^{-4}$ HZ

NOTE : THESE ACCELERATIONS ARE EXPECTED TO BE EFFECTIVELY CANCELLED BY FILTERING AND BY THE USE OF TRANSLATIONAL AND ROTATIONAL DAMPERS ON BOARD SUBSATELLITE. ESTIMATE OF OVERALL ACHIEVABLE DEGREE OF CANCELLATION : TBD.

o NATURAL MODES OF LONGITUDINAL (STRETCHING) OSCILLATIONS (TENSION WAVE MODES)

CASE A	$5.3\ 10^{-6}$ g	0.166 HZ to 0.73 HZ
CASE B	$5\ 10^{-7}$ g	1 HZ to 1.25 HZ

CHARACTERIZATION OF EXPECTED DYNAMIC NOISE (CONT.)

o ACCELERATIONS IN PAYLOAD MODULE OF SUBSATELLITE DUE TO ROTATIONAL DYNAMICS WITH RESPECT TO TETHER

	ACCELERATION MAGNITUDE	FREQUENCY SPECTRUM
CASE A	10^{-3} g (IN PLANE)	freq. = 0.2 HZ
	4 10^{-5} g (OUT OF PLANE)	" " "
	2 10^{-5} g (CENTRIFUGAL)	freq. = TBD
	$\lvert\dot{\theta}_{SAT}\rvert_{max}$ = 00022 rad/sec	freq. = 0.2 HZ
	$\lvert\dot{\varphi}_{SAT}\rvert_{max}$ = 10^{-3} rad/sec	" "
CASE B	4 10^{-5} g (IN PLANE)	freq. = 10^{-1} HZ
	2 10^{-5} g (OUT OF PLANE)	" " "
	3 10^{-7} g (CENTRIFUGAL)	freq. = TBD
	$\lvert\dot{\theta}_{SAT}\rvert_{max}$ = 0.002 rad/sec	freq.= 10^{-1} HZ
	$\lvert\dot{\varphi}_{SAT}\rvert_{max}$ = 0.001 rad/sec	" " "

NOTE: THESE ACCELERATIONS ARE EXPECTED TO BE EFFECTIVELY CANCELLED BY FILTERING AND BY THE USE OF TRANSLATIONAL AND ROTATIONAL DAMPERS ON BOARD SUBSATELLITE. ESTIMATE OF OVERALL ACHIEVABLE DEGREE OF CANCELLATION : TBD.

CHARACTERIZATION OF EXPECTED DYNAMIC NOISE (CONT.)

o LONGITUDINAL OSCILLATIONS DUE TO TETHER CONTROL

	ACCELERATION MAGNITUDE	FREQUENCY SPECTRUM
CASE A & CASE B	TBD	FREQ. EXPECTED TO BE OF THE ORDER OF 10^{-4} HZ

o LATITUDINAL OSCILLATIONS

CASE A	TBD	freq. = 5.4 10^{-4} HZ
CASE B	TBD	freq. = 9.4 10^{-4} HZ

o GROSS MOTION OF SUBSATELLITE ALONG DIRECTION OF TETHER (SPRING- MASS MODEL)

CASE A	2 10^{-3} g	freq. = 10^{-2} HZ
CASE B	TBD	freq. = 3 10^{-2} HZ

o FLUCTUATIONS OF ARTIFICIAL GRAVITY ON BOARD SUBSATELLITE

CASE A	6.8 10^{-5} g	freq. = 3.7 10^{-4} HZ
CASE B	1.35 10^{-5} g	freq. = 3.7 10^{-4} HZ

INITIAL RECOMMENDATIONS FOR BASIC PERFORMANCE SPECIFICATIONS OF SENSOR SYSTEM

WE HAVE SEEN IN THE FIRST PART OF THIS PRESENTATION HOW TO FORMULATE SENSORS' SPECIFICATIONS FROM THE VIEWPOINT OF TYPICAL POTENTIAL USERS, SUCH AS THE GEODYNAMICS COMMUNITY. WE SAW THAT THE SPECIFICATIONS TO BE IMPOSED TO THE GYROS ARE QUITE MILD, WHILE THE ONES FOR THE LINEAR ACCELEROMETERS ARE VERY THOUGH.

IN THE SECOND PART OF THIS PRESENTATION, WE HAVE SEEN ESTIMATES OF THE DYNAMICAL NOISE TO BE EXPECTED IN THE T.S.S. SUBSATELLITE FROM TETHER-RELATED SOURCES AS WELL AS FROM GEOPHYSICAL SOURCES.

BY ASSUMING, INITIALLY, THAT WE DO NOT HAVE IN USE MEANS TO ABATE THESE SOURCES (A PESSIMISTIC ASSUMPTION), HERE UNDER ARE OUR RECOMMENDATIONS FOR THE SENSOR SYSTEM REQUIRED PERFORMANCE:

- o THRESHOLD SENSITIVITY OF ACCELEROMETERS: 10^{-8}-to-10^{-10} g/$\sqrt{Hz}$, IN THE FREQUENCY BAND 10^{-4} Hz-to-1.0 Hz, UPPER BOUND OF DYNAMIC RANGE 5 10^{-2} g.ALSO SUITABLE FOR LAB TESTS IN 1 g ENVIRONMENT.
- o THRESHOLD SENSITIVITY OF GYROS (EXPRESSED IN TERMS OF REQUIRED ROTATIONAL VELOCITY STABILITY): 1 to 3 MILLIDEGREES/HOUR, IN FREQUENCY BAND 10^{-4} Hz to 1.0 Hz. DYNAMIC RANGE: TBD.

WE ALSO RECOMMEND THAT TRANSLATIONAL AND ROTATIONAL DAMPING PROVISIONS BE ADDED TO T.S.S. SUBSATELLITE TO ISOLATE IT FROM TETHER SYSTEM DYNAMICS. SPECIFICATIONS, AND REVERBERATION OF EXTENT OF FEASIBLE ISOLATION IN SPECIFICATIONS ABOVE,: TBD.

"MINIMUM PERFORMANCE"

SENSOR SYSTEM

- BY REVIEWING VALUES OF ACCELERATION MAGNITUDES FROM THE VARIOUS SOURCES OF DYNAMIC NOISE TAKEN INTO ACCOUNT IN THE PREVIOUS SLIDES, THE FOLLOWING "MINIMUM PERFORMANCE" SENSOR SYSTEM CAN BE SPECIFIED, UNDER THE ASSUMPTION THAT FOR THE FIRST T.S.S MISSION IT MIGHT BE SUFFICIENT TO MEASURE THE RAW ACCELERATIONS, WITHOUT USING DAMPERS NOR FILTERS :

  - 10^{-6} g / $\sqrt{\text{Hz}}$ ACCELEROMETERS IN THE FREQUENCY BAND 10^{-4} to 1.0 HZ, WITH DYNAMIC RANGE UPPER BOUND : 5 10^{-2} g . Also suitable for lab tests in 1 g environment;

  - 3 MILLIDEGREES/HOUR GYROS, FREQUENCY BAND 10^{-4} TO 1 HZ, DYNAMIC RANGE : TBD.

- WITH THIS INSTRUMENTATION , COLLECTED DATA WILL BE OF LIMITED USE TO USER COMMUNITIES. HOWEVER, THEY WOULD BE USEFUL IN DESIGNING FOLLOW-ON VERSIONS OF THE INSTRUMENTATION PACKAGE WITH PERFORMANCE APPROACHING UPPER BOUNDS STATED IN PREVIOUS SLIDE.

OPEN ISSUES

(CANDIDATE TOPICS FOR SPECIAL STUDIES)

- o Quantitative estimate of noise cancellation to be expected from common-mode rejection in typical users' instrument such as a gravity gradiometer
- o Formulate more accurate model of acceleration noise due to atmospheric density fluctuations
- o Definition and design of translational and rotational dampers
- o Quantitative estimate of degree of isolation achievable with dampers above
- o Quantitative estimate of overall degree of isolation by dampers and filters
- o Re-statement of accelerometers' threshold sensitivity requirements, taking into account overall achievable degree of noise abatament, inclusive of common-mode rejection

Appendix B

Some Evaluations Related to Dynamic Noise in the Payload Module of the Satellite

by

Dr. Enrico Lorenzini

This appendix derives expressions for natural frequencies related to the librational and attitudinal dynamics of the tether/subsatellite system. The expressions are evaluated for two cases, an atmospheric (downward) probe and an electrodynamic (upward) mission. See Figure B.1 for a picture of the system and definitions of the symbols.

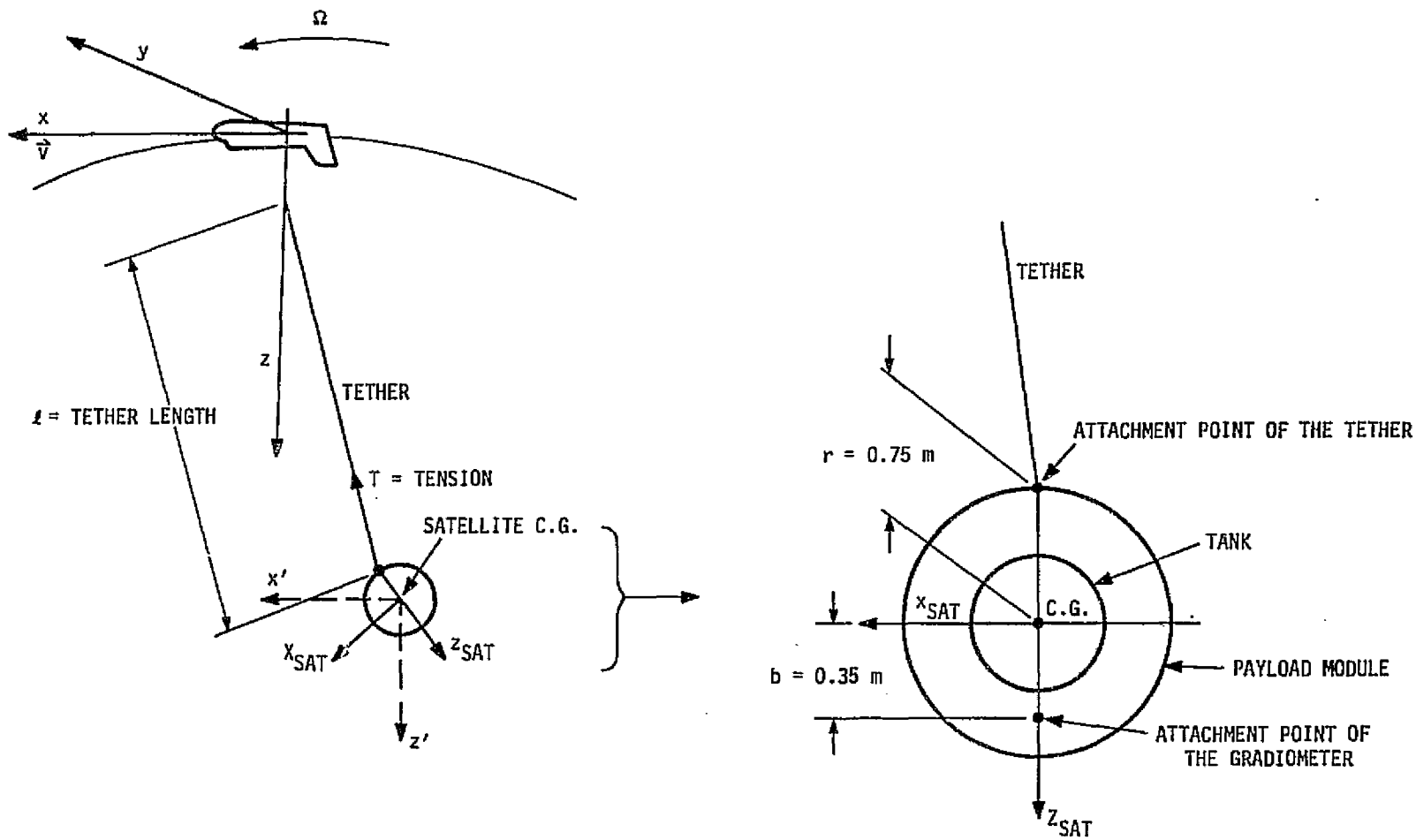
Ω
y
x
V
z
TETHER
ℓ = TETHER LENGTH
T = TENSION
SATELLITE C.G.
x'
X_SAT
Z_SAT
z'
TETHER
ATTACHMENT POINT OF THE TETHER
r = 0.75 m
TANK
X_SAT
C.G.
PAYLOAD MODULE
b = 0.35 m
ATTACHMENT POINT OF
THE GRADIOMETER
Z_SAT

Figure B-1

The attitude free oscillation frequencies of the satellite in the orbital plane (θ) and in the transverse plane (ϕ) are respectively given by:

$$\omega_\theta = \frac{Tr}{J_\theta} = \frac{3\Omega^2 m_{sat} \ell r}{J_\theta}$$
$$\omega_\phi = \frac{Tr}{J_\phi} = \frac{3\Omega^2 m_{sat} \ell r}{J_\phi} \qquad (1.1)$$

where T is the tether tension and r the satellite radius.

For small oscillation angles we can express the three components of the accelerations as:

$$a_{\theta sat} = -b\ \omega_\theta^2\ A_\theta \sin(\omega_\theta t + \gamma_\theta) \quad \text{in-plane acceleration}$$
$$a_{\phi sat} = -b\ \omega_\phi^2\ A_\phi \sin(\omega_\phi t + \gamma_\phi) \quad \text{out-of-plane acceleration}$$
$$a_{zsat} = b[\omega_\theta A_\theta \cos(\omega_\theta t + \gamma_\theta) + \omega_\phi A_\phi (\omega_\phi t + \nu_\phi)]^2 \quad \text{centrifugal acceleration} \qquad (1.2)$$

where A_θ and A_ϕ are the amplitudes of the rotational accelerations. The maximum values of the accelerations are given by:

$$\left|a_{\theta sat}\right|_{max} = b\ \omega_\theta^2\ A_\theta$$
$$\left|a_{\phi sat}\right|_{max} = b\ \omega_\phi^2\ A_\phi \qquad (1.3)$$
$$\left|a_{zsat}\right|_{max} < b\ [\omega_\theta A_\theta + \omega_\phi A_\phi]^2$$

With formulae (1.3) we are able to give an estimation of the maximum acceleration provided by the satellite rotational dynamics while the angular velocities are given by (maximum values):

$$\left|\dot{\theta}_{sat}\right|_{max} = \omega_\theta A_\theta \qquad \text{in-plane}$$

$$\left|\dot{\phi}_{sat}\right|_{max} = \omega_\phi A_\phi \qquad \text{out-of-plane} \qquad (1.4)$$

$$\left|\dot{y}_{sat}\right|_{max} = \omega_y A_y \qquad \text{yaw oscillation}$$

The accelerations depend strongly on the mission scenario and on the damping of the rotational oscillations of the satellite. Presently no damping devices for rotational oscillations are foreseen on the satellite so that we will give an estimation of the oscillations in this case. With damping devices, on the contrary, these oscillations will be damped out.

Accelerations due to the Librational Dynamics of the Tether

The tethered system, because of the atmosphere or electrodynamic drag acting on it, librates both in-plane and out-of-plane with very low frequencies.

Expressions of the tether librations are given by:

$$\theta = \beta_\theta \sin(\Omega_\theta t + \gamma_\theta)$$
$$\phi = \beta_\phi \sin(\Omega_\phi t + \gamma_\phi) \qquad (2.1)$$

where β_θ and β_ϕ are the amplitudes and Ω_θ, Ω_ϕ the angular frequencies. Maximum angular rates are given by:

$$\left|\dot{\theta}\right|_{max} = \beta_\theta \Omega_\theta$$
$$\left|\dot{\phi}\right|_{max} = \beta_\phi \Omega_\phi \qquad (2.2)$$

Accelerations can be easily derived in the small oscillation case as:

$$a_\theta = -\ell\Omega_\theta^2\beta_\theta \sin(\Omega_\theta t + \gamma_\theta)$$

$$a_\phi = -\ell\Omega_\phi^2\beta_\phi \sin(\Omega_\phi t + \gamma_\phi) \qquad (2.3)$$

$$a_z = \ell[\Omega_\theta\beta_\theta \cos(\Omega_\theta t + \gamma_\theta) + \Omega_\phi\beta_\phi \cos(\Omega_\phi t + \gamma_\phi)]^2$$

and their maximum values by:

$$\left|a_\theta\right|_{max} = \ell\Omega_\theta^2\beta_\theta$$

$$\left|a_\phi\right|_{max} = \ell\Omega_\phi^2\beta_\phi \qquad (2.4)$$

Preliminary Evaluation of the Effect of Rotational Dynamics and Tether Librations for some Mission Cases

Let us consider some typical mission cases that give an idea of what the acceleration values could be in the case that no rotational damping devices are operating on the satellite.

Satellite Characteristics

m_{sat} = 500 kg

$J_\theta = J_\phi \sim 100$ kg m^2

r = satellite radius = 0.75 m

b = distance between satellite c.g. and gradiometer = 0.35 m

1st Case: Atmospheric Mission (Downward)

Orbit inclination = 28°

Tether length = 100 km

Orbiter altitude = 230 km

Orbiter rate = Ω = 1.178 x 10^{-3} rad/sec

The satellite oscillation amplitude and angular frequencies are approximately given by:

$\beta_\theta \simeq 1°$

$\beta_\phi \simeq 0.04°$

$\Omega_\theta = 2\Omega = 2.36 \times 10^{-3}$ rad/sec

$\Omega_\phi = \Omega = 1.178 \times 10^{-3}$ rad/sec

Tether libration amplitudes and forced frequencies (atmospheric drag)

$A_\theta \simeq 1°$

$A_\phi \simeq 0.04°$

$\omega_\theta = 1.25$ rad/sec (Period $\simeq$ 5 sec)

$\omega_\phi = 1.25$ rad/sec (Period $\simeq$ 5 sec)

Attitude oscillation amplitudes and free frequencies

An estimation of the maximum values of the related accelerations and frequencies is therefore as follows:

$|a_{\theta sat}|_{max} = 0.010$ m/sec^2 ; $f_{\theta sat} = 0.2$ hertz ($\tau = 5$ sec)

$|a_{\phi sat}|_{max} = 3.8 \times 10^{-4}$ m/sec^2 ; $f_{\phi sat} = 0.2$ hertz ($\tau = 5$ sec)

$|a_{zsat}|_{max} = 1.8 \times 10^{-4}$ m/sec^2 ; f_{zsat} = difficult to be estimated

$|a_\theta|_{max} = 0.009$ m/sec^2 ; $f_\theta = 3.74 \times 10^{-4}$hertz ($\tau = 45$ min)

$|a_\phi|_{max} = 9.7 \times 10^{-5}$ m/sec^2 ; $f_\phi = 1.87 \times 10^{-4}$hertz ($\tau = 90$ min)

and the velocities:

$$\left|\dot{\theta}_{sat}\right|_{max} = 0.022 \text{ rad/sec} \quad ; \text{ same frequencies as above}$$

$$\left|\dot{\phi}_{sat}\right|_{max} = 8.73 \times 10^{-4} \text{rad/sec} \; ; \quad "$$

$$\left|\dot{\theta}\right|_{max} = 4.12 \times 10^{-5} \text{rad/sec} \quad ; \quad "$$

$$\left|\dot{\phi}\right|_{max} = 2.06 \times 10^{-5} \text{rad/sec} \quad ; \quad "$$

2nd Case: Electrodynamic Mission (Upward)

Orbit inclination = 28°

Tether length = 20 km

Orbiter Altitude = 295 km

Orbital rate = 1.175×10^{-3} rad/sec

Current intensity ≈ 0.35 Amp

Satellite oscillation amplitudes and angular frequencies are approximately as follows:

$\beta_\theta = 0.2°$

$\beta_\phi = 0.1°$

$\Omega_\theta = 2.04 \times 10^{-3}$ rad/sec

$\Omega_\phi = 2.35 \times 10^{-3}$ rad/sec

Amplitudes and frequencies of the tether librations

$A_\theta = 0.2°$

$A_\phi = 0.1°$

$\omega_\theta = 0.56$ rad/sec (Period = 11 sec)

$\omega_\phi = 0.56$ rad/sec (Period = 11 sec)

Amplitudes and free oscillation frequencies of the rotational satellite dynamics

Acceleration and frequencies in the payload modules are given by:

$$|a_{\theta sat}|_{max} = 3.8 \times 10^{-4} \text{ m/sec}^2 \; ; \; f_{\theta sat} = 8.91 \times 10^{-2} \text{hertz} \; (\tau = 11 \text{ sec})$$

$$|a_{\phi sat}|_{max} = 1.92 \times 10^{-4} \text{ m/sec}^2 \; ; \; f_{\phi sat} = 8.91 \times 10^{-2} \text{hertz} \; (\tau = 11 \text{ sec})$$

$$|a_{zsat}|_{max} = 3.01 \times 10^{-6} \text{ m/sec}^2 \; ; \; f_{zsat} = \text{difficult to be evaluated}$$

$$|a_{\theta}|_{max} = 2.88 \times 10^{-4} \text{ m/sec}^2 \; ; \; f_{\theta} = 3.25 \times 10^{-4} \text{hertz} \; (\tau = 51 \text{ min})$$

$$|a_{\phi}|_{max} = 1.93 \times 10^{-4} \text{ m/sec}^2 \; ; \; f_{\phi} = 3.74 \times 10^{-4} \text{hertz} \; (\tau = 45 \text{ min})$$

and the angular velocities:

$$|\dot{\theta}_{sat}|_{max} = 0.002 \text{ rad/sec} \; ; \quad \text{same frequenices as above}$$

$$|\dot{\phi}_{sat}|_{max} = 0.001 \text{ rad/sec} \; ; \quad "$$

$$|\dot{\theta}|_{max} = 7.12 \times 10^{-6} \text{ rad/sec} \; ; \quad "$$

$$|\dot{\phi}|_{max} = 4.1 \times 10^{-6} \text{ rad/sec} \; ; \quad "$$

The yaw oscillation velocity has not been calculated because it depends on many parameters that still require a complete definition.

APPENDIX C

A Presentation Made By

Dr. Gordon E. Gullahorn

to

NASA Geodynamics Conference

American Geophysical Union 1984 Spring Meeting

Cincinnati, Ohio

May 14-17, 1984

Feasibility of Gravity Gradient Measurements from a Tethered Subsatellite

FEASIBILITY OF GRAVITY GRADIENT MEASUREMENTS FROM A TETHERED SUBSATELLITE PLATFORM

G. E. GULLAHORN
F. FULIGNI*
M. D. GROSSI

MAY 1984

SMITHSONIAN INSTITUTION
ASTROPHYSICAL OBSERVATORY
CAMBRIDGE, MASSACHUSETTS 02138

* VISTING SCIENTIST, IFSI-CNR, FRASCATI, ITALY

408-090

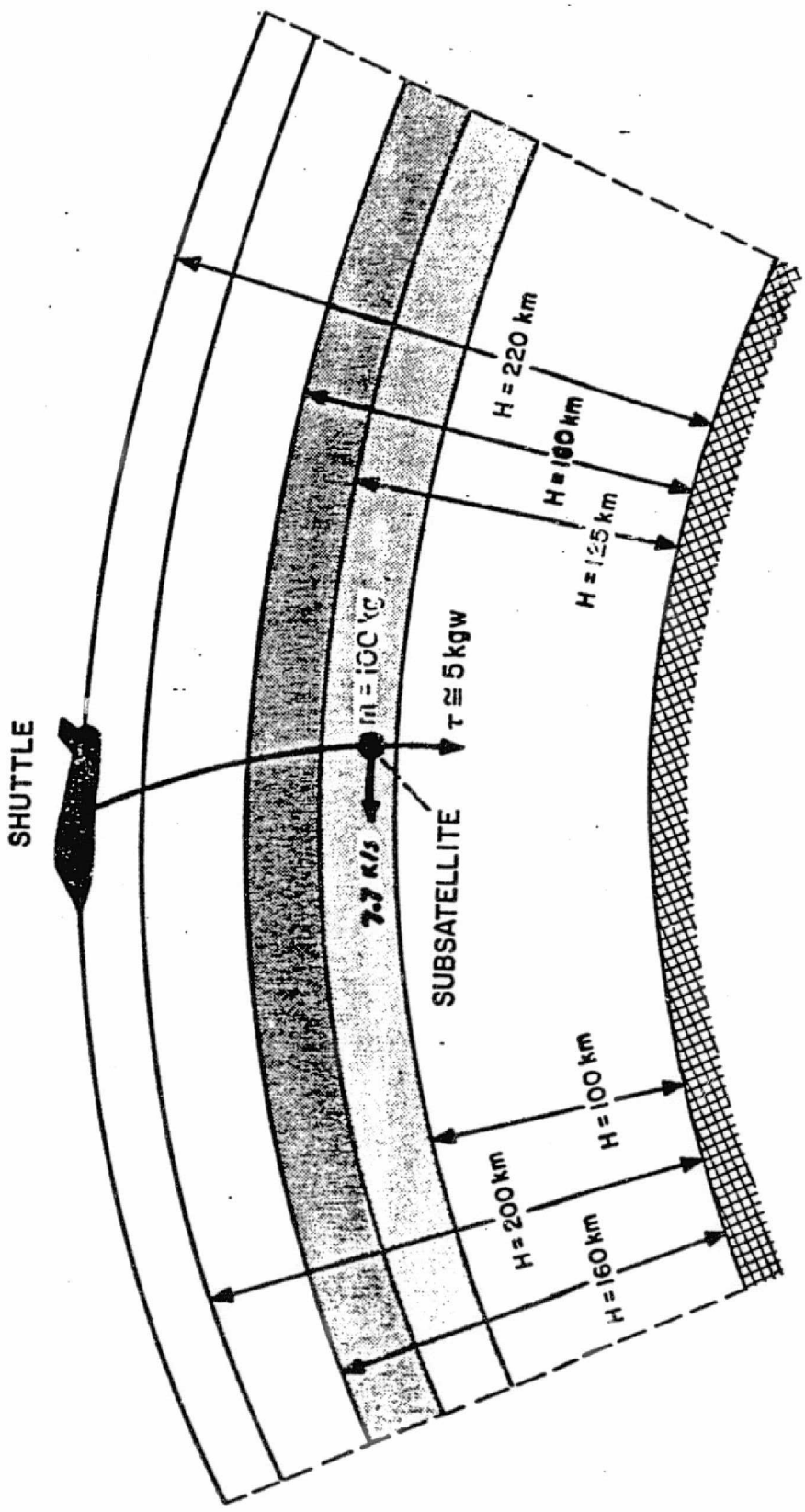

"TRADITIONAL" GRAVITY MEASUREMENT

EARTH SURFACE :

- -- MEASURE ABSOLUTE ACCELERATION DIRECTLY
- -- USE MASS ON SPRING, PENDULUM, FALLING BODY
- -- SHORT DISTANCE SCALE EFFECTS
- -- HISTORICAL BASE

SATELLITE ORBIT OBSERVATION :

- -- LASER RANGING, DOPPLER RANGING, OPTICAL POSITIONS
- -- LONG SCALE EFFECTS
- -- INTEGRATED EFFECT OVER MANY ORBITS
- -- STATION COORDINATES
- -- POSSIBILITY OF DIRECTLY OBSERVING CONTINENTAL DRIFT

G R A V I T Y G R A D I O M E T R Y

-- ORBITING PLATFORM
-- MEASURE SPACE DERIVATIVES OF GRAVITATIONAL ACCELERATION
-- DIRECT MEASUREMENT
-- MEASURE ANOMALIES AT ALL SCALES DOWN TO ORBIT ALTITUDE
-- ORBIT CAUSES US TO SCAN ACROSS FEATURES

PROPOSED PLATFORMS :

- -- HIGH ALTITUDE FREE SATELLITE
- -- LOW ALTITUDE "DRAG-FREE" SATELLITE
- -- LOW ALTITUDE TETHERED SUBSATELLITE
- -- SATELLITE - SATELLITE DOPPLER

DEFINITIONS AND UNITS

$$\Gamma_{IJ} = \frac{\partial G_I}{\partial X_J} = -\frac{\partial^2 U}{\partial X_I \partial X_J}$$

---- 5 INDEPENDENT COMPONENTS, BY SYMMETRIES AND POISSON EQUATION

---- BY MEASURING MORE THAN 5, CAN ALLOW FOR EFFECTS OF ROTATION

UNIT OF GRAVITY : 1 GAL = 1 CM / SEC

1 G = 10^3 GAL

UNIT OF GRADIENT : 1 EOTVOS UNIT (EU) = 10^{-9} SEC^{-2}

= 10^{-9} GAL / CM

BASELINE GRAVITY GRADIENT = 3000 EU

SENSITIVITY GOAL = 3×10^{-4} EU $Hz^{-1/2}$

POINT ANOMALY -- GRADIENT IMPULSE FUNCTION

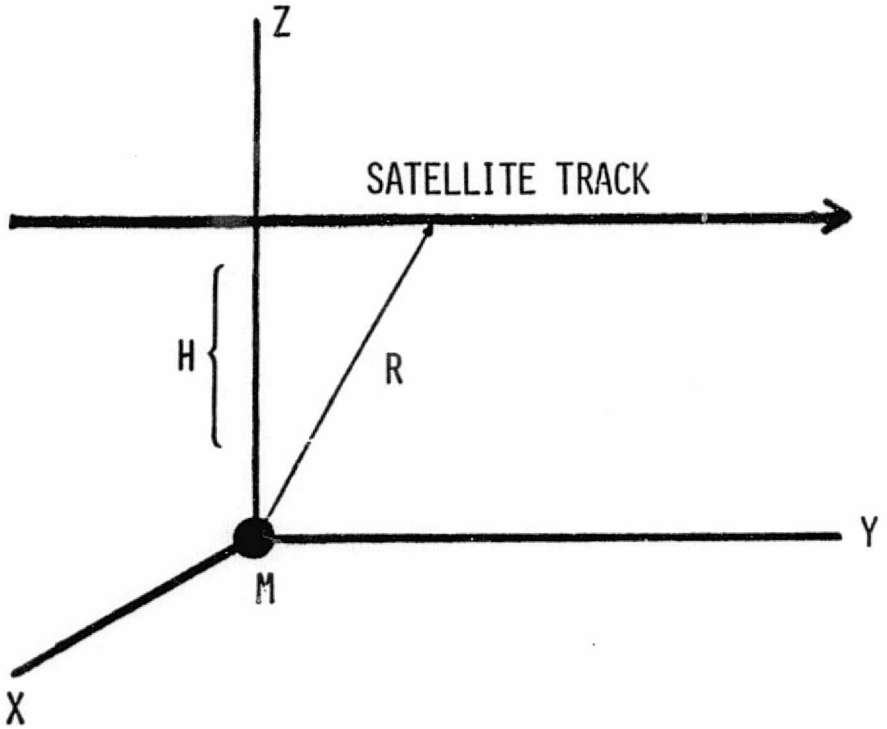

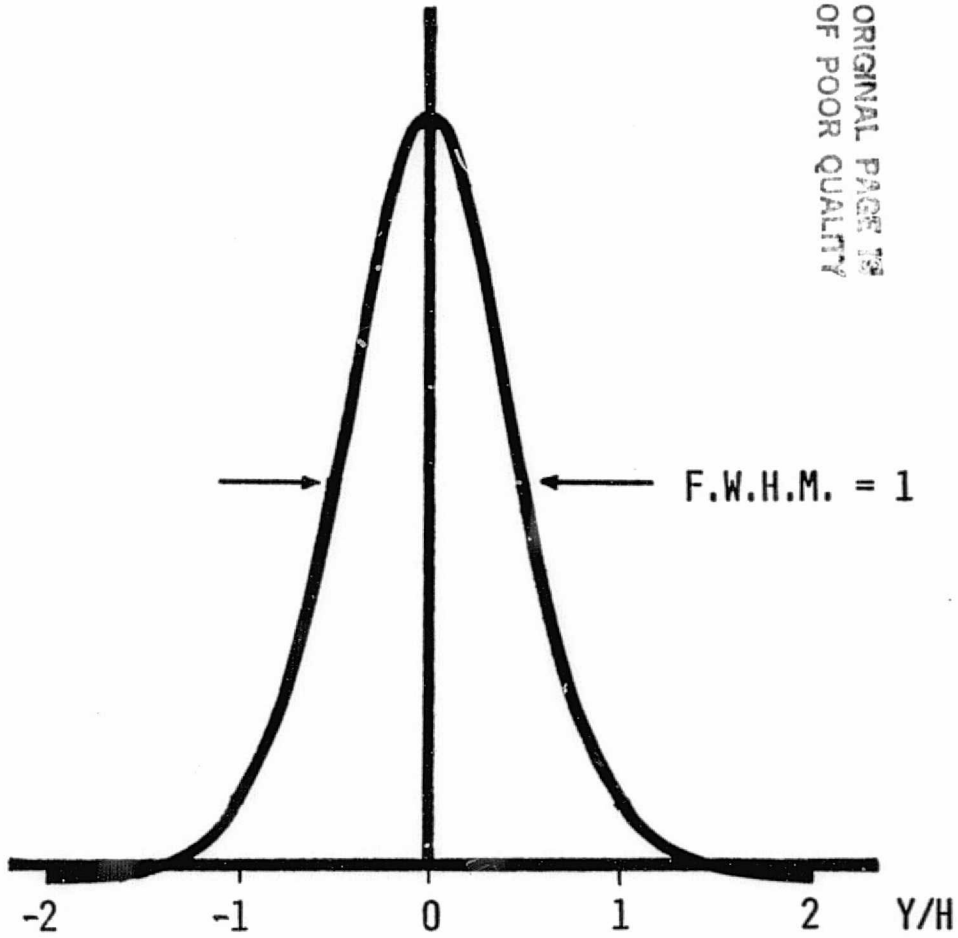

$$\Gamma_{ZZ} = \left[\frac{G\,M}{H^3}\right]\left[\frac{3 - (R/H)^2}{(R/H)^5}\right]$$

TETHERED SUBSATELLITE

ADVANTAGES:

-- RESPOND TO SMALL ANOMALIES, DOWN TO SCALE ABOUT (1/ ALTITUDE)

-- STRONG SIGNAL, PROPORTIONAL TO $(1 / \text{ALTITUDE})^3$

-- MODERATE LENGTH MISSION

DISADVANTAGES:

-- NOISY ACCELERATION ENVIRONMENT

-- T.S.S. NOT FULLY DEVELOPED

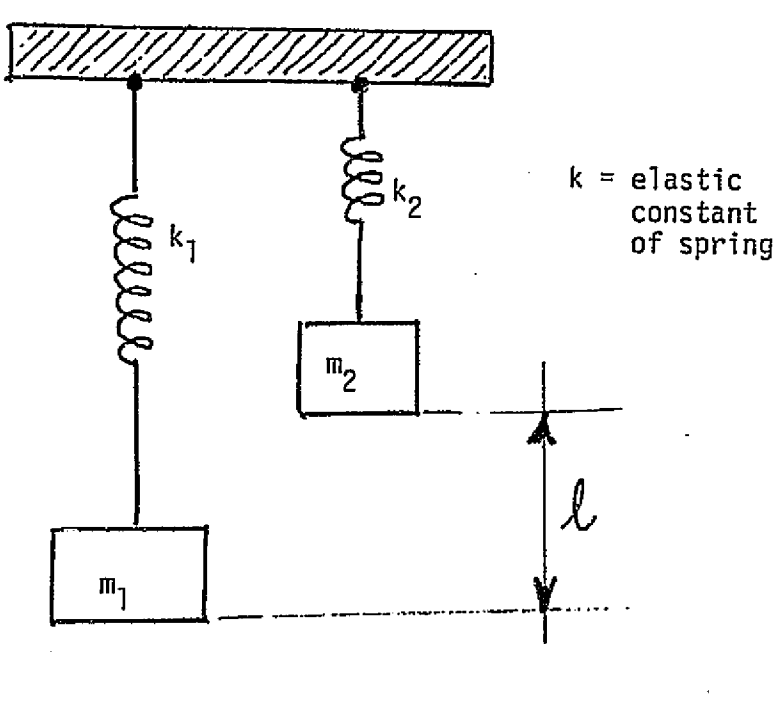

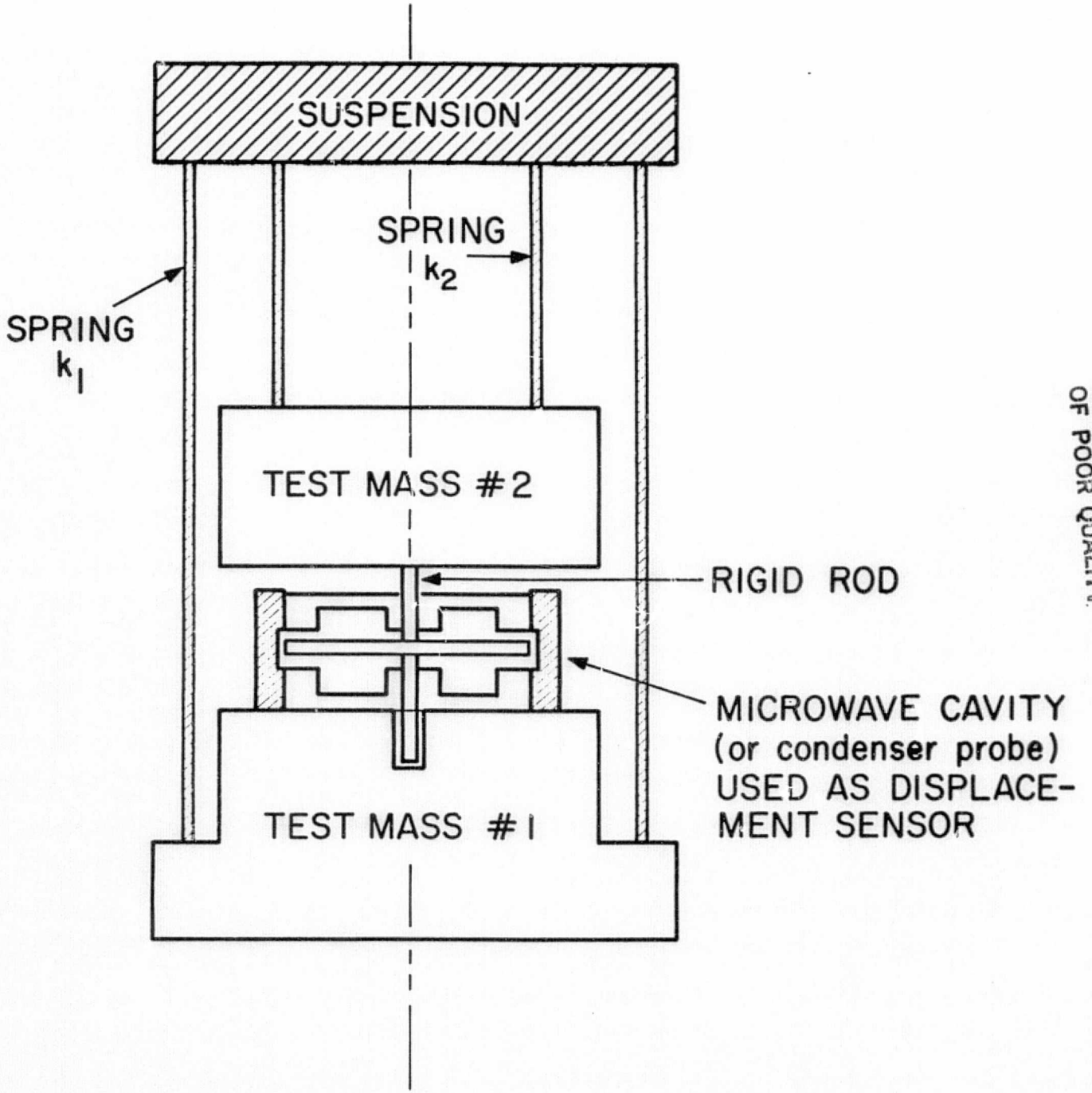

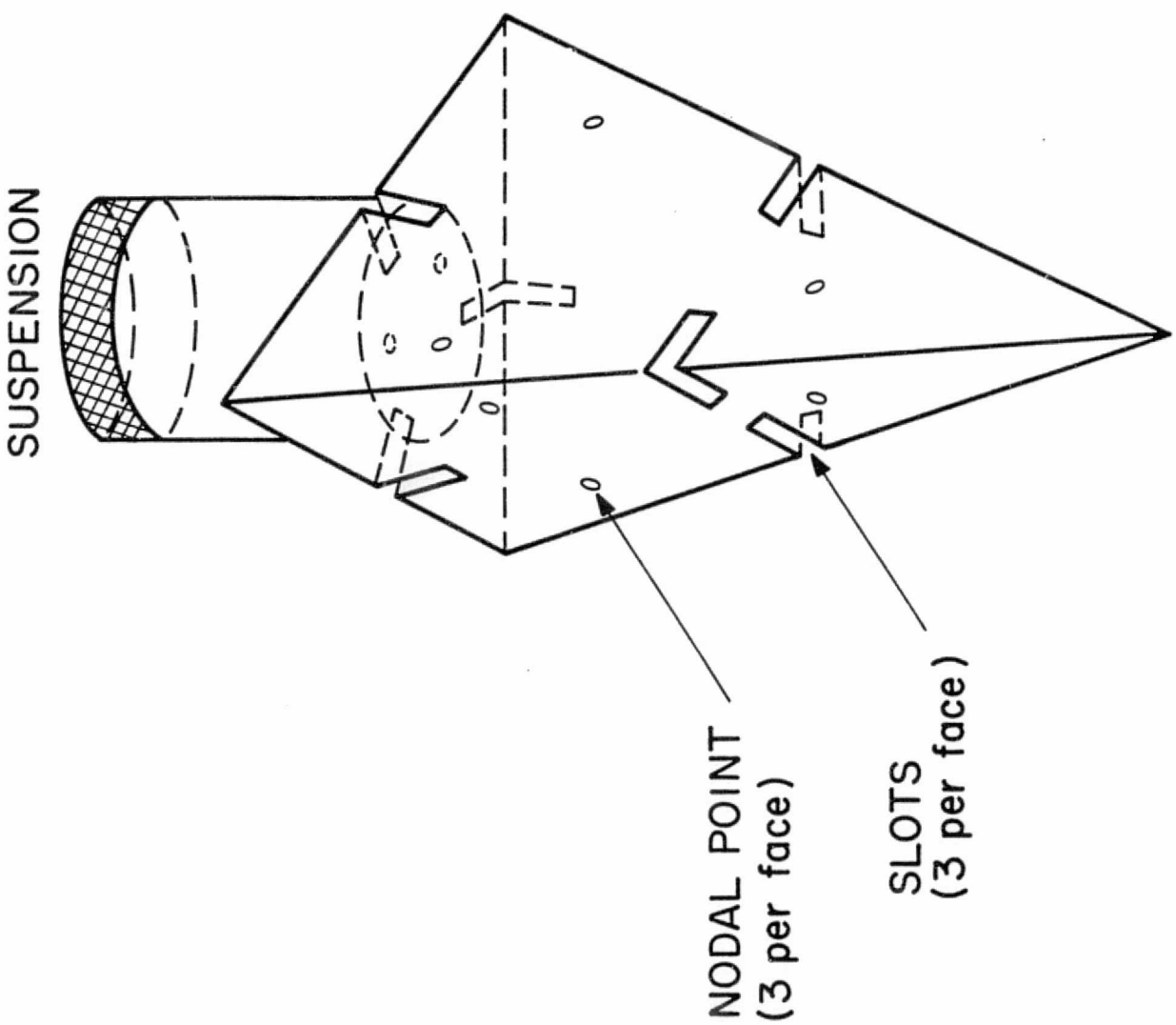

GRADIOMETRIC EFFECT OF DYNAMIC NOISE

LINEAR ACCELERATION NOISE

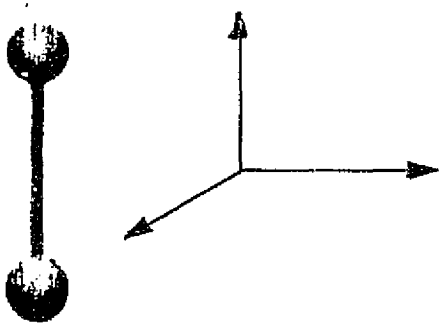

REJECTED BY
COMMON MODE ACCELERATION

TORSIONAL ACCELERATION NOISE

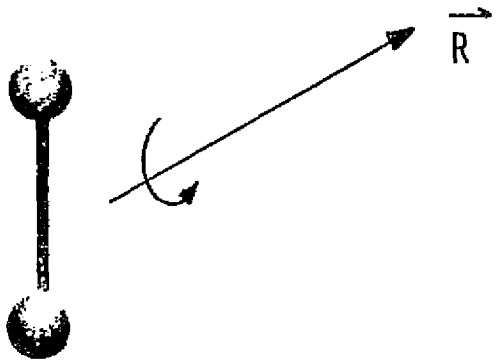

PRODUCES AN ADDITIONAL GRADIENT COMPONENT:

$$A = \dot{T} + T^2$$

$$T = \begin{bmatrix} 0 & -R_3 & R_2 \\ R_3 & 0 & -R_1 \\ -R_2 & R_1 & 0 \end{bmatrix}$$

SOURCES OF DYNAMIC NOISE

-- VARIABLE DRAG DUE TO ATMOSPHERIC DENSITY FLUCTUATIONS

-- TETHER OSCILLATIONS :
   - LONGITUDINAL (STRETCHING) MODES
   - LATITUDINAL MODES

-- GROSS MOTION OF SUBSATELLITE ALONG TETHER DIRECTION ("SPRING-MASS" MODE)

-- SUBSATELLITE ROTATIONAL DYNAMICS

-- TETHER PENDULAR LIBRATIONS

-- TETHER REEL CONTROL

-- ORBITAL ALTITUDE VARIATIONS

-- MOTION ON BOARD DEPLOYER

-- MAGNETIC FIELD VARIATIONS

ATMOSPHERIC DENSITY FLUCTUATIONS

--- AT ALTITUDES OF INTEREST (120 - 150 KM) THE ONLY DATA IS FROM PERIGEE PASSAGES OF SPADES AND ATMOSPHERE EXPLORER-C SATELLITES

-- GIVES ONLY BRIEF SAMPLES

-- VERTICAL AND HORIZONTAL CORRELATIONS CONFUSED

-- FLUCTUATIONS OF UP TO 20 % ON SCALES OF 10'S TO 100'S OF KILOMETERS (REBER, ET AL 1975)

--- THERE IS GOOD DATA AT HIGHER ALTITUDES FROM ATMOSPHERE EXPLORER-E (300 KM) AND ATMOSPHERE EXPLORER-C (250 KM)

-- LONG OBSERVATION SPANS

-- CONSTANT ALTITUDE

-- A.E.-C RESULTS (GROSS, REBER AND HUANG 1984):

- POWER LAW SPECTRUM WITH SOME SHARP PEAKS
- INDIVIDUAL WAVES EXTENDING ONLY A FEW PERIODS

--- PRIMARY EFFECT IS HORIZONTAL DRAG ON SUBSATELLITE

-- DRAG FLUCTUATION IS PROPORTIONAL TO DENSITY FLUCTUATION

-- BASELINE DRAG ACCELERATION AT 120 KM = 0.5 GAL = 5×10^{-3} G

TETHER DYNAMICS

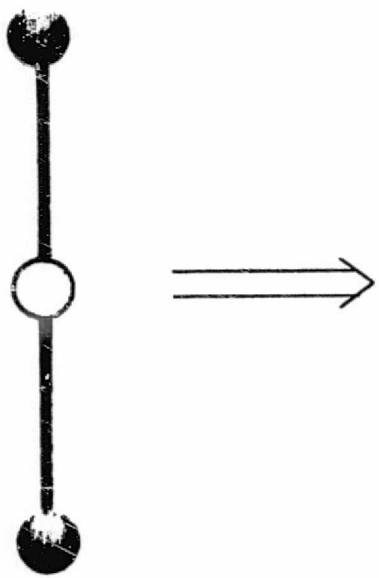

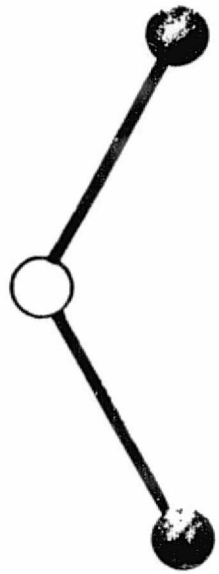

LONGITUDINAL	LATITUDINAL	SPRING-MASS
$0.03\ N$ HZ	$10^{-3}\ N$ HZ	0.01 HZ
$\frac{30}{N}$ SEC	$\frac{1000}{N}$ SEC	110 SEC

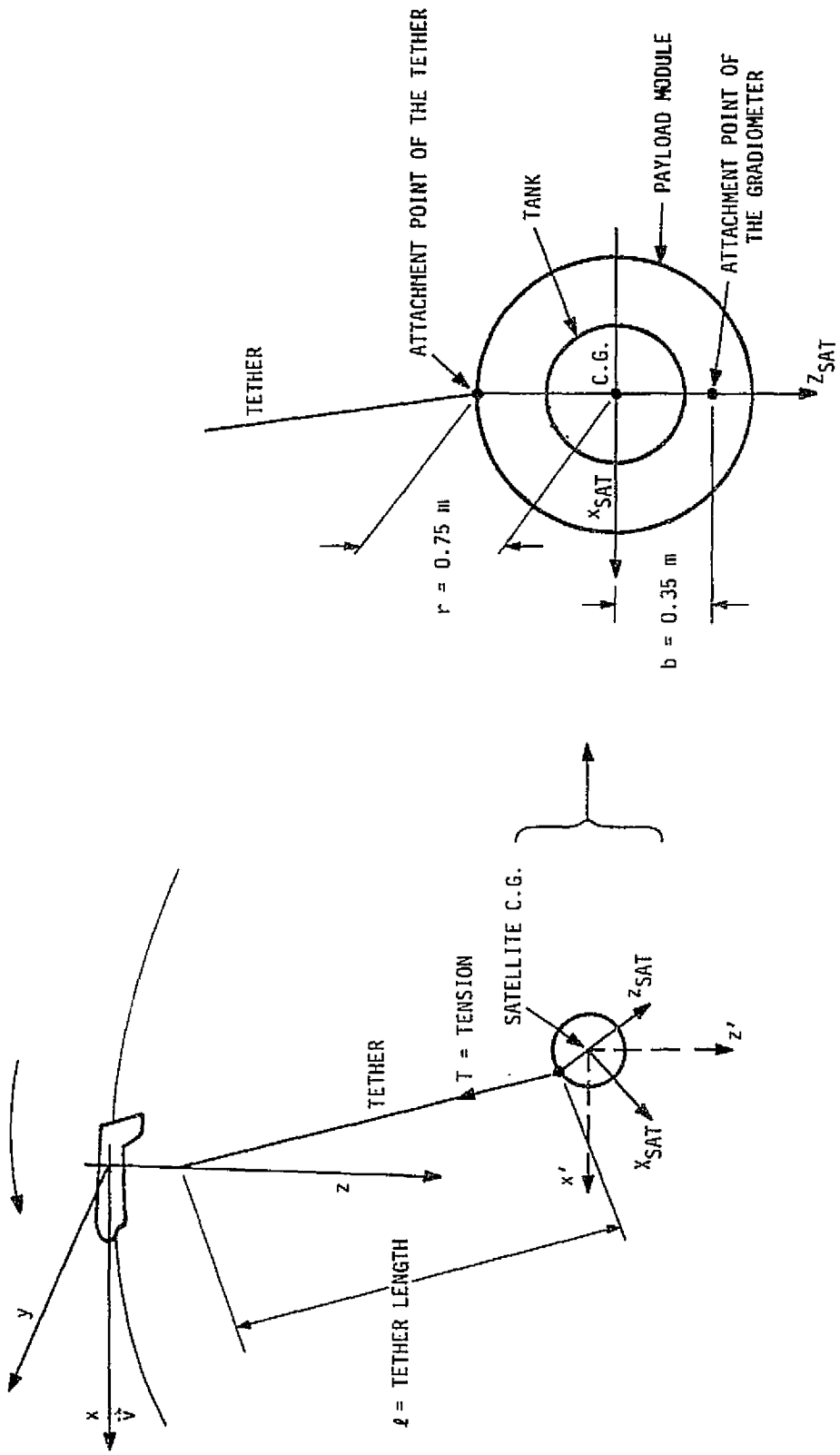

ACCELERATION IMPULSE RESPONSE P.S.D.

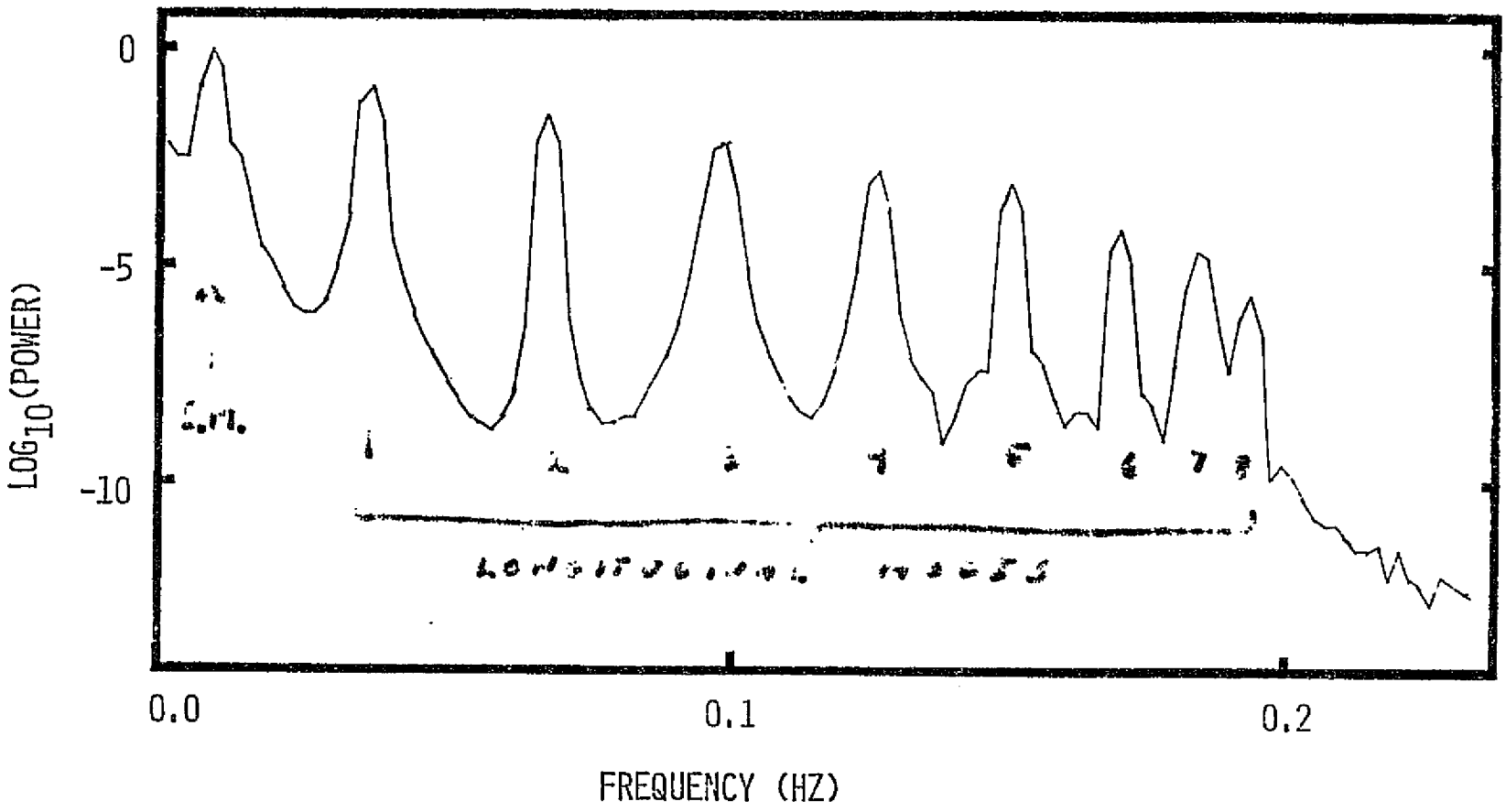

PRELIMINARY MAGNITUDE ESTIMATES

SOURCE	MAGNITUDE	FREQUENCY
DENSITY FLUCTUATIONS (10%)	0.05 GAL	BROADBAND
SUBSATELLITE ROTATION (RESIDUAL FROM DEPLOYMENT)	0.01 - 1 GAL	0.2 HZ
	0.001 - 0.02 RAD/SEC	0.2 HZ
LONGITUDINAL OSCILLATIONS (FORCED BY ABOVE)	0.0001 - 0.001 GAL	0.03 N HZ
SPRING - MASS OSCILLATION (RESIDUAL FROM DEPLOYMENT)	1 GAL	0.01 HZ

FUTURE DIRECTIONS

- LINEAR ACCELERATION NOISE ⇒ ROTATIONAL NOISE
  - ATMOSPHERIC DRAG FLUCTUATIONS
  - TETHER OSCILLATIONS
- INVESTIGATE USE OF FULL Γ_{ij} TO ELIMINATE ROTATION EFFECTS
- STUDY GRAVIMETER SUSPENSION AND TETHER DAMPING
  - DEGREE OF COMMON MODE REJECTION
  - AVOID / ELIMINATE ROTATION IN INSTRUMENT
- IMPROVE MODELLING
  - RANDOM VIBRATION ANALYSIS
  - INCLUDE GRAVIMETER AND ITS SUSPENSION

PROPOSED MISSIONS

T.S.S. DEMONSTRATION FLIGHTS

MISSION I (UPWARD):

- -- STUDY SYSTEM RESPONSE USING KNOWN THRUSTER FORCES
- -- COMPARE WITH THEORY, ESTIMATE DAMPING AND SYSTEM PARAMETERS

MISSION II (DOWNWARD):

- -- OBSERVE EFFECTS OF ATMOSPHERIC FLUCTUATIONS
- -- MEASURE RESPONSE AND PARAMETERS OF A DIFFERENT SYSTEM
- -- POSSIBLY FLY A ONE-AXIS, NON-CRYOGENIC GRADIOMETER TO STUDY GRADIOMETRIC NOISE

DEVOTED FLIGHTS

- -- FULL TENSOR GRADIOMETER, CRYOGENIC
- -- OBTAIN GEOPHYSICAL DATA

APPENDIX D

Detailed Plots of Simulation Results

Figure D-1. This figure plots the acceleration perpendicular to the tether as a function of time, following a perturbation due to an atmospheric density enhancement. For details of the case studied, see Section 7. The two columns of numbers to the left of the plot are (1) the time since the beginning of the simulation and (2) the acceleration in gal's (cm/sec^2). The plot begins at t = 16 seconds, since during the actual perturbation the (from about t=10 to t=15) the acceleration is several orders of magnitude greater; thus, a full span plot is simply a step function. Note the overall smooth appearance of the plot when compared with Figure D-2 below, which shows the acceleration component tangent to the tether. Also note the jump in acceleration near t = 420; an explanation for this has not been ascertained, but it is probably an artifact of the simulation.

ACROSS-TETHER ACCELERATION

MIN, MAX: -0.8102100000D-05 0.4904170000D-04

16.00	0.11482000D-05	:
17.00	0.14185000D-05	:
18.00	0.17157000D-05	:
19.00	0.20378000D-05	:
20.00	0.23822000D-05	:
21.00	0.27475000D-05	:
22.00	0.31320000D-05	:
23.00	0.35343000D-05	:
24.00	0.39529000D-05	:
25.00	0.43859000D-05	:
26.00	0.48320000D-05	:
27.00	0.52900000D-05	:
28.00	0.57584000D-05	:
29.00	0.62360000D-05	:
30.00	0.67214000D-05	:
31.00	0.72133000D-05	:
32.00	0.77105000D-05	:
33.00	0.82122000D-05	:
34.00	0.87170000D-05	:
35.00	0.92239000D-05	:
36.00	0.97320000D-05	:
37.00	0.10240600D-04	:
38.00	0.10749600D-04	:
39.00	0.11259500D-04	:
40.00	0.11771700D-04	:
41.00	0.12289800D-04	:
42.00	0.12819200D-04	:
43.00	0.13367800D-04	:
44.00	0.13945000D-04	:
45.00	0.14560300D-04	:
46.00	0.15221800D-04	:
47.00	0.15933300D-04	:
48.00	0.16693500D-04	:
49.00	0.17494800D-04	:
50.00	0.18326300D-04	:
51.00	0.19176200D-04	:
52.00	0.20034500D-04	:
53.00	0.20895800D-04	:
54.00	0.21758200D-04	:
55.00	0.22621100D-04	:
56.00	0.23483300D-04	:
57.00	0.24341000D-04	:
58.00	0.25189000D-04	:
59.00	0.26022200D-04	:
60.00	0.26837400D-04	:
61.00	0.27633400D-04	:
62.00	0.28409800D-04	:
63.00	0.29165800D-04	:
64.00	0.29899200D-04	:
65.00	0.30607100D-04	:
66.00	0.31287700D-04	:
67.00	0.31941100D-04	:
68.00	0.32568300D-04	:
69.00	0.33171100D-04	:
70.00	0.33750900D-04	:
71.00	0.34310000D-04	:

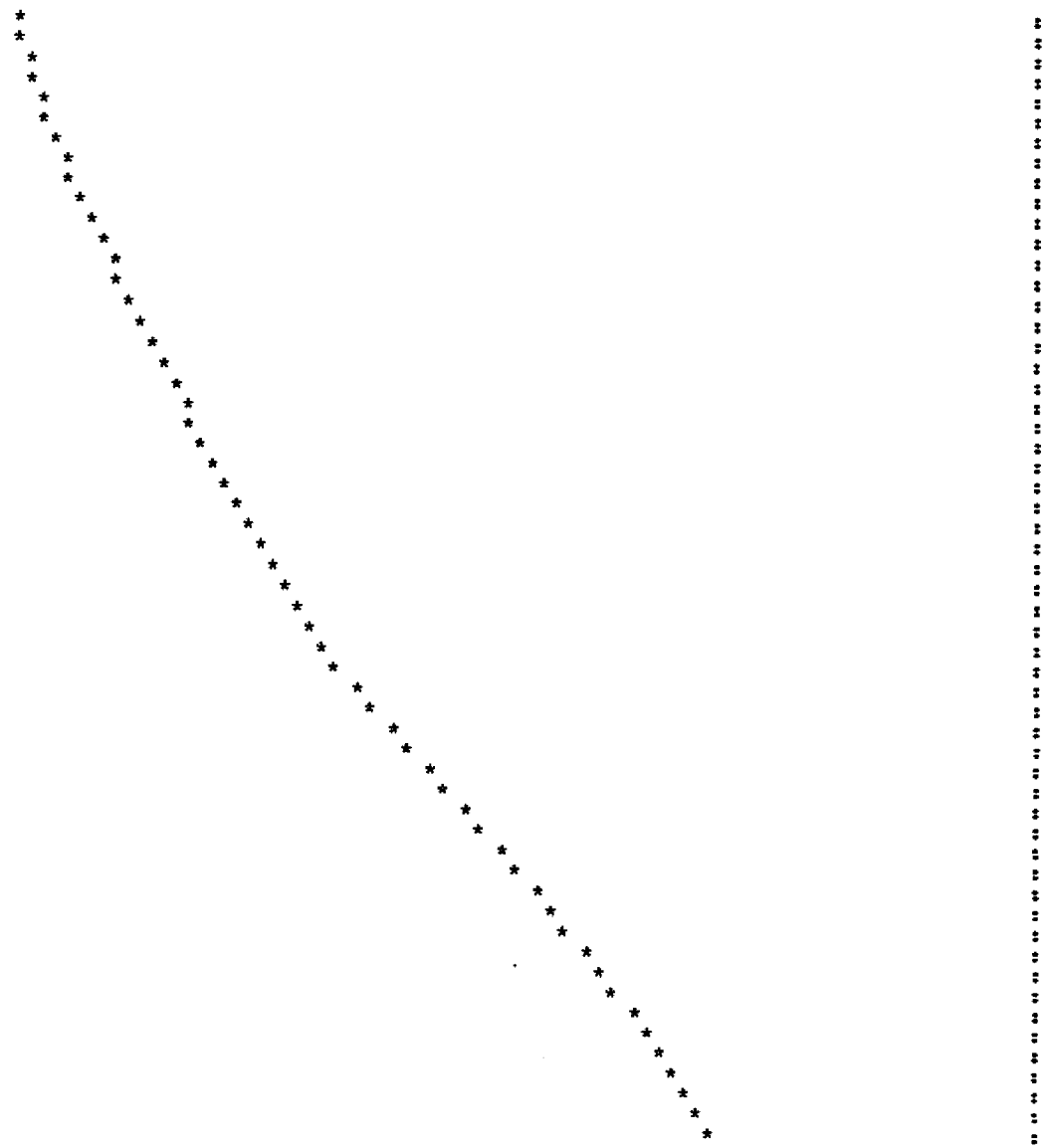

72.00	0.34851500D-04
73.00	0.35380100D-04
74.00	0.35901300D-04
75.00	0.36419600D-04
76.00	0.36936300D-04
77.00	0.37449500D-04
78.00	0.37953200D-04
79.00	0.38438600D-04
80.00	0.38893800D-04
81.00	0.39306400D-04
82.00	0.39664200D-04
83.00	0.39958900D-04
84.00	0.40186800D-04
85.00	0.40349000D-04
86.00	0.40449400D-04
87.00	0.40491600D-04
88.00	0.40477300D-04
89.00	0.40405300D-04
90.00	0.40273000D-04
91.00	0.40078400D-04
92.00	0.39821400D-04
93.00	0.39504600D-04
94.00	0.39132200D-04
95.00	0.38709000D-04
96.00	0.38238800D-04
97.00	0.37723600D-04
98.00	0.37164700D-04
99.00	0.36564200D-04
100.00	0.35926400D-04
101.00	0.35257900D-04
102.00	0.34565400D-04
103.00	0.33854500D-04
104.00	0.33128300D-04
105.00	0.32387200D-04
106.00	0.31630500D-04
107.00	0.30856800D-04
108.00	0.30062800D-04
109.00	0.29242500D-04
110.00	0.28387500D-04
111.00	0.27488400D-04
112.00	0.26537600D-04
113.00	0.25532600D-04
114.00	0.24475800D-04
115.00	0.23374000D-04
116.00	0.22236600D-04
117.00	0.21073300D-04
118.00	0.19892600D-04
119.00	0.18700800D-04
120.00	0.17501800D-04
121.00	0.16290200D-04
122.00	0.15091200D-04
123.00	0.13883500D-04
124.00	0.12679100D-04
125.00	0.11484600D-04
126.00	0.10308200D-04
127.00	0.91576000D-05
128.00	0.80388000D-05
129.00	0.69546000D-05
130.00	0.59061000D-05
131.00	0.48942000D-05
132.00	0.39221000D-05
133.00	0.29942000D-05
134.00	0.21148000D-05
135.00	0.12853000D-05
136.00	0.50280000D-06
137.00	-0.23880000D-06

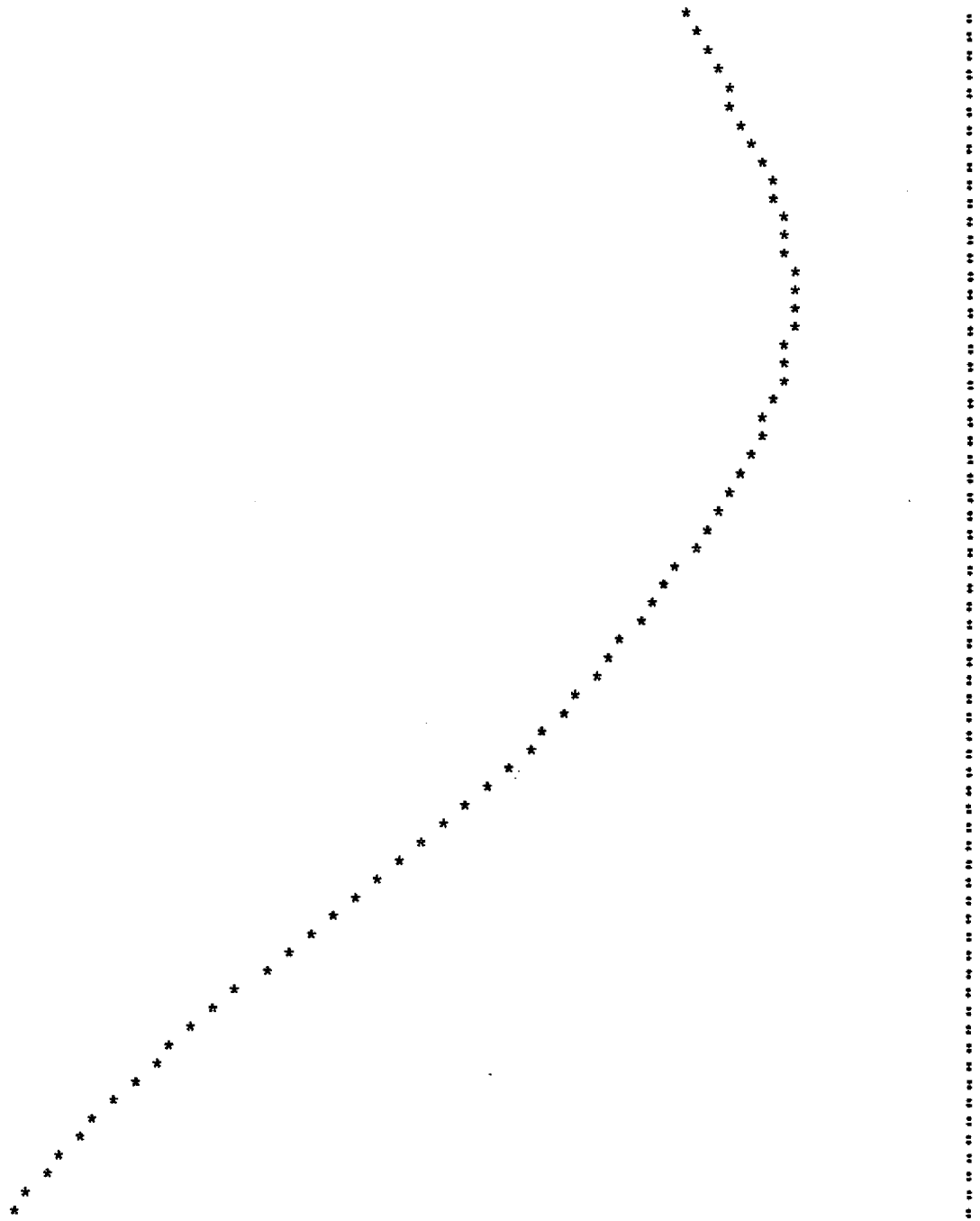

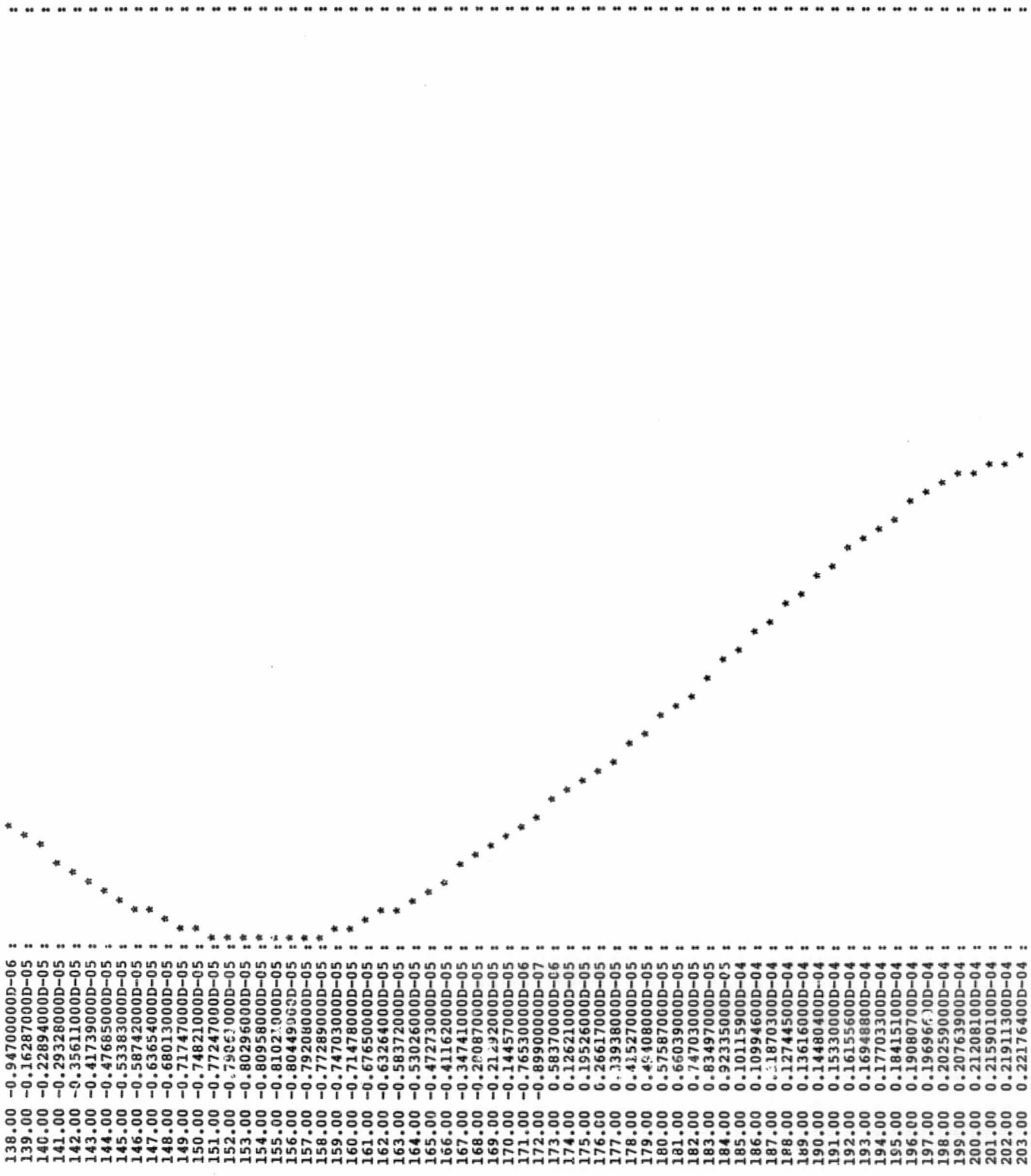

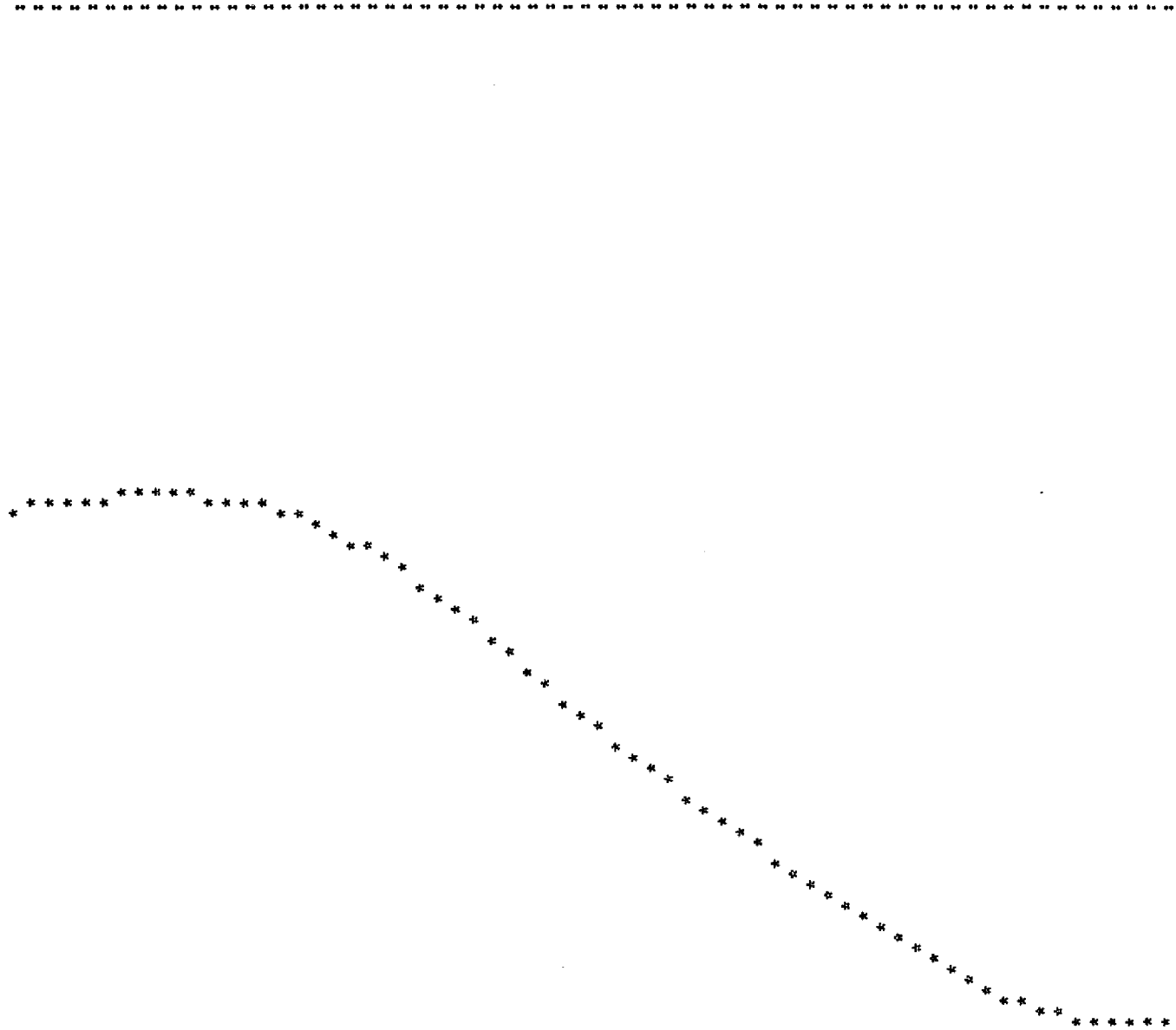

204.00	0.223931000D-04
205.00	0.225712000D-04
206.00	0.227208000D-04
207.00	0.228500000D-04
208.00	0.229636000D-04
209.00	0.230620000D-04
210.00	0.231418000D-04
211.00	0.231971000D-04
212.00	0.232216000D-04
213.00	0.232096000D-04
214.00	0.231574000D-04
215.00	0.230627000D-04
216.00	0.229236000D-04
217.00	0.227392000D-04
218.00	0.225097000D-04
219.00	0.222374000D-04
220.00	0.219247000D-04
221.00	0.215730000D-04
222.00	0.211799000D-04
223.00	0.207395000D-04
224.00	0.202456000D-04
225.00	0.196947000D-04
226.00	0.190886000D-04
227.00	0.184332000D-04
228.00	0.177355000D-04
229.00	0.170007000D-04
230.00	0.162326000D-04
231.00	0.154341000D-04
232.00	0.146107000D-04
233.00	0.137705000D-04
234.00	0.129238000D-04
235.00	0.120822000D-04
236.00	0.112559000D-04
237.00	0.104533000D-04
238.00	0.967850000D-05
239.00	0.893150000D-05
240.00	0.820800000D-05
241.00	0.750150000D-05
242.00	0.680510000D-05
243.00	0.611270000D-05
244.00	0.542070000D-05
245.00	0.472830000D-05
246.00	0.403680000D-05
247.00	0.335010000D-05
248.00	0.267240000D-05
249.00	0.200730000D-05
250.00	0.135710000D-05
251.00	0.722500000D-06
252.00	0.103800000D-06
253.00	-0.499000000D-06
254.00	-0.108610000D-05
255.00	-0.165730000D-05
256.00	-0.221160000D-05
257.00	-0.274630000D-05
258.00	-0.325530000D-05
259.00	-0.373010000D-05
260.00	-0.416460000D-05
261.00	-0.453940000D-05
262.00	-0.486010000D-05
263.00	-0.512010000D-05
264.00	-0.531750000D-05
265.00	-0.544940000D-05
266.00	-0.551140000D-05
267.00	-0.549920000D-05
268.00	-0.541070000D-05
269.00	-0.524910000D-05

270.00	-0.50236000D-05
271.00	-0.47470000D-05
272.00	-0.44317000D-05
273.00	-0.40868000D-05
274.00	-0.37164000D-05
275.00	-0.33207000D-05
276.00	-0.28978000D-05
277.00	-0.24454000D-05
278.00	-0.19606000D-05
279.00	-0.14405000D-05
280.00	-0.88290000D-06
281.00	-0.28710000D-06
282.00	0.34560000D-06
283.00	0.10119000D-05
284.00	0.17089000D-05
285.00	0.24353000D-05
286.00	0.31921000D-05
287.00	0.39821000D-05
288.00	0.48088000D-05
289.00	0.56759000D-05
290.00	0.65870000D-05
291.00	0.75461000D-05
292.00	0.85556000D-05
293.00	0.96162000D-05
294.00	0.10725200D-04
295.00	0.11877600D-04
296.00	0.13067400D-04
297.00	0.14288500D-04
298.00	0.15534900D-04
299.00	0.16800000D-04
300.00	0.18076000D-04
301.00	0.19352800D-04
302.00	0.20618600D-04
303.00	0.21862400D-04
304.00	0.23075700D-04
305.00	0.24255300D-04
306.00	0.25403800D-04
307.00	0.26528600D-04
308.00	0.27638000D-04
309.00	0.28737400D-04
310.00	0.29827700D-04
311.00	0.30905600D-04
312.00	0.31966600D-04
313.00	0.33007200D-04
314.00	0.34026500D-04
315.00	0.35024200D-04
316.00	0.36000500D-04
317.00	0.36955200D-04
318.00	0.37889400D-04
319.00	0.38805300D-04
320.00	0.39706400D-04
321.00	0.40594700D-04
322.00	0.41469900D-04
323.00	0.42328500D-04
324.00	0.43164300D-04
325.00	0.43970100D-04
326.00	0.44738600D-04
327.00	0.45462700D-04
328.00	0.46135100D-04
329.00	0.46749000D-04
330.00	0.47297800D-04
331.00	0.47775700D-04
332.00	0.48178400D-04
333.00	0.48503000D-04
334.00	0.48748900D-04
335.00	0.48917300D-04

ORIGINAL PAGE IS
OF POOR QUALITY

336.00	0.49012500D-04
337.00	0.49041700D-04
338.00	0.49015200D-04
339.00	0.48943400D-04
340.00	0.48834900D-04
341.00	0.48693200D-04
342.00	0.48515900D-04
343.00	0.48297500D-04
344.00	0.48033800D-04
345.00	0.47721000D-04
346.00	0.47364500D-04
347.00	0.46969200D-04
348.00	0.46540800D-04
349.00	0.46083600D-04
350.00	0.45599200D-04
351.00	0.45087800D-04
352.00	0.44548500D-04
353.00	0.43978900D-04
354.00	0.43376500D-04
355.00	0.42737700D-04
356.00	0.42057900D-04
357.00	0.41332000D-04
358.00	0.40555700D-04
359.00	0.39726300D-04
360.00	0.38844600D-04
361.00	0.37913900D-04
362.00	0.36939400D-04
363.00	0.35926600D-04
364.00	0.34880400D-04
365.00	0.33807500D-04
366.00	0.32717000D-04
367.00	0.31621000D-04
368.00	0.30532400D-04
369.00	0.29461900D-04
370.00	0.28417300D-04
371.00	0.27402200D-04
372.00	0.26418000D-04
373.00	0.25463400D-04
374.00	0.24535900D-04
375.00	0.23632300D-04
376.00	0.22750800D-04
377.00	0.21893400D-04
378.00	0.21065900D-04
379.00	0.20276800D-04
380.00	0.19532800D-04
381.00	0.18836600D-04
382.00	0.18185700D-04
383.00	0.17574600D-04
384.00	0.16997000D-04
385.00	0.16449000D-04
386.00	0.15929200D-04
387.00	0.15438000D-04
388.00	0.14976600D-04
389.00	0.14546100D-04
390.00	0.14148000D-04
391.00	0.13785900D-04
392.00	0.13466000D-04
393.00	0.13197100D-04
394.00	0.12918700D-04
395.00	0.12849400D-04
396.00	0.12786100D-04
397.00	0.12804200D-04
398.00	0.12908100D-04
399.00	0.13101900D-04
400.00	0.13388500D-04
401.00	0.13768200D-04

402.00	0.142375000-04
403.00	0.147894000-04
404.00	0.154142000-04
405.00	0.161030000-04
406.00	0.168493000-04
407.00	0.176498000-04
408.00	0.185048000-04
409.00	0.194160000-04
410.00	0.203845000-04
411.00	0.214093000-04
412.00	0.224859000-04
413.00	0.236071000-04
414.00	0.247635000-04
415.00	0.259454000-04
416.00	0.271448000-04
417.00	0.283567000-04
418.00	0.295798000-04
419.00	0.308165000-04
420.00	0.320706000-04
421.00	0.333459000-04
422.00	0.346443000-04
423.00	0.359664000-04
424.03	0.238275000-04
425.00	0.978330000-05
426.00	0.100981000-04
427.00	0.104191000-04
428.00	0.107459000-04
429.00	0.110772000-04
430.00	0.114108000-04
431.00	0.117444000-04
432.00	0.120759000-04
433.00	0.124031000-04
434.00	0.127241000-04
435.00	0.130366000-04
436.00	0.133382000-04
437.00	0.136269000-04
438.00	0.139018000-04
439.00	0.141626000-04
440.00	0.144100000-04
441.00	0.146438000-04
442.00	0.148638000-04
443.00	0.150687000-04
444.00	0.152567000-04
445.00	0.154260000-04
446.00	0.155753000-04
447.00	0.157039000-04
448.00	0.158120000-04
449.00	0.159007000-04
450.00	0.159719000-04
451.00	0.160271000-04
452.00	0.160675000-04
453.00	0.160940000-04
454.00	0.161073000-04
455.00	0.161074000-04
456.00	0.160942000-04
457.00	0.160675000-04
458.00	0.160267000-04
459.00	0.159717000-04
460.00	0.159016000-04
461.00	0.158155000-04
462.00	0.157119000-04
463.00	0.155892000-04
464.00	0.154464000-04
465.00	0.152827000-04
466.00	0.150990000-04
467.00	0.148963000-04

468.00	0.14675700D-04
469.00	0.14438600D-04
470.00	0.14186300D-04
471.00	0.13920500D-04
472.00	0.13642900D-04
473.00	0.13354800D-04
474.00	0.13057700D-04
475.00	0.12752000D-04
476.00	0.12438000D-04
477.00	0.12116200D-04
478.00	0.11787900D-04
479.00	0.11455700D-04
480.00	0.11123000D-04
481.00	0.10793600D-04
482.00	0.10470200D-04
483.00	0.10154500D-04
484.00	0.98473000D-05
485.00	0.95487000D-05
486.00	0.92589000D-05
487.00	0.89779000D-05
488.00	0.87057000D-05
489.00	0.84420000D-05
490.00	0.81869000D-05
491.00	0.79399000D-05
492.00	0.77010000D-05
493.00	0.74703000D-05
494.00	0.72477000D-05
495.00	0.70335000D-05
496.00	0.68285000D-05
497.00	0.66343000D-05
498.00	0.64531000D-05
499.00	0.62871000D-05
500.00	0.61385000D-05
501.00	0.60088000D-05
502.00	0.58988000D-05
503.00	0.58093000D-05
504.00	0.57406000D-05
505.00	0.56929000D-05
506.00	0.56663000D-05
507.00	0.56612000D-05
508.00	0.56776000D-05
509.00	0.57171000D-05
510.00	0.57797000D-05
511.00	0.58668000D-05
512.00	0.59795000D-05
513.00	0.61184000D-05
514.00	0.62827000D-05
515.00	0.64712000D-05
516.00	0.66808000D-05
517.00	0.69082000D-05
518.00	0.71507000D-05
519.00	0.74063000D-05
520.00	0.76740000D-05
521.00	0.79528000D-05
522.00	0.82420000D-05
523.00	0.85401000D-05
524.00	0.88456000D-05
525.00	0.91578000D-05
526.00	0.94761000D-05
527.00	0.98013000D-05
528.00	0.10133800D-04
529.00	0.10473900D-04
530.00	0.10822100D-04
531.00	0.11177900D-04
532.00	0.11540800D-04
533.00	0.11909600D-04

ORIGINAL PAGE IS
OF POOR QUALITY

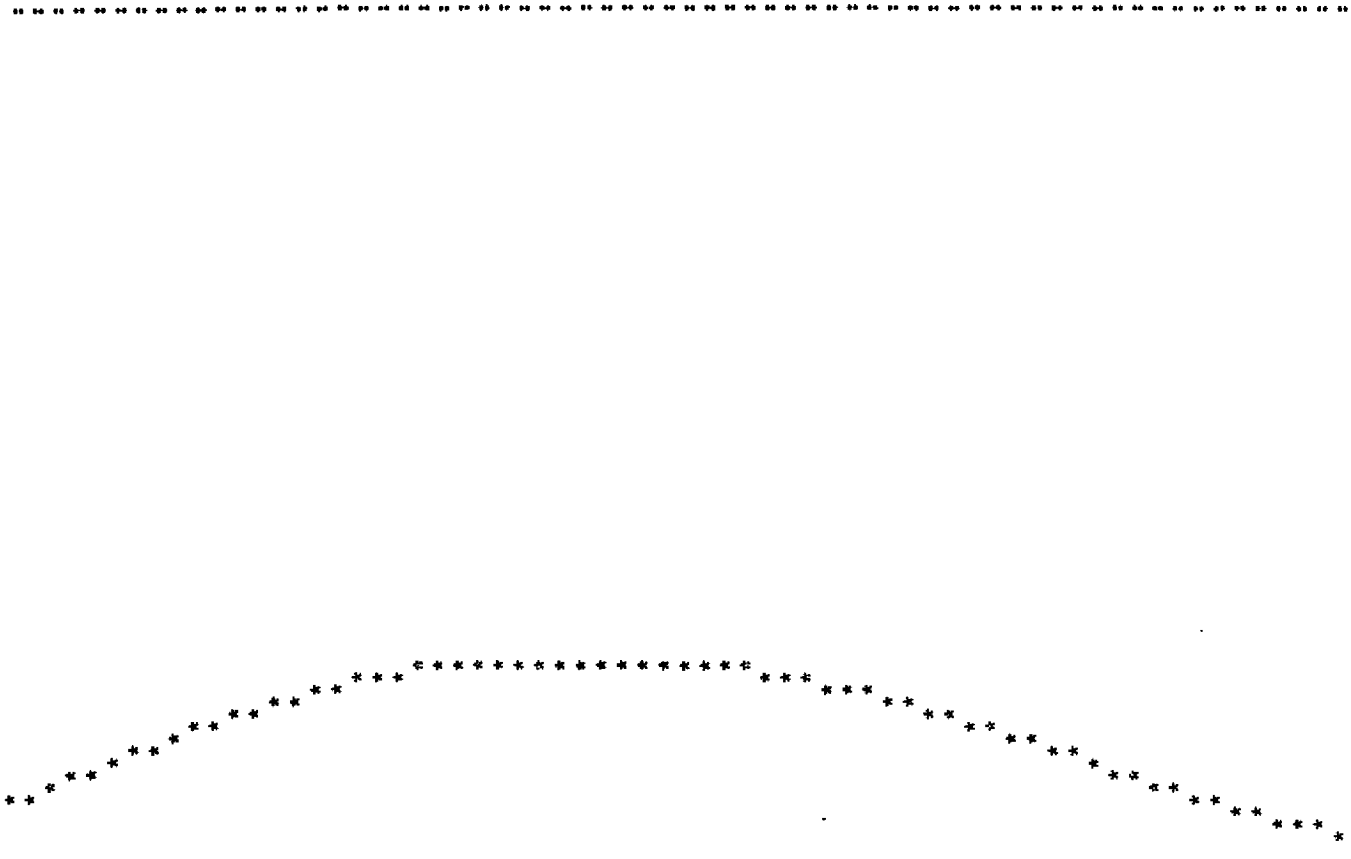

534.00	0.12282900D-04
535.00	0.12658700D-04
536.00	0.13035100D-04
537.00	0.13410600D-04
538.00	0.13784200D-04
539.00	0.14155200D-04
540.00	0.14523200D-04
541.00	0.14887600D-04
542.00	0.15247500D-04
543.00	0.15601200D-04
544.00	0.15947000D-04
545.00	0.16282500D-04
546.00	0.16605000D-04
547.00	0.16911600D-04
548.00	0.17199200D-04
549.00	0.17465200D-04
550.00	0.17708200D-04
551.00	0.17927800D-04
552.00	0.18124700D-04
553.00	0.18299900D-04
554.00	0.18454400D-04
555.00	0.18588300D-04
556.00	0.18701900D-04
557.00	0.18795400D-04
558.00	0.18869600D-04
559.00	0.18926000D-04
560.00	0.18966000D-04
561.00	0.18990800D-04
562.00	0.19000400D-04
563.00	0.18994700D-04
564.00	0.18972400D-04
565.00	0.18932300D-04
566.00	0.18873900D-04
567.00	0.18797100D-04
568.00	0.18702600D-04
569.00	0.18590900D-04
570.00	0.18463000D-04
571.00	0.18319200D-04
572.00	0.18160100D-04
573.00	0.17986100D-04
574.00	0.17797400D-04
575.00	0.17593600D-04
576.00	0.17373700D-04
577.00	0.17136500D-04
578.00	0.16881900D-04
579.00	0.16610500D-04
580.00	0.16323700D-04
581.00	0.16023700D-04
582.00	0.15712900D-04
583.00	0.15394200D-04
584.00	0.15070600D-04
585.00	0.14745300D-04
586.00	0.14420700D-04
587.00	0.14098800D-04
588.00	0.13780700D-04
589.00	0.13467200D-04
590.00	0.13159500D-04
591.00	0.12859300D-04
592.00	0.12567600D-04
593.00	0.12285600D-04
594.00	0.12013000D-04
595.00	0.11749400D-04
596.00	0.11493800D-04
597.00	0.11245600D-04
598.00	0.11005400D-04
599.00	0.10774200D-04

ORIGINAL PAGE IS
OF POOR QUALITY

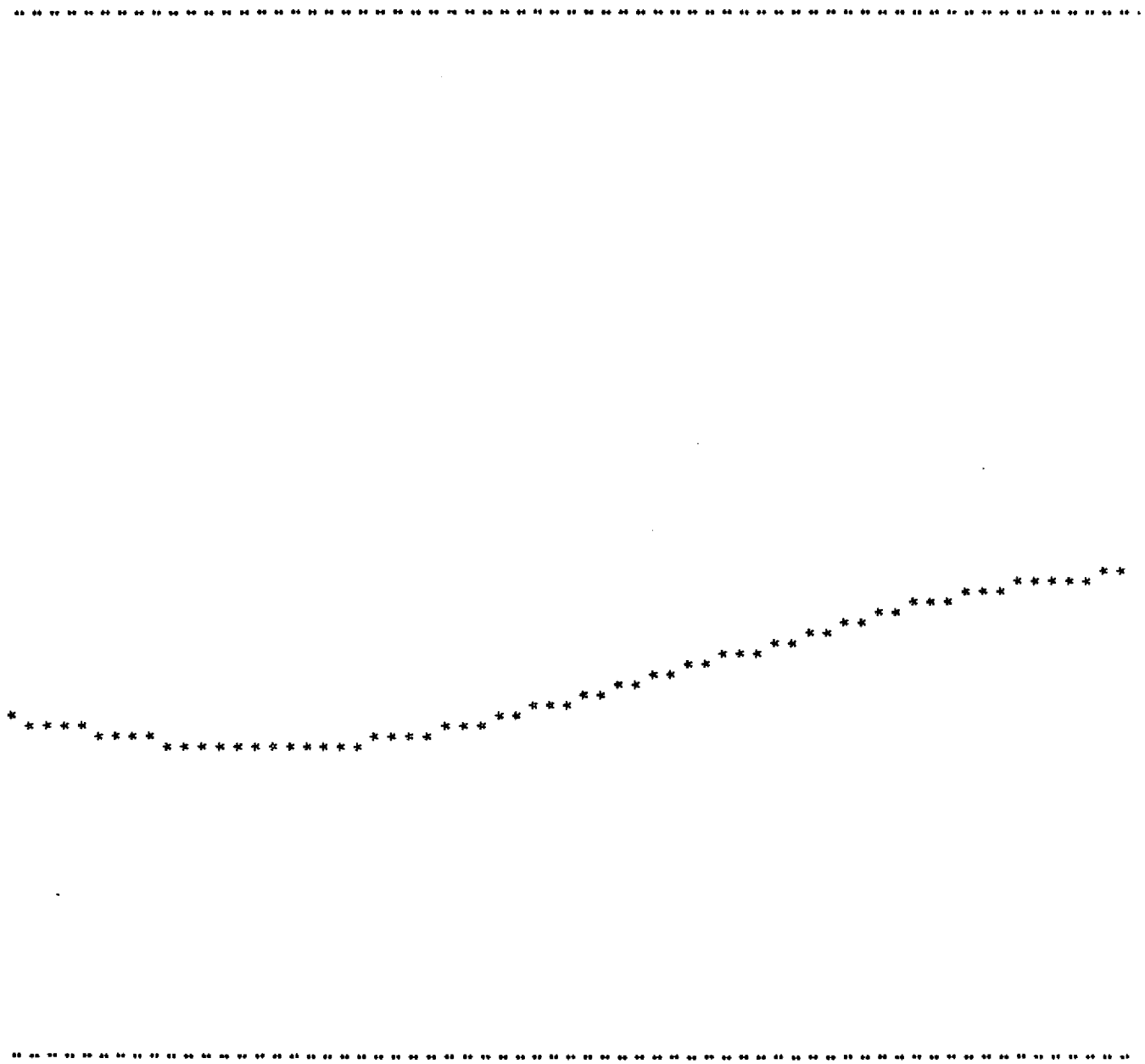

600.00	0.10553800D-04
601.00	0.10345700D-04
602.00	0.10150500D-04
603.00	0.99682000D-05
604.00	0.97983000D-05
605.00	0.96402000D-05
606.00	0.94935000D-05
607.00	0.93581000D-05
608.00	0.92342000D-05
609.00	0.91221000D-05
610.00	0.90229000D-05
611.00	0.89382000D-05
612.00	0.88702000D-05
613.00	0.88212000D-05
614.00	0.87936000D-05
615.00	0.87887000D-05
616.00	0.88073000D-05
617.00	0.88492000D-05
618.00	0.89137000D-05
619.00	0.89997000D-05
620.00	0.91059000D-05
621.00	0.92313000D-05
622.00	0.93746000D-05
623.00	0.95343000D-05
624.00	0.97090000D-05
625.00	0.98973000D-05
626.00	0.10097300D-04
627.00	0.10307400D-04
628.00	0.10526200D-04
629.00	0.10752500D-04
630.00	0.10985500D-04
631.00	0.11225200D-04
632.00	0.11472000D-04
633.00	0.11725900D-04
634.00	0.11985700D-04
635.00	0.12249800D-04
636.00	0.12515600D-04
637.00	0.12781200D-04
638.00	0.13045900D-04
639.00	0.13310000D-04
640.00	0.13574600D-04
641.00	0.13840500D-04
642.00	0.14108600D-04
643.00	0.14379200D-04
644.00	0.14652300D-04
645.00	0.14928300D-04
646.00	0.15206500D-04
647.00	0.15485600D-04
648.00	0.15763500D-04
649.00	0.16037600D-04
650.00	0.16304800D-04
651.00	0.16563200D-04
652.00	0.16810500D-04
653.00	0.17045400D-04
654.00	0.17266700D-04
655.00	0.17473400D-04
656.00	0.17664400D-04
657.00	0.17838700D-04
658.00	0.17995700D-04
659.00	0.18134500D-04
660.00	0.18255500D-04
661.00	0.18359200D-04
662.00	0.18446400D-04
663.00	0.18517700D-04
664.00	0.18573300D-04

```
 666.00  0.18637200D-04 :
 667.00  0.18644600D-04 :
 668.00  0.18635600D-04 :
 669.00  0.18610300D-04 :
 670.00  0.18569900D-04 :
 671.00  0.18516400D-04 :
 672.00  0.18452500D-04 :
 673.00  0.18380100D-04 :
 674.00  0.18300500D-04 :
 675.00  0.18213500D-04 :
 676.00  0.18118000D-04 :
 677.00  0.18012800D-04 :
 678.00  0.17896500D-04 :
 679.00  0.17768200D-04 :
 680.00  0.17626900D-04 :
 681.00  0.17472100D-04 :
 682.00  0.17303000D-04 :
 683.00  0.17119300D-04 :
 684.00  0.16921400D-04 :
 685.00  0.16710500D-04 :
 686.00  0.16488100D-04 :
 687.00  0.16256400D-04 :
 688.00  0.16016600D-04 :
 689.00  0.15769700D-04 :
 690.00  0.15516900D-04 :
 691.00  0.15259600D-04 :
 692.00  0.14999800D-04 :
 693.00  0.14739900D-04 :
 694.00  0.14481900D-04 :
 695.00  0.14226900D-04 :
 696.00  0.13975700D-04 :
 697.00  0.13728600D-04 :
 698.00  0.13486500D-04 :
 699.00  0.13250500D-04 :
```

Figure D-2. A plot similar to D-1, except that here we plot the acceleration component tangent to the tether. We are also able to plot the full span of the simulation, including the initial unperturbed state and during the encounter with the atmospheric enhancement from t = 10 to t = 16 seconds. The accelerations produced in this direction are several orders of magnitude greater than those in the orthogonal direction, and the maximum accelerations are comparable to the acceleration produced directly by the perturbing drag (0.084 gal).

ALONG-TETHER ACCELERATION

MIN, MAX: -0.8636856000D-01 0.9640561000D-01

0.00	0.00000000D+00	:
1.00	0.00000000D+00	:
2.00	0.00000000D+00	:
3.00	0.00000000D+00	:
4.00	0.00000000D+00	:
5.00	0.00000000D+00	:
6.00	0.00000000D+00	:
7.00	0.00000000D+00	:
8.00	0.00000000D+00	:
9.00	0.00000000D+00	:
10.00	0.00000000D+00	:
11.00	0.29310300D-02	:
12.00	0.49946400D-02	:
13.00	0.10199520D-01	:
14.00	0.16616680D-01	:
15.00	0.22660300D-01	:
16.00	0.23828530D-01	:
17.00	0.23976360D-01	:
18.00	0.22261060D-01	:
19.00	0.20511640D-01	:
20.00	0.19330600D-01	:
21.00	0.18410500D-01	:
22.00	0.17349990D-01	:
23.00	0.16127630D-01	:
24.00	0.14971180D-01	:
25.00	0.14008000D-01	:
26.00	0.13141850D-01	:
27.00	0.12228650D-01	:
28.00	0.11257280D-01	:
29.00	0.10332340D-01	:
30.00	0.95132200D-02	:
31.00	0.87574200D-02	:
32.00	0.79899000D-02	:
33.00	0.72081100D-02	:
34.00	0.64878600D-02	:
35.00	0.59048200D-02	:
36.00	0.55119100D-02	:
37.00	0.54137600D-02	:
38.00	0.58614600D-02	:
39.00	0.72672100D-02	:
40.00	0.10091100D-01	:
41.00	0.14678290D-01	:
42.00	0.21068170D-01	:
43.00	0.28825420D-01	:
44.00	0.36881540D-01	:
45.00	0.43585190D-01	:
46.00	0.47067980D-01	:
47.00	0.45967140D-01	:
48.00	0.40150200D-01	:
49.00	0.31055360D-01	:
50.00	0.21247840D-01	:
51.00	0.13359260D-01	:
52.00	0.88674100D-02	:
53.00	0.74522500D-02	:
54.00	0.73139000D-02	:
55.00	0.63465700D-02	:

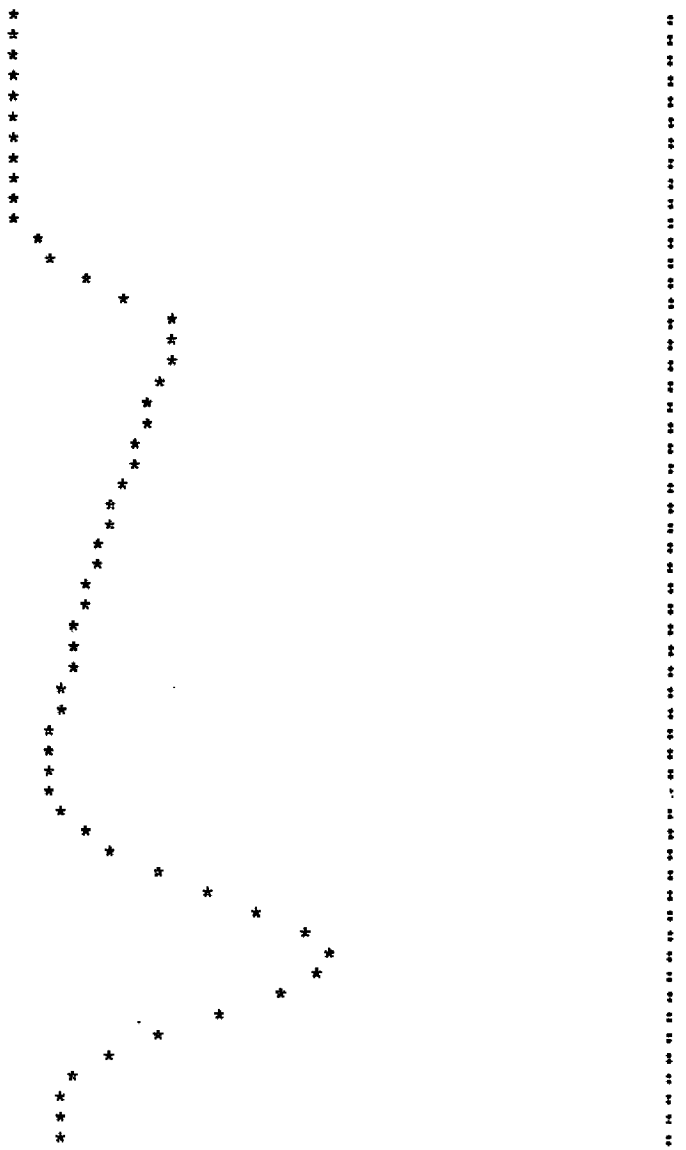

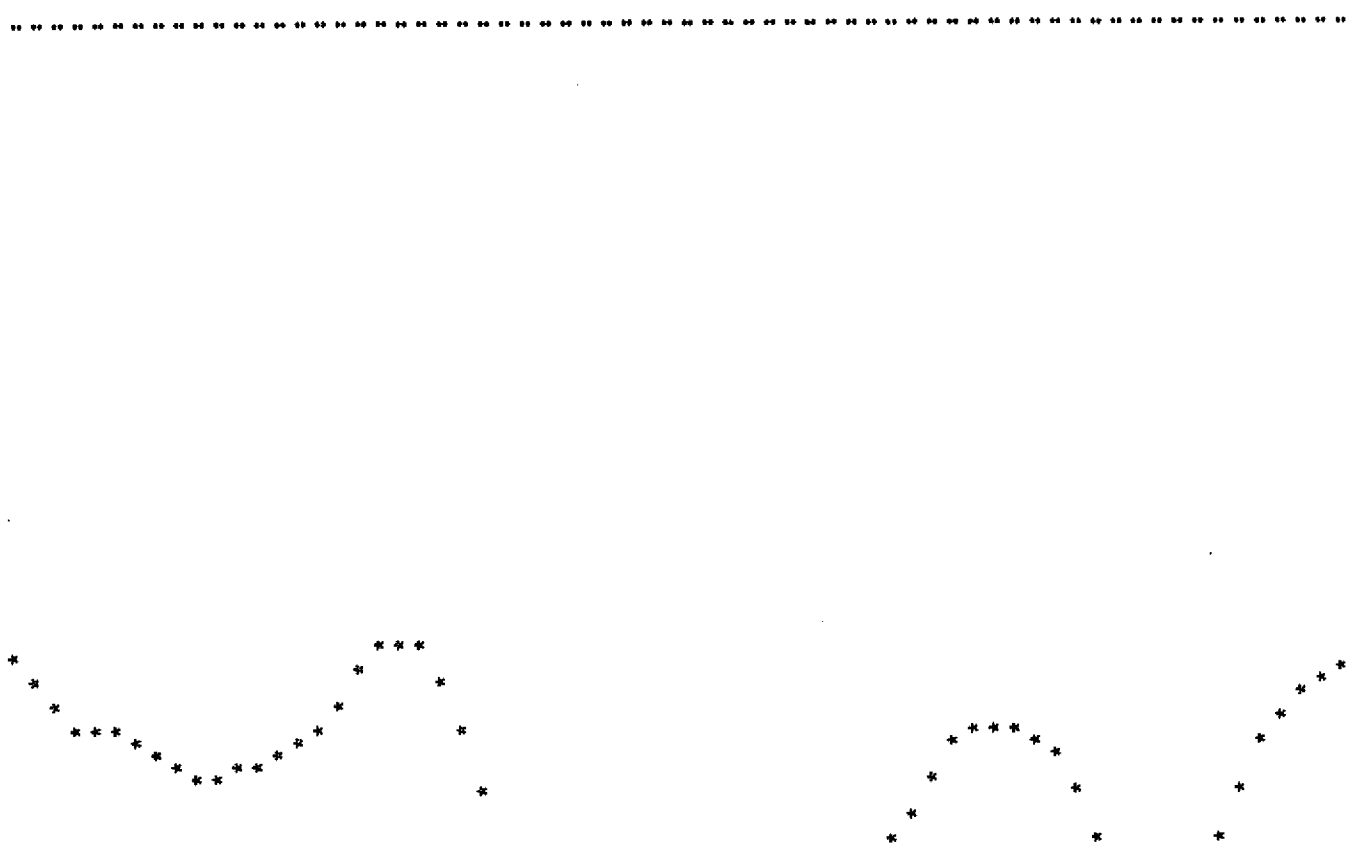

56.00	0.344530000D-02
57.00	-0.894580000D-03
58.00	-0.509341000D-02
59.00	-0.773403000D-02
60.00	-0.859868000D-02
61.00	-0.871879000D-02
62.00	-0.943068000D-02
63.00	-0.112562100D-01
64.00	-0.133347800D-01
65.00	-0.150746300D-01
66.00	-0.153781500D-01
67.00	-0.141373700D-01
68.00	-0.127621500D-01
69.00	-0.115066400D-01
70.00	-0.998858000D-02
71.00	-0.742784000D-02
72.00	-0.352673000D-02
73.00	0.967410000D-03
74.00	0.457346000D-02
75.00	0.587844000D-02
76.00	0.416350000D-02
77.00	-0.571850000D-03
78.00	-0.796383000D-02
79.00	-0.174204700D-01
80.00	-0.279090400D-01
81.00	-0.377365700D-01
82.00	-0.448894200D-01
83.00	-0.475491900D-01
84.00	-0.470141900D-01
85.00	-0.437834800D-01
86.00	-0.406711600D-01
87.00	-0.394707100D-01
88.00	-0.405216800D-01
89.00	-0.427850700D-01
90.00	-0.446462300D-01
91.00	-0.448154000D-01
92.00	-0.428779800D-01
93.00	-0.393849700D-01
94.00	-0.355396100D-01
95.00	-0.325618200D-01
96.00	-0.309626100D-01
97.00	-0.301276600D-01
98.00	-0.286422200D-01
99.00	-0.252599100D-01
100.00	-0.200970000D-01
101.00	-0.143784600D-01
102.00	-0.991268000D-02
103.00	-0.766770000D-02
104.00	-0.732780000D-02
105.00	-0.798767000D-02
106.00	-0.928503000D-02
107.00	-0.118736200D-01
108.00	-0.167066400D-01
109.00	-0.238180600D-01
110.00	-0.317037400D-01
111.00	-0.379236500D-01
112.00	-0.403942700D-01
113.00	-0.384203400D-01
114.00	-0.328116300D-01
115.00	-0.252306400D-01
116.00	-0.173919500D-01
117.00	-0.105752900D-01
118.00	-0.549069000D-02
119.00	-0.228848000D-02
120.00	-0.571350000D-03
121.00	0.552280000D-03

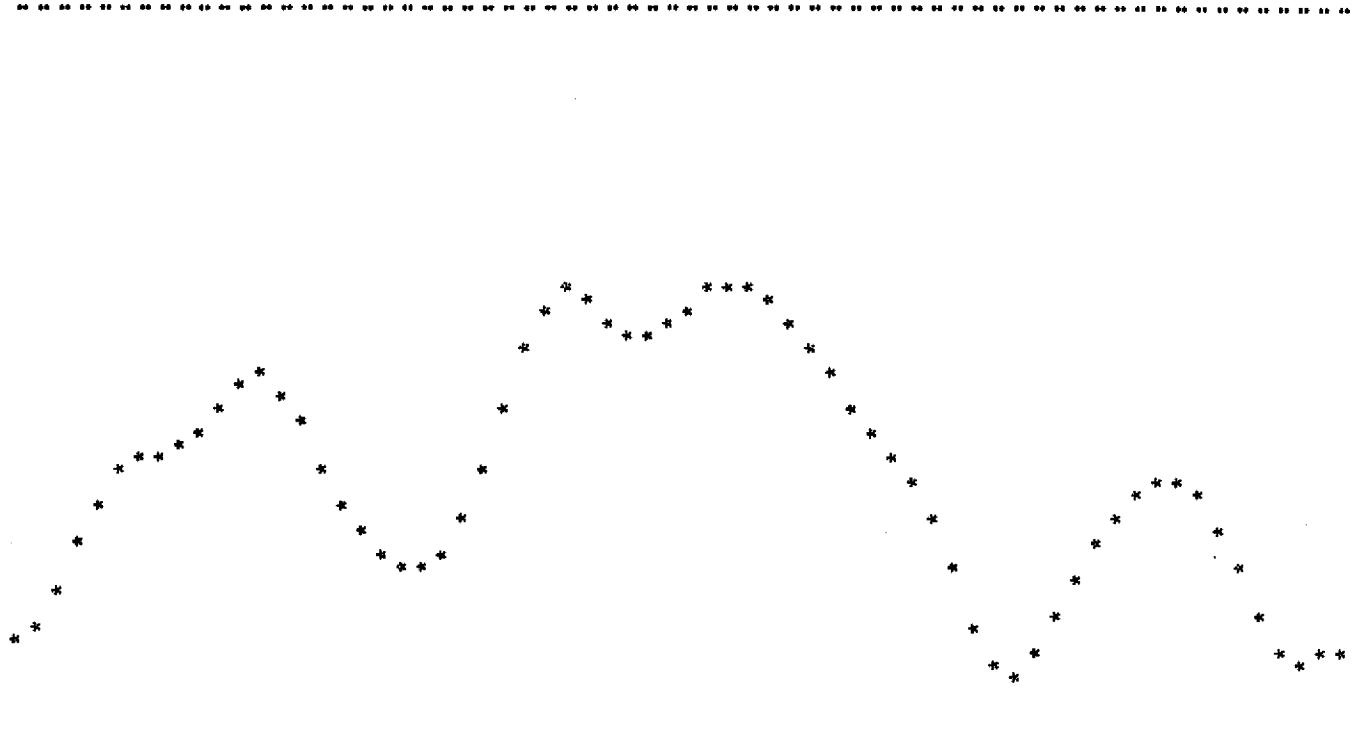

122.00	0.22543400D-02
123.00	0.55641400D-02
124.00	0.10847280D-01
125.00	0.17462570D-01
126.00	0.23915570D-01
127.00	0.28619830D-01
128.00	0.30889790D-01
129.00	0.31506170D-01
130.00	0.32244650D-01
131.00	0.35556470D-01
132.00	0.38356330D-01
133.00	0.41930750D-01
134.00	0.43115480D-01
135.00	0.40820770D-01
136.00	0.35683290D-01
137.00	0.29454180D-01
138.00	0.23764830D-01
139.00	0.19363260D-01
140.00	0.16289570D-01
141.00	0.14558190D-01
142.00	0.14571010D-01
143.00	0.16959570D-01
144.00	0.22078060D-01
145.00	0.29611080D-01
146.00	0.38474660D-01
147.00	0.46976980D-01
148.00	0.53238620D-01
149.00	0.55899720D-01
150.00	0.54902680D-01
151.00	0.51770240D-01
152.00	0.48974100D-01
153.00	0.48457060D-01
154.00	0.50543940D-01
155.00	0.53875340D-01
156.00	0.56535350D-01
157.00	0.57353890D-01
158.00	0.56351850D-01
159.00	0.54171450D-01
160.00	0.51260540D-01
161.00	0.47665450D-01
162.00	0.43467570D-01
163.00	0.39145510D-01
164.00	0.35267340D-01
165.00	0.31764630D-01
166.00	0.27657590D-01
167.00	0.23772790D-01
168.00	0.13973380D-01
169.00	0.58225400D-02
170.00	-0.11062000D-03
171.00	-0.17912300D-02
172.00	0.97845000D-03
173.00	0.65524700D-02
174.00	0.12648490D-01
175.00	0.17729690D-01
176.00	0.21521170D-01
177.00	0.24424610D-01
178.00	0.26523120D-01
179.00	0.27110210D-01
180.00	0.25155440D-01
181.00	0.20261280D-01
182.00	0.13337750D-01
183.00	0.63946800D-02
184.00	0.15390300D-02
185.00	-0.19566000D-03
186.00	0.54554000D-03
187.00	0.17643500D-02

188.00	0.12038200D-02
189.00	-0.24284700D-02
190.00	-0.88182700D-02
191.00	-0.16358150D-01
192.00	-0.23178230D-01
193.00	-0.28200010D-01
194.00	-0.31542680D-01
195.00	-0.34121150D-01
196.00	-0.36847760D-01
197.00	-0.40041910D-01
198.00	-0.43340560D-01
199.00	-0.45992500D-01
200.00	-0.47151250D-01
201.00	-0.46081780D-01
202.00	-0.42342070D-01
203.00	-0.36030780D-01
204.00	-0.27986130D-01
205.00	-0.19709490D-01
206.00	-0.12940660D-01
207.00	-0.90840400D-02
208.00	-0.87512700D-02
209.00	-0.11591490D-01
210.00	-0.16435940D-01
211.00	-0.21731350D-01
212.00	-0.26168380D-01
213.00	-0.29212340D-01
214.00	-0.31152680D-01
215.00	-0.32523300D-01
216.00	-0.33374070D-01
217.00	-0.33148580D-01
218.00	-0.31463320D-01
219.00	-0.29081540D-01
220.00	-0.27947100D-01
221.00	-0.29853210D-01
222.00	-0.34735460D-01
223.00	-0.40210980D-01
224.00	-0.43056180D-01
225.00	-0.41528770D-01
226.00	-0.36550390D-01
227.00	-0.30784710D-01
228.00	-0.26454210D-01
229.00	-0.23792680D-01
230.00	-0.21280200D-01
231.00	-0.17119820D-01
232.00	-0.10542660D-01
233.00	-0.20363100D-02
234.00	0.71947000D-02
235.00	0.15785400D-01
236.00	0.22411890D-01
237.00	0.25934890D-01
238.00	0.25772290D-01
239.00	0.22302010D-01
240.00	0.16822250D-01
241.00	0.10993260D-01
242.00	0.61874500D-02
243.00	0.32116700D-02
244.00	0.24068700D-02
245.00	0.37325800D-02
246.00	0.66818400D-02
247.00	0.10235080D-01
248.00	0.13230650D-01
249.00	0.14974550D-01
250.00	0.15574090D-01
251.00	0.15626470D-01
252.00	0.15600850D-01
253.00	0.15569740D-01

ORIGINAL PAGE IS
OF POOR QUALITY

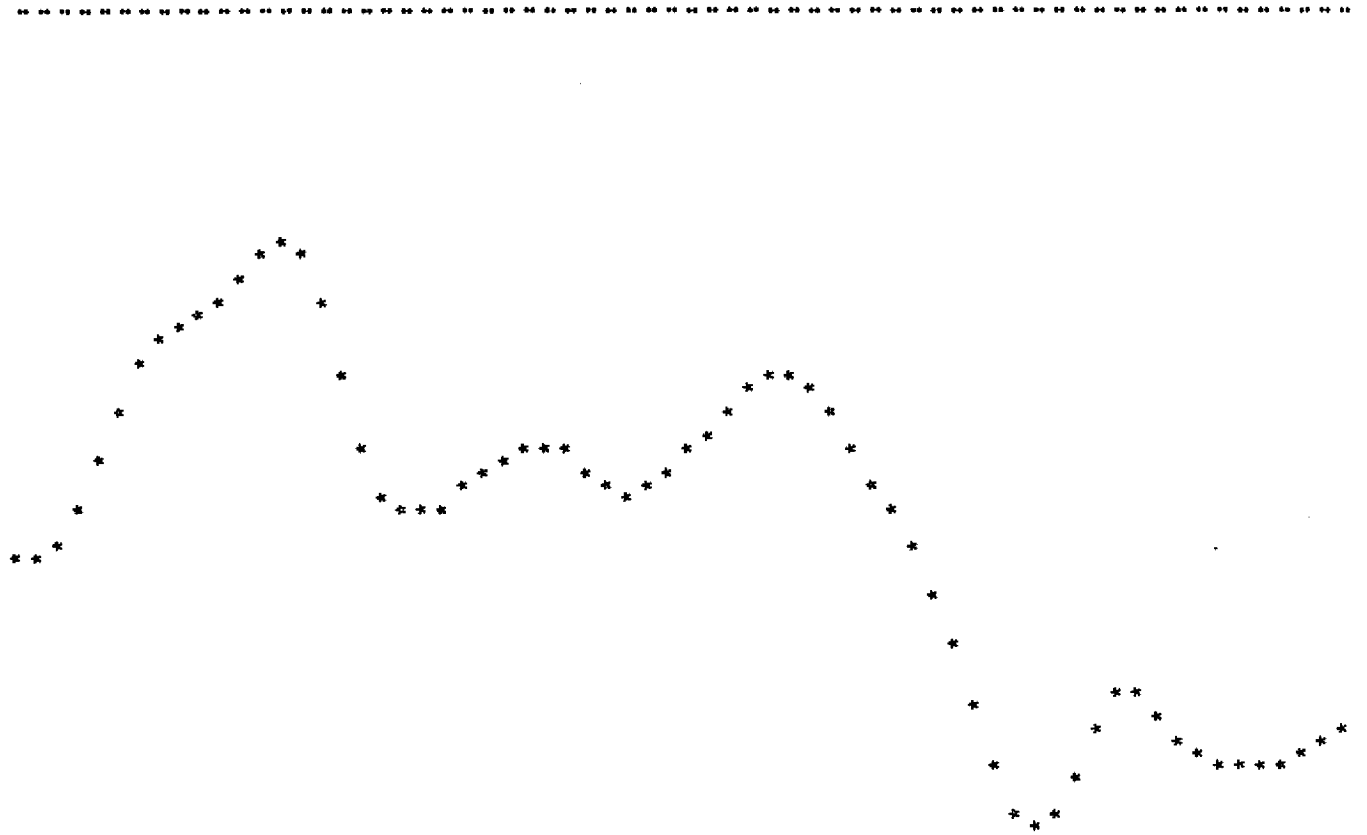

254.00	0.155734200-01
255.00	0.161657000-01
256.00	0.184195200-01
257.00	0.232013700-01
258.00	0.303001900-01
259.00	0.382421100-01
260.00	0.450570900-01
261.00	0.494658000-01
262.00	0.516470300-01
263.00	0.530307300-01
264.00	0.552379100-01
265.00	0.588336800-01
266.00	0.626849200-01
267.00	0.646108200-01
268.00	0.617897200-01
269.00	0.543005800-01
270.00	0.437346000-01
271.00	0.333357500-01
272.00	0.259926200-01
273.00	0.227635000-01
274.00	0.227634100-01
275.00	0.243292700-01
276.00	0.263282200-01
277.00	0.285151700-01
278.00	0.308765500-01
279.00	0.328708200-01
280.00	0.335085900-01
281.00	0.322103300-01
282.00	0.295405400-01
283.00	0.269942100-01
284.00	0.259811400-01
285.00	0.269116200-01
286.00	0.291960200-01
287.00	0.320145400-01
288.00	0.349739300-01
289.00	0.380795200-01
290.00	0.411429400-01
291.00	0.433825900-01
292.00	0.437460000-01
293.00	0.416822100-01
294.00	0.376011800-01
295.00	0.326003200-01
296.00	0.276476200-01
297.00	0.229253000-01
298.00	0.178027700-01
299.00	0.113871100-01
300.00	0.323242000-02
301.00	-0.619604000-02
302.00	-0.154269900-01
303.00	-0.223369300-01
304.00	-0.249653500-01
305.00	-0.225791900-01
306.00	-0.164236500-01
307.00	-0.944555000-02
308.00	-0.486174000-02
309.00	-0.435209000-02
310.00	-0.718989000-02
311.00	-0.110156900-01
312.00	-0.136648100-01
313.00	-0.145404900-01
314.00	-0.144792700-01
315.00	-0.144693600-01
316.00	-0.145336600-01
317.00	-0.138366700-01
318.00	-0.118010900-01
319.00	-0.902031000-02

C-2

ORIGINAL PAGE IS
OF POOR QUALITY

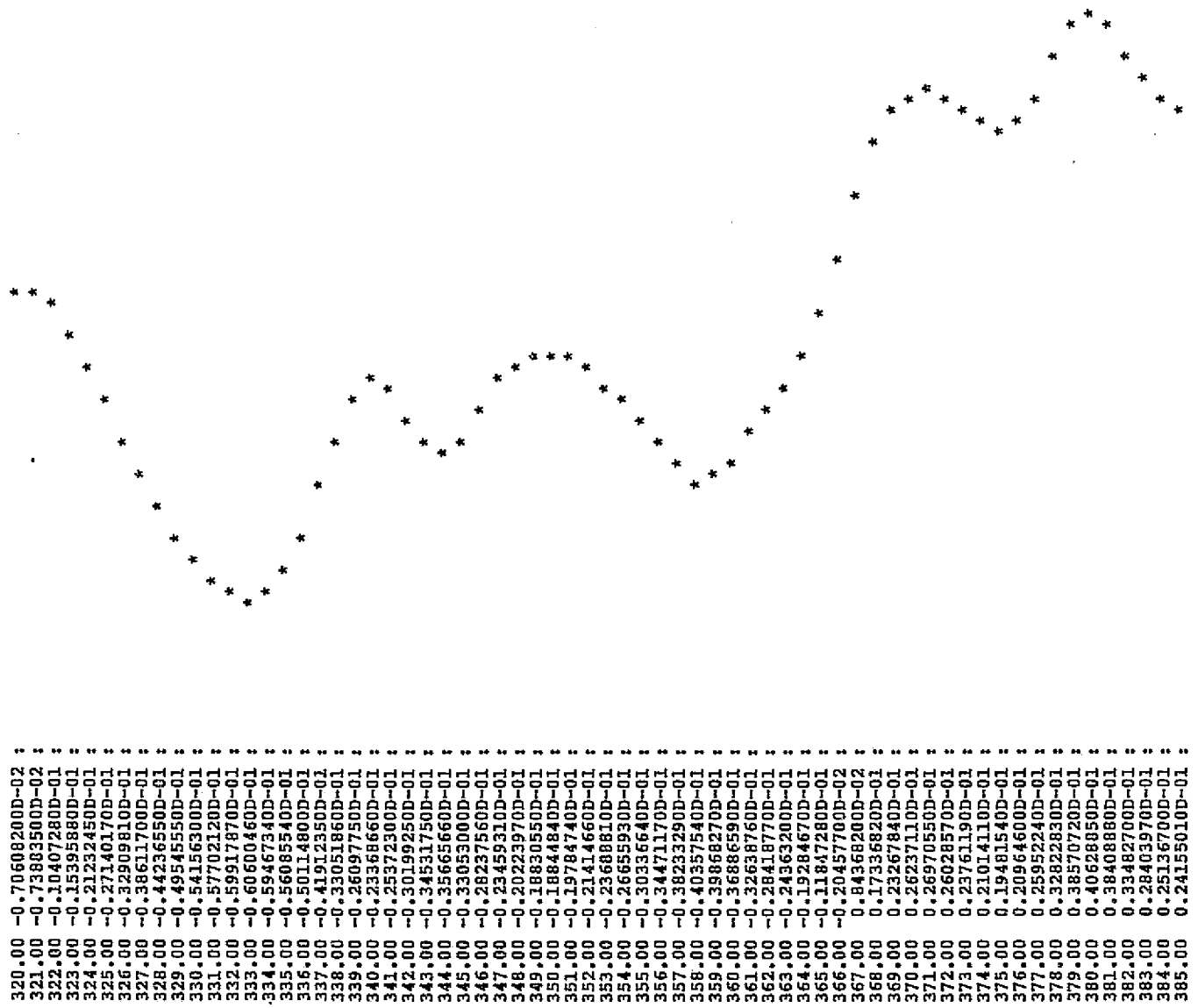

320.00	-0.706082000D-02
321.00	-0.738835000D-02
322.00	-0.104072800D-01
323.00	-0.153958800D-01
324.00	-0.212324500D-01
325.00	-0.271401700D-01
326.00	-0.329098100D-01
327.00	-0.386117000D-01
328.00	-0.442365500D-01
329.00	-0.495455500D-01
330.00	-0.541563000D-01
331.00	-0.577021200D-01
332.00	-0.599178700D-01
333.00	-0.606004600D-01
334.00	-0.594673400D-01
335.00	-0.560855400D-01
336.00	-0.501148000D-01
337.00	-0.419123500D-01
338.00	-0.330518600D-01
339.00	-0.260977500D-01
340.00	-0.233686600D-01
341.00	-0.253723000D-01
342.00	-0.301992500D-01
343.00	-0.345317500D-01
344.00	-0.356656600D-01
345.00	-0.330530000D-01
346.00	-0.282375600D-01
347.00	-0.234593100D-01
348.00	-0.202239700D-01
349.00	-0.188305500D-01
350.00	-0.188448400D-01
351.00	-0.197847400D-01
352.00	-0.214146600D-01
353.00	-0.236888100D-01
354.00	-0.266559300D-01
355.00	-0.303366400D-01
356.00	-0.344711700D-01
357.00	-0.382332900D-01
358.00	-0.403575400D-01
359.00	-0.398682700D-01
360.00	-0.368865900D-01
361.00	-0.326387600D-01
362.00	-0.284187700D-01
363.00	-0.243632000D-01
364.00	-0.192846700D-01
365.00	-0.118472800D-01
366.00	-0.204577000D-02
367.00	0.843682000D-02
368.00	0.173368200D-01
369.00	0.232678400D-01
370.00	0.262371100D-01
371.00	0.269705500D-01
372.00	0.260285700D-01
373.00	0.237611900D-01
374.00	0.210141100D-01
375.00	0.194815400D-01
376.00	0.209646000D-01
377.00	0.259522400D-01
378.00	0.328228300D-01
379.00	0.385707200D-01
380.00	0.406280500D-01
381.00	0.384088800D-01
382.00	0.334827000D-01
383.00	0.284039700D-01
384.00	0.251367000D-01
385.00	0.241550100D-01

ORIGINAL PAGE IS
OF POOR QUALITY

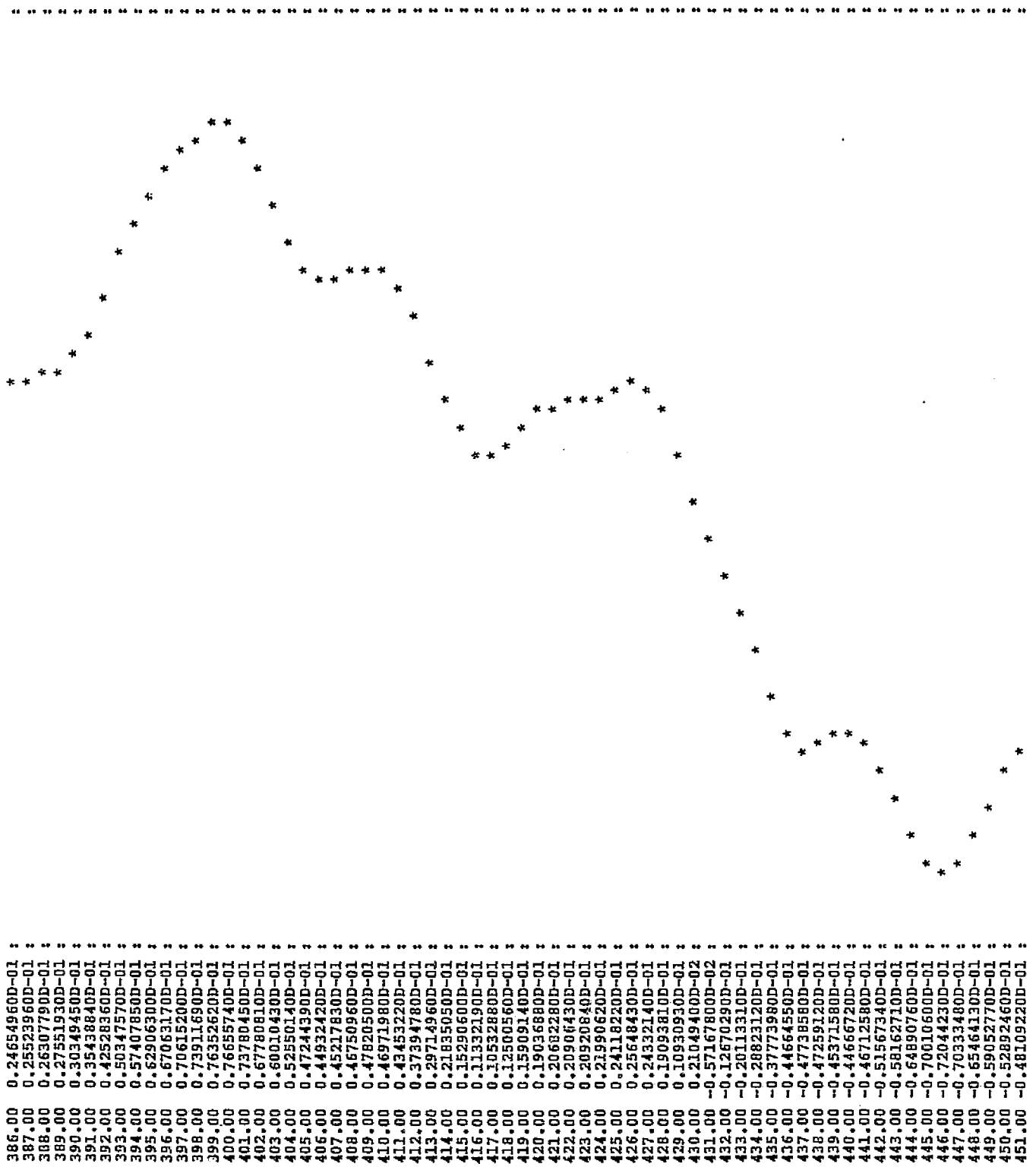

386.00	0.2465496D-01
387.00	0.2552396D-01
388.00	0.2630779D-01
389.00	0.2755193D-01
390.00	0.3034945D-01
391.00	0.3543884D-01
392.00	0.4252836D-01
393.00	0.5034757D-01
394.00	0.5740785D-01
395.00	0.6290630D-01
396.00	0.6706317D-01
397.00	0.7061520D-01
398.00	0.7391169D-01
399.00	0.7635262D-01
400.00	0.7665574D-01
401.00	0.7378045D-01
402.00	0.6778081D-01
403.00	0.6001043D-01
404.00	0.5255014D-01
405.00	0.4724439D-01
406.00	0.4493242D-01
407.00	0.4521783D-01
408.00	0.4675096D-01
409.00	0.4782050D-01
410.00	0.4697198D-01
411.00	0.4345322D-01
412.00	0.3739478D-01
413.00	0.2971496D-01
414.00	0.2183505D-01
415.00	0.1529060D-01
416.00	0.1133219D-01
417.00	0.1053288D-01
418.00	0.1250056D-01
419.00	0.1590914D-01
420.00	0.1903688D-01
421.00	0.2068228D-01
422.00	0.2090643D-01
423.00	0.2092084D-01
424.00	0.2199062D-01
425.00	0.2411822D-01
426.00	0.2564843D-01
427.00	0.2433214D-01
428.00	0.1909381D-01
429.00	0.1093093D-01
430.00	0.2104940D-02
431.00	-0.5716780D-02
432.00	-0.1267029D-01
433.00	-0.2011331D-01
434.00	-0.2882312D-01
435.00	-0.3777398D-01
436.00	-0.4466455D-01
437.00	-0.4773858D-01
438.00	-0.4725912D-01
439.00	-0.4537158D-01
440.00	-0.4466672D-01
441.00	-0.4671258D-01
442.00	-0.5156734D-01
443.00	-0.5816271D-01
444.00	-0.6489076D-01
445.00	-0.7001060D-01
446.00	-0.7204423D-01
447.00	-0.7033348D-01
448.00	-0.6546413D-01
449.00	-0.5905277D-01
450.00	-0.5289246D-01
451.00	-0.4810922D-01

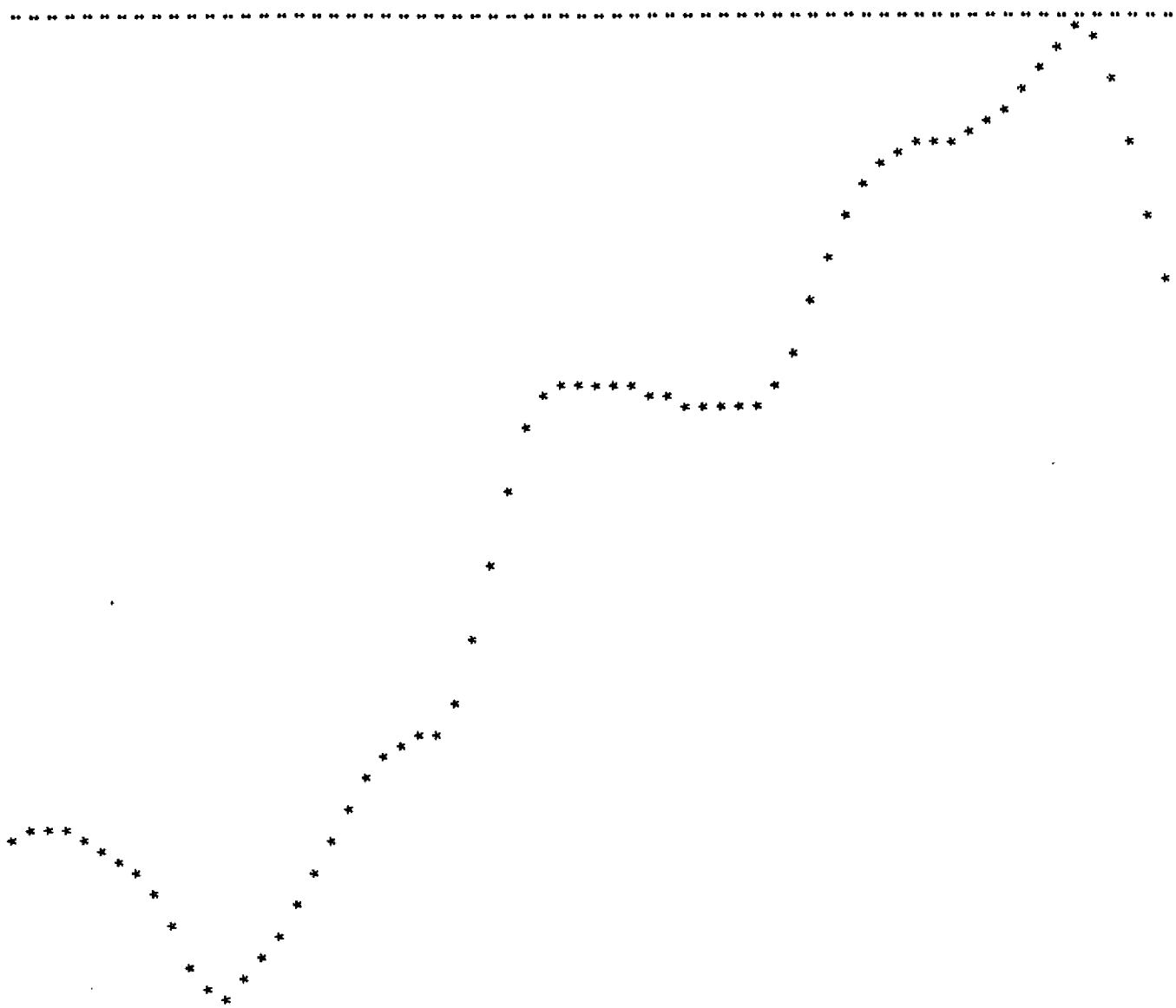

452.00	-0.44965520D-01
453.00	-0.43280670D-01
454.00	-0.42859420D-01
455.00	-0.43478990D-01
456.00	-0.44715720D-01
457.00	-0.46103850D-01
458.00	-0.47648220D-01
459.00	-0.50063850D-01
460.00	-0.54215000D-01
461.00	-0.60073470D-01
462.00	-0.66230510D-01
463.00	-0.70578120D-01
464.00	-0.71646490D-01
465.00	-0.69500730D-01
466.00	-0.65422970D-01
467.00	-0.60767410D-01
468.00	-0.56056190D-01
469.00	-0.50989330D-01
470.00	-0.45188730D-01
471.00	-0.38930480D-01
472.00	-0.33248520D-01
473.00	-0.29339260D-01
474.00	-0.27636400D-01
475.00	-0.27142590D-01
476.00	-0.25561620D-01
477.00	-0.20382170D-01
478.00	-0.10484030D-01
479.00	0.28325300D-02
480.00	0.16312450D-01
481.00	0.26596630D-01
482.00	0.32188090D-01
483.00	0.34003470D-01
484.00	0.34190330D-01
485.00	0.34332810D-01
486.00	0.34605350D-01
487.00	0.34381700D-01
488.00	0.33396820D-01
489.00	0.32159150D-01
490.00	0.31332170D-01
491.00	0.31012550D-01
492.00	0.30803290D-01
493.00	0.30643850D-01
494.00	0.31406720D-01
495.00	0.34448930D-01
496.00	0.40456630D-01
497.00	0.48712500D-01
498.00	0.57429850D-01
499.00	0.64860300D-01
500.00	0.70171910D-01
501.00	0.73508460D-01
502.00	0.75452290D-01
503.00	0.76537820D-01
504.00	0.77718220D-01
505.00	0.77748330D-01
506.00	0.78676220D-01
507.00	0.80283620D-01
508.00	0.82759080D-01
509.00	0.86156030D-01
510.00	0.90259930D-01
511.00	0.94234020D-01
512.00	0.96405610D-01
513.00	0.94735140D-01
514.00	0.86005400D-01
515.00	0.76985640D-01
516.00	0.64478440D-01
517.00	0.53870659D-01

ORIGINAL PAGE IS
OF POOR QUALITY

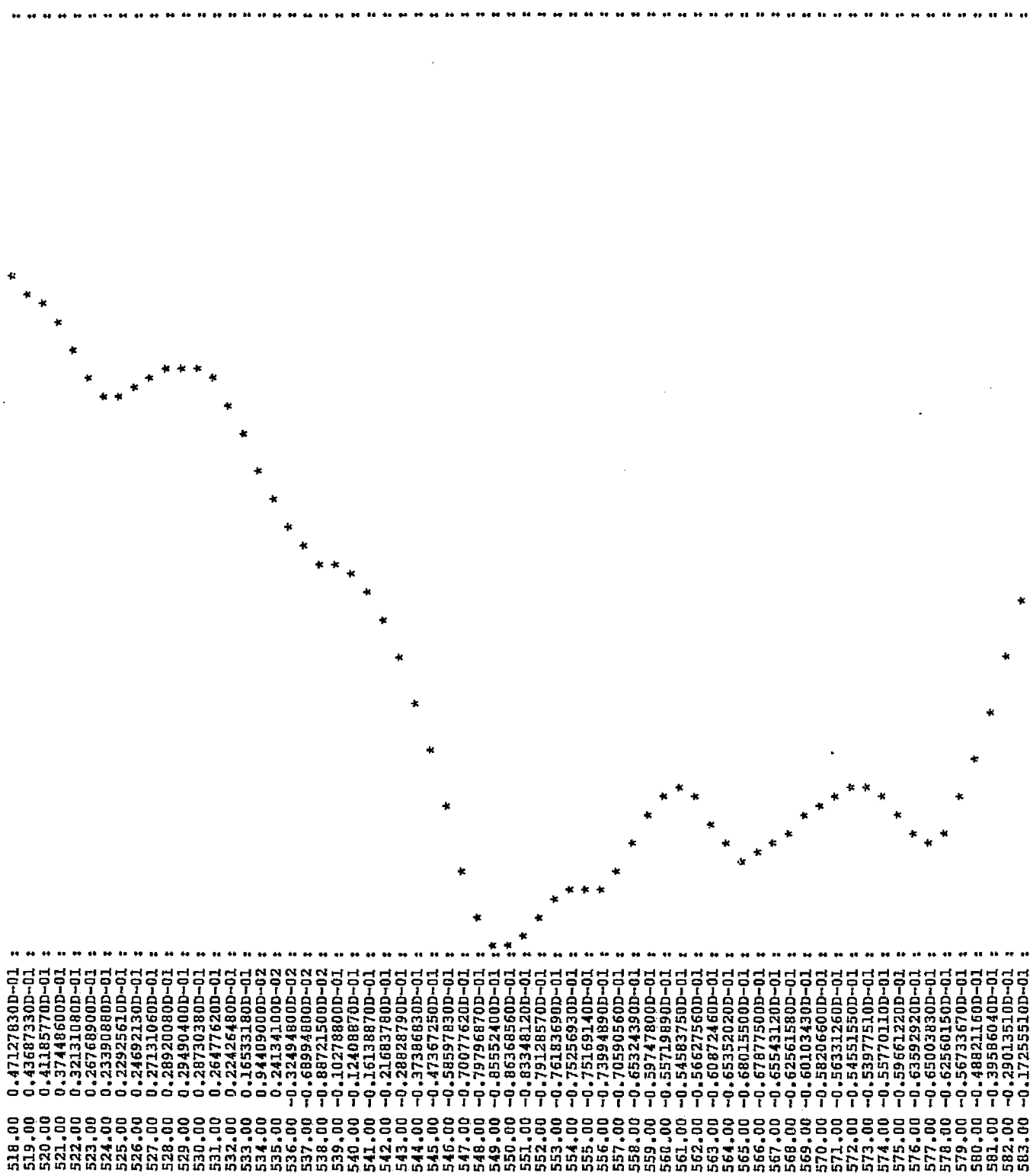

518.00	0.47127830D-01
519.00	0.43687330D-01
520.00	0.41185770D-01
521.00	0.37448600D-01
522.00	0.32131080D-01
523.00	0.26768900D-01
524.00	0.23390880D-01
525.00	0.22925610D-01
526.00	0.24692130D-01
527.00	0.27131060D-01
528.00	0.28920080D-01
529.00	0.29490400D-01
530.00	0.28730380D-01
531.00	0.26477620D-01
532.00	0.22426480D-01
533.00	0.16533180D-01
534.00	0.94409000D-02
535.00	0.24134100D-02
536.00	-0.32494800D-02
537.00	-0.68994800D-02
538.00	-0.88721500D-02
539.00	-0.10278800D-01
540.00	-0.12408870D-01
541.00	-0.16138870D-01
542.00	-0.21683780D-01
543.00	-0.28828790D-01
544.00	-0.37386830D-01
545.00	-0.47367250D-01
546.00	-0.58597830D-01
547.00	-0.70077620D-01
548.00	-0.79796870D-01
549.00	-0.85552400D-01
550.00	-0.86368560D-01
551.00	-0.83348120D-01
552.00	-0.79128570D-01
553.00	-0.75183690D-01
554.00	-0.72569300-01
555.00	-0.71691400-01
556.00	-0.73994890D-01
557.00	-0.70590560D-01
558.00	-0.65324390D-01
559.00	-0.59747800D-01
560.00	-0.55719890D-01
561.00	-0.54583750D-01
562.00	-0.56627560D-01
563.00	-0.60872460D-01
564.00	-0.65352020D-01
565.00	-0.68015500D-01
566.00	-0.67877500D-01
567.00	-0.65543120D-01
568.00	-0.62561580D-01
569.00	-0.60103430D-01
570.00	-0.58206600D-01
571.00	-0.56331260D-01
572.00	-0.54551550D-01
573.00	-0.53977510D-01
574.00	-0.55770110D-01
575.00	-0.59661220D-01
576.00	-0.63592920D-01
577.00	-0.65003830D-01
578.00	-0.62560150D-01
579.00	-0.56733670D-01
580.00	-0.48821160D-01
581.00	-0.39586040D-01
582.00	-0.29013510D-01
583.00	-0.17255510D-01

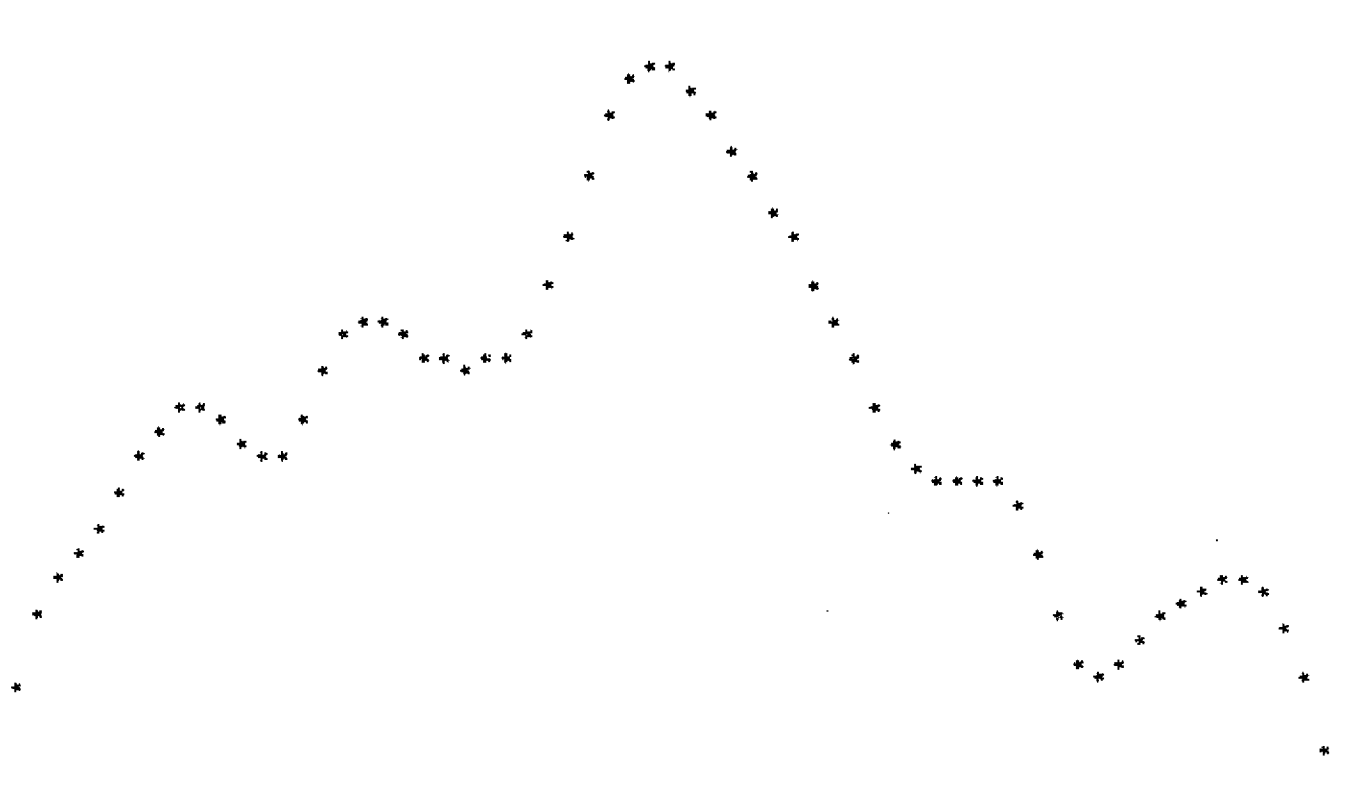

584.00	-0.55211000D-02
585.00	0.42772400D-02
586.00	0.10921420D-01
587.00	0.14940920D-01
588.00	0.18239310D-01
589.00	0.22570050D-01
590.00	0.28162160D-01
591.00	0.33599460D-01
592.00	0.36893820D-01
593.00	0.36887160D-01
594.00	0.34065860D-01
595.00	0.30403670D-01
596.00	0.28402320D-01
597.00	0.29812160D-01
598.00	0.34659540D-01
599.00	0.41167340D-01
600.00	0.46741340D-01
601.00	0.49460170D-01
602.00	0.49087000D-01
603.00	0.46897630D-01
604.00	0.44559250D-01
605.00	0.43070400D-01
606.00	0.42577110D-01
607.00	0.42991020D-01
608.00	0.44648130D-01
609.00	0.48290090D-01
610.00	0.54424370D-01
611.00	0.62701230D-01
612.00	0.71821000D-01
613.00	0.80024920D-01
614.00	0.85766200D-01
615.00	0.88214100D-01
616.00	0.87445580D-01
617.00	0.84304280D-01
618.00	0.79977400D-01
619.00	0.75430130D-01
620.00	0.71005600D-01
621.00	0.66443690D-01
622.00	0.61370710D-01
623.00	0.55675900D-01
624.00	0.49586170D-01
625.00	0.43384860D-01
626.00	0.37250760D-01
627.00	0.31494700D-01
628.00	0.26877430D-01
629.00	0.24406160D-01
630.00	0.24443450D-01
631.00	0.25808740D-01
632.00	0.25940380D-01
633.00	0.22418150D-01
634.00	0.14845220D-01
635.00	0.55270200D-02
636.00	-0.18435000D-02
637.00	-0.46133400D-02
638.00	-0.27960100D-02
639.00	0.13277100D-02
640.00	0.51591800D-02
641.00	0.75292500D-02
642.00	0.88486400D-02
643.00	0.98115100D-02
644.00	0.10100500D-01
645.00	0.83525100D-02
646.00	0.33156200D-02
647.00	-0.50027800D-02
648.00	-0.15216480D-01
649.00	-0.25440700D-01

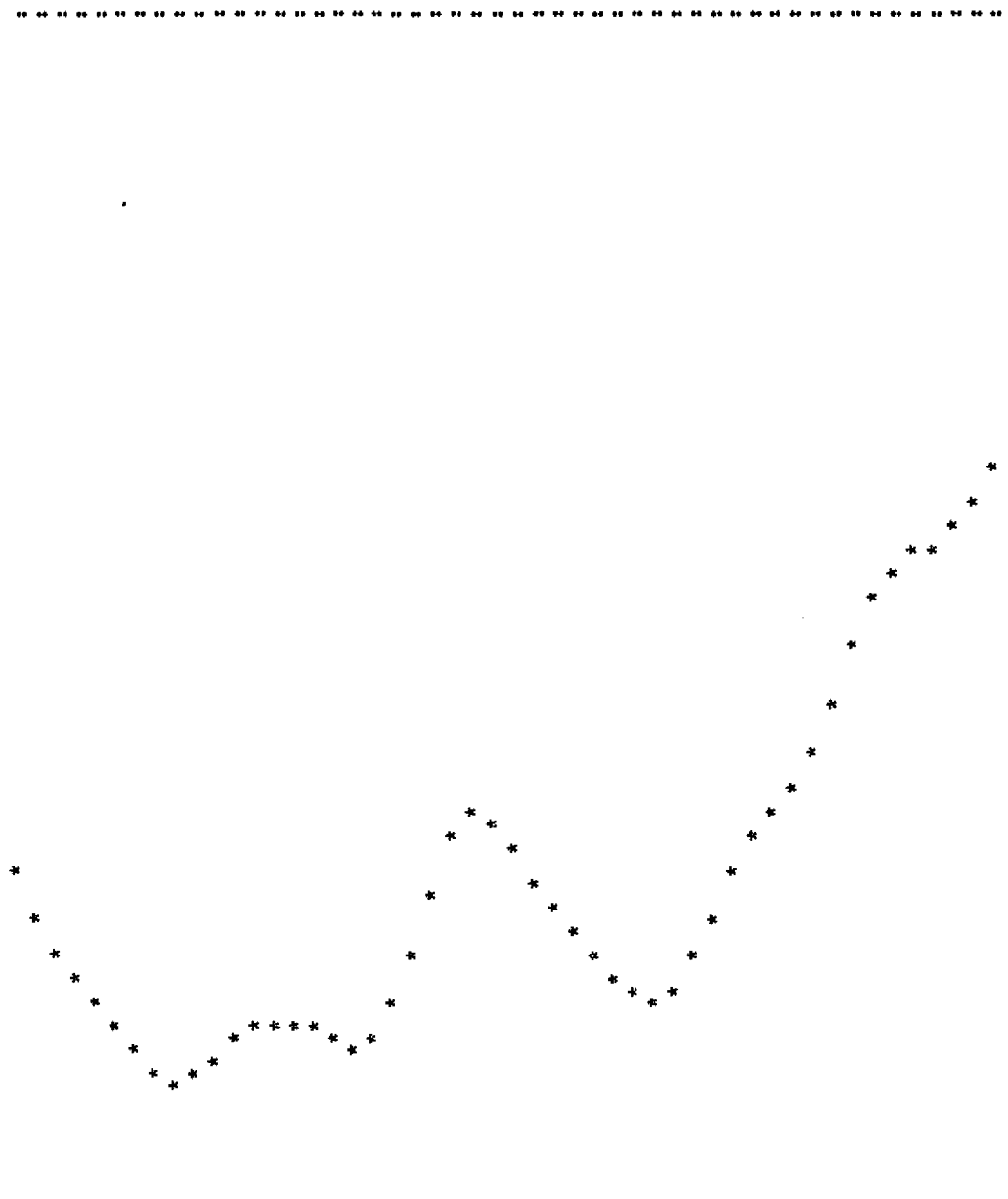

650.00	-0.34283480D-01
651.00	-0.41243120D-01
652.00	-0.46502310D-01
653.00	-0.50603820D-01
654.00	-0.54226590D-01
655.00	-0.57931050D-01
656.00	-0.61767570D-01
657.00	-0.65042200D-01
658.00	-0.66663380D-01
659.00	-0.66000670D-01
660.00	-0.63462890D-01
661.00	-0.60364780D-01
662.00	-0.58038350D-01
663.00	-0.57097870D-01
664.00	-0.57415260D-01
665.00	-0.58553870D-01
666.00	-0.59969990D-01
667.00	-0.60760960D-01
668.00	-0.59501260D-01
669.00	-0.54856070D-01
670.00	-0.46753630D-01
671.00	-0.37072230D-01
672.00	-0.28954020D-01
673.00	-0.25038220D-01
674.00	-0.25960050D-01
675.00	-0.30245110D-01
676.00	-0.35551170D-01
677.00	-0.40176670D-01
678.00	-0.43729690D-01
679.00	-0.46710350D-01
680.00	-0.49585820D-01
681.00	-0.52085080D-01
682.00	-0.53161450D-01
683.00	-0.51617810D-01
684.00	-0.47025630D-01
685.00	-0.40309540D-01
686.00	-0.33412780D-01
687.00	-0.28044010D-01
688.00	-0.24366580D-01
689.00	-0.20802630D-01
690.00	-0.15345800D-01
691.00	-0.73935200D-02
692.00	0.15334200D-02
693.00	0.89306600D-02
694.00	0.13286080D-01
695.00	0.15198200D-01
696.00	0.16651460D-01
697.00	0.19377390D-01
698.00	0.23869030D-01
699.00	0.29715080D-01

Figure D-3. Spectral analysis of the orthogonal acceleration component plotted as a function of time in Figure D-1. Data beginning immediately after the perturbation ended, for 512 samples, were used. Note the strong peak at low frequencies comprising the spring-mass mode and possibly including several latitudinal tether oscillation modes (see Section 4.2.1). Two small peaks at somewhat higher frequencies are apparent, but the overall behavior at high frequencies is much smoother than for the tangent acceleration analyzed in Figure D-4 below. The logarithm of the absolute value of the spectrum is plotted. The columns to the left of the plot list (1) the frequency (Hz), (2) the associated period (seconds) and (3) the value plotted. As discussed in Section 6.1, the spectrum is smoothed by about 1 frequency bin on either side of a peak because of the Hanning window imposed to reduce leakage of sharp spectral lines.

ORTHOGONAL ACCELERATION, LOG10 MIN, MAX: -0.4028542774D+01 0.0000000000D+00

0.0000	999.00	-0.1397087 5D+01:
0.0020	512.01	-0.1 93 98246D+00:
0.0039	256.00	-0.11 97266 8D+00:
0.0059	170.67	-0.23097 958D+00:
0.0078	128.00	0.00000000D+00:
0.0098	102.40	-0.17146 920D+00:
0.0117	85.33	-0.10644296D+01:
0.0137	73.14	-0.10559333D+01:
0.0156	64.00	-0.12340641D+01:
0.0176	56.89	-0.1317 9651D+01:
0.0195	51.20	-0.1377053 9D+01:
0.0215	46.55	-0.14285937D+01:
0.0234	42.67	-0.14766440D+01:
0.0254	39.38	-0.1518907 0D+01:
0.0273	36.57	-0.155536 95D+01:
0.0293	34.13	-0.1587531 0D+01:
0.0313	32.00	-0.16189816D+01:
0.0332	30.12	-0.16625813D+01:
0.0352	28.44	-0.14891508D+01:
0.0371	26.95	-0.14766 946D+01:
0.0391	25.60	-0.2018702 8D+01:
0.0410	24.38	-0.17696877D+01:
0.0430	23.27	-0.17846395D+01:
0.0449	22.26	-0.18037299D+01:
0.0469	21.33	-0.18215850D+01:
0.0488	20.48	-0.18381267D+01:
0.0508	19.69	-0.18541760D+01:
0.0527	18.96	-0.1870347 5D+01:
0.0547	18.29	-0.1886518 2D+01:
0.0566	17.66	-0.19021314D+01:
0.0586	17.07	-0.1916937 9D+01:
0.0605	16.52	-0.19312545D+01:
0.0625	16.00	-0.1945801 8D+01:
0.0645	15.52	-0.1960540 5D+01:
0.0664	15.06	-0.1947379 3D+01:
0.0684	14.63	-0.1897809 9D+01:
0.0703	14.22	-0.20647754D+01:
0.0723	13.84	-0.20163528D+01:
0.0742	13.47	-0.2027977 0D+01:
0.0762	13.13	-0.2038877 3D+01:
0.0781	12.80	-0.2049438 4D+01:
0.0801	12.49	-0.20599856D+01:
0.0820	12.19	-0.20706834D+01:
0.0840	11.91	-0.20813916D+01:
0.0859	11.64	-0.20918856D+01:
0.0879	11.38	-0.21020059D+01:
0.0898	11.13	-0.2111 9699D+01:
0.0918	10.89	-0.2121 9348D+01:
0.0938	10.67	-0.21315964D+01:
0.0957	10.45	-0.21362432D+01:
0.0977	10.24	-0.2184254 8D+01:

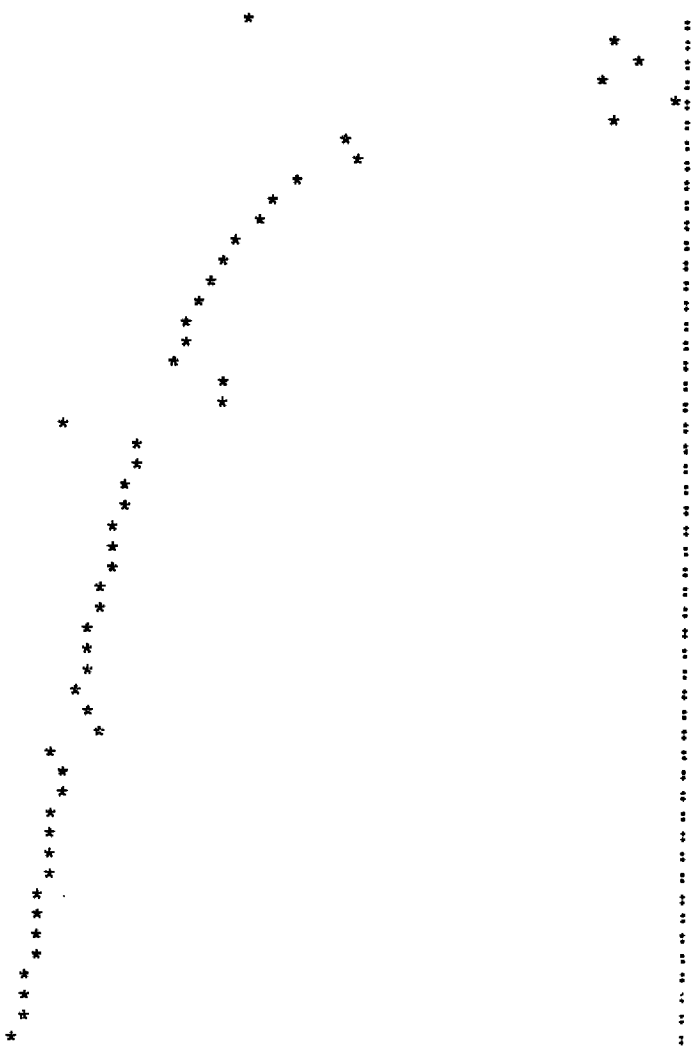

0.0996	10.04	-0.21598348D+01
0.1016	9.85	-0.21566079D+01
0.1035	9.66	-0.21748895D+01
0.1055	9.48	-0.21848133D+01
0.1074	9.31	-0.21936252D+01
0.1094	9.14	-0.22020690D+01
0.1113	8.98	-0.22105241D+01
0.1133	8.83	-0.22189515D+01
0.1152	8.68	-0.22272041D+01
0.1172	8.53	-0.22352071D+01
0.1191	8.39	-0.22431210D+01
0.1211	8.26	-0.22513277D+01
0.1230	8.13	-0.22603494D+01
0.1250	8.00	-0.22660733D+01
0.1270	7.88	-0.22580791D+01
0.1289	7.76	-0.22835087D+01
0.1309	7.64	-0.22883402D+01
0.1328	7.53	-0.22958035D+01
0.1348	7.42	-0.23029915D+01
0.1367	7.31	-0.23100476D+01
0.1387	7.21	-0.23169743D+01
0.1406	7.11	-0.23239922D+01
0.1426	7.01	-0.23309235D+01
0.1445	6.92	-0.23378721D+01
0.1465	6.83	-0.23444316D+01
0.1484	6.74	-0.23560110D+01
0.1504	6.65	-0.23539189D+01
0.1523	6.56	-0.23599988D+01
0.1543	6.48	-0.23706099D+01
0.1563	6.40	-0.23767502D+01
0.1582	6.32	-0.23832243D+01
0.1602	6.24	-0.23895666D+01
0.1621	6.17	-0.23959225D+01
0.1641	6.10	-0.24021978D+01
0.1660	6.02	-0.24083737D+01
0.1680	5.95	-0.24159198D+01
0.1699	5.89	-0.24200151D+01
0.1719	5.82	-0.24255564D+01
0.1738	5.75	-0.24326400D+01
0.1758	5.69	-0.24386062D+01
0.1777	5.63	-0.24445726D+01
0.1797	5.57	-0.24505409D+01
0.1816	5.51	-0.24563427D+01
0.1836	5.45	-0.24636328D+01
0.1855	5.39	-0.24673150D+01
0.1875	5.33	-0.24735218D+01
0.1895	5.28	-0.24795046D+01
0.1914	5.22	-0.24850842D+01
0.1934	5.17	-0.24912274D+01
0.1953	5.12	-0.24967887D+01
0.1973	5.07	-0.25023133D+01
0.1992	5.02	-0.25080043D+01
0.2012	4.97	-0.25136122D+01
0.2031	4.92	-0.25191714D+01
0.2051	4.88	-0.25247027D+01
0.2070	4.83	-0.25302333D+01
0.2090	4.79	-0.25357349D+01
0.2109	4.74	-0.25412777D+01
0.2129	4.70	-0.25467611D+01
0.2148	4.65	-0.25522526D+01
0.2168	4.61	-0.25576140D+01
0.2188	4.57	-0.25631322D+01
0.2207	4.53	-0.25686162D+01
0.2227	4.49	-0.25739408D+01
0.2246	4.45	-0.25793026D+01
0.2266	4.41	-0.25848003D+01

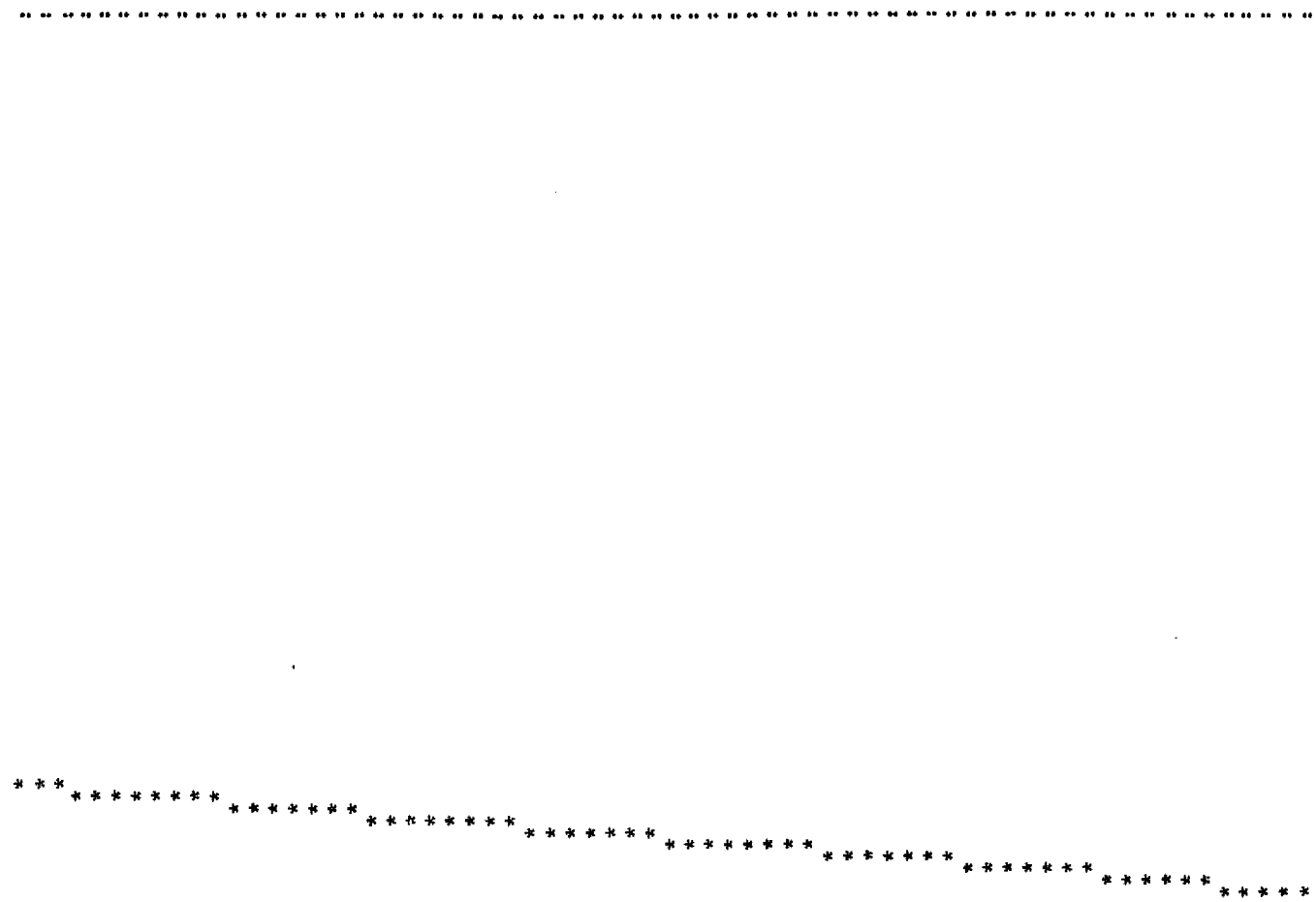

0.2285	4.38	-0.25901579D+01
0.2305	4.34	-0.25955116D+01
0.2324	4.30	-0.26008906D+01
0.2344	4.27	-0.26062185D+01
0.2363	4.23	-0.26115053D+01
0.2383	4.20	-0.26168944D+01
0.2402	4.16	-0.26222348D+01
0.2422	4.13	-0.26275228D+01
0.2441	4.10	-0.26329126D+01
0.2461	4.06	-0.26382205D+01
0.2480	4.03	-0.26435060D+01
0.2500	4.00	-0.26488937D+01
0.2520	3.97	-0.26541594D+01
0.2539	3.94	-0.26594788D+01
0.2559	3.91	-0.26647920D+01
0.2578	3.88	-0.26702541D+01
0.2598	3.85	-0.26754658D+01
0.2617	3.82	-0.26808537D+01
0.2637	3.79	-0.26861796D+01
0.2656	3.76	-0.26915512D+01
0.2676	3.74	-0.26969080D+01
0.2695	3.71	-0.27021815D+01
0.2715	3.68	-0.27075239D+01
0.2734	3.66	-0.27129422D+01
0.2754	3.63	-0.27183836D+01
0.2773	3.61	-0.27237879D+01
0.2793	3.58	-0.27290957D+01
0.2813	3.56	-0.27345293D+01
0.2832	3.53	-0.27399980D+01
0.2852	3.51	-0.27453531D+01
0.2871	3.48	-0.27508643D+01
0.2891	3.46	-0.27564281D+01
0.2910	3.44	-0.27618376D+01
0.2930	3.41	-0.27672883D+01
0.2949	3.39	-0.27727719D+01
0.2969	3.37	-0.27784411D+01
0.2988	3.35	-0.27838998D+01
0.3008	3.32	-0.27895919D+01
0.3027	3.30	-0.27951120D+01
0.3047	3.28	-0.28007385D+01
0.3066	3.26	-0.28064626D+01
0.3086	3.24	-0.28121573D+01
0.3105	3.22	-0.28177951D+01
0.3125	3.20	-0.28234735D+01
0.3145	3.18	-0.28293741D+01
0.3164	3.16	-0.28351637D+01
0.3184	3.14	-0.28409265D+01
0.3203	3.12	-0.28467166D+01
0.3223	3.10	-0.28526997D+01
0.3242	3.08	-0.28585720D+01
0.3262	3.07	-0.28645500D+01
0.3281	3.05	-0.28705437D+01
0.3301	3.03	-0.28766337D+01
0.3320	3.01	-0.28825931D+01
0.3340	2.99	-0.28888262D+01
0.3359	2.98	-0.28949403D+01
0.3379	2.96	-0.29011754D+01
0.3398	2.94	-0.29073075D+01
0.3418	2.93	-0.29135685D+01
0.3438	2.91	-0.29200987D+01
0.3457	2.89	-0.29264460D+01
0.3477	2.88	-0.29328092D+01
0.3496	2.86	-0.29393796D+01
0.3516	2.84	-0.29457814D+01
0.3535	2.83	-0.29525130D+01
0.3555	2.81	-0.29593239D+01

0.3574	2.80	-0.2965913D+01:
0.3594	2.78	-0.2972867D+01:
0.3613	2.77	-0.2979731D+01:
0.3633	2.75	-0.2986506D+01:
0.3652	2.74	-0.2993664D+01:
0.3672	2.72	-0.3000690D+01:
0.3691	2.71	-0.3007927D+01:
0.3711	2.69	-0.3015160D+01:
0.3730	2.68	-0.3022606D+01:
0.3750	2.67	-0.3029896D+01:
0.3770	2.65	-0.3037342D+01:
0.3789	2.64	-0.3045033D+01:
0.3809	2.63	-0.3052707D+01:
0.3828	2.61	-0.3060411D+01:
0.3848	2.60	-0.3068616D+01:
0.3867	2.59	-0.3076360D+01:
0.3887	2.57	-0.3084512D+01:
0.3906	2.56	-0.3092789D+01:
0.3926	2.55	-0.3100965D+01:
0.3945	2.53	-0.3109485D+01:
0.3965	2.52	-0.3118199D+01:
0.3984	2.51	-0.3126810D+01:
0.4004	2.50	-0.3135755D+01:
0.4023	2.49	-0.3144808D+01:
0.4043	2.47	-0.3154067D+01:
0.4063	2.46	-0.3163273D+01:
0.4082	2.45	-0.3172734D+01:
0.4102	2.44	-0.3182458D+01:
0.4121	2.43	-0.3192306D+01:
0.4141	2.42	-0.3202276D+01:
0.4160	2.40	-0.3212484D+01:
0.4180	2.39	-0.3223085D+01:
0.4199	2.38	-0.3233781D+01:
0.4219	2.37	-0.3244699D+01:
0.4238	2.36	-0.3256433D+01:
0.4258	2.35	-0.3266896D+01:
0.4277	2.34	-0.3278856D+01:
0.4297	2.33	-0.3290368D+01:
0.4316	2.32	-0.3302673D+01:
0.4336	2.31	-0.3315442D+01:
0.4355	2.30	-0.3328083D+01:
0.4375	2.29	-0.3341391D+01:
0.4395	2.28	-0.3354862D+01:
0.4414	2.27	-0.3368983D+01:
0.4434	2.26	-0.3383162D+01:
0.4453	2.25	-0.3397284D+01:
0.4473	2.24	-0.3412769D+01:
0.4492	2.23	-0.3428296D+01:
0.4512	2.22	-0.3445183D+01:
0.4531	2.21	-0.3461651D+01:
0.4551	2.20	-0.3478598D+01:
0.4570	2.19	-0.3496759D+01:
0.4590	2.18	-0.3515444D+01:
0.4609	2.17	-0.3534505D+01:
0.4629	2.16	-0.3555255D+01:
0.4648	2.15	-0.3575300D+01:
0.4668	2.14	-0.3597047D+01:
0.4688	2.13	-0.3620167D+01:
0.4707	2.12	-0.3643655D+01:
0.4727	2.12	-0.3668274D+01:
0.4746	2.11	-0.3693994D+01:
0.4766	2.10	-0.3720891D+01:
0.4785	2.09	-0.3749831D+01:
0.4805	2.08	-0.3778176D+01:
0.4824	2.07	-0.3807999D+01:
0.4844	2.06	-0.3840669D+01:

```
 0.4863   2.06  -0.3871496D+01:  *
 0.4883   2.05  -0.3903125ZD+01:   *
 0.4902   2.04  -0.3934155ZD+01:    *
 0.4922   2.03  -0.3963406ZD+01:   *
 0.4941   2.02  -0.3990361ZD+01:*
 0.4961   2.02  -0.4011094ZD+01:*
 0.4980   2.01  -0.4022992ZD+01:*
 0.5000   2.00  -0.4028542ZD+01:*
```

Figure D-4. A spectral analysis similar to Figure D-3 except that the acceleration component tangent to the tether is analyzed. Note the several sharp peaks out to about 0.2 Hz, and the jagged nature of the baseline thereafter compared with the baseline in D-3. The peaks correspond to the spring-mass mode and longitudinal tether oscillation modes as discussed in Section 7.1. The limited number of peaks is due to the finite number of masses used in the simulation. The difference in the baselines for the tangent and orthogonal components has not been analyzed.

ALONG-TETHER ACCELERATION, LOG10

0.0000	999.00	-0.106841600+01:
0.0020	512.01	-0.121764720+01:
0.0039	256.00	-0.118634860+01:
0.0059	170.67	-0.436361440+00:
0.0078	128.00	0.000000000+00:
0.0098	102.40	-0.226884130+00:
0.0117	85.33	-0.103676770+01:
0.0137	73.14	-0.118429150+01:
0.0156	64.00	-0.173118650+01:
0.0176	56.89	-0.229935980+01:
0.0195	51.20	-0.245304770+01:
0.0215	46.55	-0.272687320+01:
0.0234	42.67	-0.298552410+01:
0.0254	39.38	-0.304503260+01:
0.0273	36.57	-0.305752920+01:
0.0293	34.13	-0.288805760+01:
0.0313	32.00	-0.250176040+01:
0.0332	30.12	-0.190410590+01:
0.0352	28.44	-0.614389490+00:
0.0371	26.95	-0.408161970+00:
0.0391	25.60	-0.810698990+00:
0.0410	24.38	-0.216619250+01:
0.0430	23.27	-0.268531100+01:
0.0449	22.26	-0.307637500+01:
0.0469	21.33	-0.335519310+01:
0.0488	20.48	-0.360620770+01:
0.0508	19.69	-0.384493670+01:
0.0527	18.96	-0.401167820+01:
0.0547	18.29	-0.418265800+01:
0.0566	17.66	-0.429497530+01:
0.0586	17.07	-0.434807440+01:
0.0605	16.52	-0.422458950+01:
0.0625	16.00	-0.385135920+01:
0.0645	15.52	-0.315352060+01:
0.0664	15.06	-0.103273160+01:
0.0684	14.63	-0.717743100+00:
0.0703	14.22	-0.160+7237D+01:
0.0723	13.84	-0.306829210+01:
0.0742	13.47	-0.376681530+01:
0.0762	13.13	-0.414417920+01:
0.0781	12.80	-0.426008690+01:
0.0801	12.49	-0.426740900+01:
0.0820	12.19	-0.419913880+01:
0.0840	11.91	-0.416712560+01:
0.0859	11.64	-0.393298810+01:
0.0879	11.38	-0.371253130+01:
0.0898	11.13	-0.349159210+01:
0.0918	10.89	-0.313864490+01:
0.0938	10.67	-0.266636160+01:
0.0957	10.45	-0.188510180+01:
0.0977	10.24	-0.110115750+01:

0.0996	10.04	-0.1056221D+01:
0.1016	9.85	-0.1677786D+01:
0.1035	9.66	-0.2599935D+01:
0.1055	9.48	-0.3100037D+01:
0.1074	9.31	-0.3418552D+01:
0.1094	9.14	-0.3741842D+01:
0.1113	8.98	-0.3983382D+01:
0.1133	8.83	-0.4147441D+01:
0.1152	8.68	-0.4210430D+01:
0.1172	8.53	-0.4059796D+01:
0.1191	8.39	-0.3639853D+01:
0.1211	8.26	-0.3170303D+01:
0.1230	8.13	-0.2492717D+01:
0.1250	8.00	-0.1470719D+01:
0.1270	7.88	-0.1332538D+01:
0.1289	7.76	-0.1817375D+01:
0.1309	7.64	-0.2929516D+01:
0.1328	7.53	-0.3472467D+01:
0.1348	7.42	-0.3760487D+01:
0.1367	7.31	-0.3922613D+01:
0.1387	7.21	-0.4455239D+01:
0.1406	7.11	-0.4204489D+01:
0.1426	7.01	-0.3828191D+01:
0.1445	6.92	-0.3684511D+01:
0.1465	6.83	-0.3664005D+01:
0.1484	6.74	-0.1820651D+01:
0.1504	6.65	-0.1523493D+01:
0.1523	6.56	-0.1808168D+01:
0.1543	6.48	-0.3408140D+01:
0.1563	6.40	-0.3552774D+01:
0.1582	6.32	-0.3952744D+01:
0.1602	6.24	-0.4251451D+01:
0.1621	6.17	-0.4123001D+01:
0.1641	6.10	-0.4111030D+01:
0.1660	6.02	-0.4274228D+01:
0.1680	5.95	-0.2305401D+01:
0.1699	5.89	-0.2049970D+01:
0.1719	5.82	-0.2397563D+01:
0.1738	5.75	-0.3910217D+01:
0.1758	5.69	-0.4054665D+01:
0.1777	5.63	-0.4421639D+01:
0.1797	5.57	-0.3605391D+01:
0.1816	5.51	-0.2758926D+01:
0.1836	5.45	-0.2262721D+01:
0.1855	5.39	-0.2370117D+01:
0.1875	5.33	-0.3117238D+01:
0.1895	5.28	-0.3666633D+01:
0.1914	5.22	-0.3002596D+01:
0.1934	5.17	-0.2823798D+01:
0.1953	5.12	-0.3206429D+01:
0.1973	5.07	-0.4876103D+01:
0.1992	5.02	-0.4751500D+01:
0.2012	4.97	-0.4896218D+01:
0.2031	4.92	-0.5140921D+01:
0.2051	4.88	-0.5318358D+01:
0.2070	4.83	-0.5412973D+01:
0.2090	4.79	-0.5456441D+01:
0.2109	4.74	-0.5584989D+01:
0.2129	4.70	-0.5763999D+01:
0.2148	4.65	-0.5768[illegible]D+01:
0.2168	4.61	-0.5663983D+01:
0.2188	4.57	-0.6076565D+01:
0.2207	4.53	-0.5703933D+01:
0.2227	4.49	-0.6011552D+01:
0.2246	4.45	-0.6108214D+01:
0.2266	4.41	-0.6383678D+01:

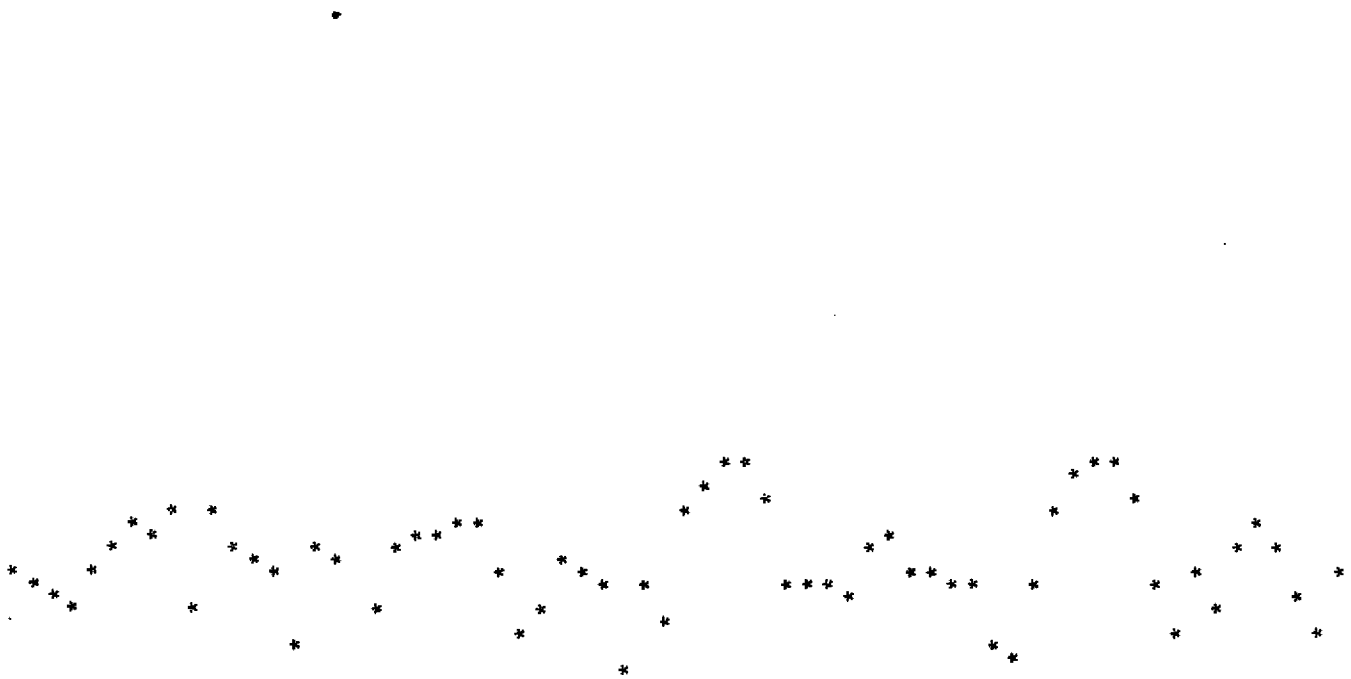

0.2285	4.38	-0.601940220+01:
0.2305	4.34	-0.614451900+01:
0.2324	4.30	-0.620637090+01:
0.2344	4.27	-0.622672070+01:
0.2363	4.23	-0.620566979D+01:
0.2383	4.20	-0.589140390+01:
0.2402	4.16	-0.574434770+01:
0.2422	4.13	-0.579050700+01:
0.2441	4.10	-0.555209380+01:
0.2461	4.06	-0.629565640+01:
0.2480	4.03	-0.568087350+01:
0.2500	4.00	-0.585808170+01:
0.2520	3.97	-0.599100700+01:
0.2539	3.94	-0.600717310+01:
0.2559	3.91	-0.650641510+01:
0.2578	3.88	-0.587149670+01:
0.2598	3.85	-0.595396280+01:
0.2617	3.82	-0.761780280+01:*
0.2637	3.79	-0.625665490+01:
0.2656	3.76	-0.592302040+01:
0.2676	3.74	-0.582245690+01:
0.2695	3.71	-0.580249040+01:
0.2715	3.68	-0.570939010+01:
0.2734	3.66	-0.576879400+01:
0.2754	3.63	-0.605750330+01:
0.2773	3.61	-0.640151260+01:
0.2793	3.58	-0.625411520+01:
0.2813	3.56	-0.598694360+01:
0.2832	3.53	-0.602974050+01:
0.2852	3.51	-0.610634030+01:
0.2871	3.48	-0.667055130+01:
0.2891	3.46	-0.608776730+01:
0.2910	3.44	-0.637966300+01:
0.2930	3.41	-0.566840330+01:
0.2949	3.39	-0.551917200+01:
0.2969	3.37	-0.536708280+01:
0.2988	3.35	-0.531053830+01:
0.3008	3.32	-0.556601320+01:
0.3027	3.30	-0.611104310+01:
0.3047	3.28	-0.613159130+01:
0.3066	3.26	-0.614276950+01:
0.3086	3.24	-0.620666020+01:
0.3105	3.22	-0.587784180+01:
0.3125	3.20	-0.581848880+01:
0.3145	3.18	-0.601982610+01:
0.3164	3.16	-0.600718460+01:
0.3184	3.14	-0.615579570+01:
0.3203	3.12	-0.613009390+01:
0.3223	3.10	-0.653916530+01:
0.3242	3.08	-0.658405060+01:
0.3262	3.07	-0.609157130+01:
0.3281	3.05	-0.566905500+01:
0.3301	3.03	-0.542297020+01:
0.3320	3.01	-0.537889390+01:
0.3340	2.99	-0.535340850+01:
0.3359	2.98	-0.559600130+01:
0.3379	2.96	-0.609623680+01:
0.3398	2.94	-0.639173080+01:
0.3418	2.93	-0.604142510+01:
0.3438	2.91	-0.626270640+01:
0.3457	2.89	-0.591466520+01:
0.3477	2.88	-0.571139130+01:
0.3496	2.86	-0.585962330+01:
0.3516	2.84	-0.623272610+01:
0.3535	2.83	-0.643830010+01:
0.3555	2.81	-0.601077940+01:

0.3574	2.80	-0.623880840+01:
0.3594	2.78	-0.655881090+01:
0.3613	2.77	-0.612052510+01:
0.3633	2.75	-0.590305590+01:
0.3652	2.74	-0.564090080+01:
0.3672	2.72	-0.549731920+01:
0.3691	2.71	-0.556830890+01:
0.3711	2.69	-0.584002880+01:
0.3730	2.68	-0.614270250+01:
0.3750	2.67	-0.611909730+01:
0.3770	2.65	-0.634703170+01:
0.3789	2.64	-0.640449720+01:
0.3809	2.63	-0.599804700+01:
0.3828	2.61	-0.596299290+01:
0.3848	2.60	-0.642936830+01:
0.3867	2.59	-0.620780520+01:
0.3887	2.57	-0.614004430+01:
0.3906	2.56	-0.606460260+01:
0.3926	2.55	-0.597328290+01:
0.3945	2.53	-0.584528000+01:
0.3965	2.52	-0.622345350+01:
0.3984	2.51	-0.648516150+01:
0.4004	2.50	-0.621464310+01:
0.4023	2.49	-0.608788960+01:
0.4043	2.47	-0.594124190+01:
0.4063	2.46	-0.596214420+01:
0.4082	2.45	-0.624362330+01:
0.4102	2.44	-0.601701460+01:
0.4121	2.43	-0.598021800+01:
0.4141	2.42	-0.627864370+01:
0.4160	2.40	-0.654265560+01:
0.4180	2.39	-0.612336890+01:
0.4199	2.38	-0.618776400+01:
0.4219	2.37	-0.643529610+01:
0.4238	2.36	-0.627043840+01:
0.4258	2.35	-0.663251920+01:
0.4277	2.34	-0.679197810+01:
0.4297	2.33	-0.639268330+01:
0.4316	2.32	-0.656106070+01:
0.4336	2.31	-0.613867290+01:
0.4355	2.30	-0.626390000+01:
0.4375	2.29	-0.650030740+01:
0.4395	2.28	-0.594233120+01:
0.4414	2.27	-0.579661350+01:
0.4434	2.26	-0.590084680+01:
0.4453	2.25	-0.587189230+01:
0.4473	2.24	-0.580190460+01:
0.4492	2.23	-0.612130300+01:
0.4512	2.22	-0.614439540+01:
0.4531	2.21	-0.604825170+01:
0.4551	2.20	-0.608352450+01:
0.4570	2.19	-0.591374060+01:
0.4590	2.18	-0.593463540+01:
0.4609	2.17	-0.605205580+01:
0.4629	2.16	-0.623921500+01:
0.4648	2.15	-0.607597310+01:
0.4668	2.14	-0.589661610+01:
0.4688	2.13	-0.610222950+01:
0.4707	2.12	-0.603423690+01:
0.4727	2.12	-0.662686350+01:
0.4746	2.11	-0.616299020+01:
0.4766	2.10	-0.606167190+01:
0.4785	2.09	-0.596887040+01:
0.4805	2.08	-0.638764220+01:
0.4824	2.07	-0.616988440+01:
0.4844	2.06	-0.593953300+01:

```
0.4863   2.06 -0.59624030D+01:                    *
0.4883   2.05 -0.60576918D+01:                   *
0.4902   2.04 -0.61886563D+01:                 *
0.4922   2.03 -0.64184235D+01:             *
0.4941   2.02 -0.60149091D+01:                   *
0.4961   2.02 -0.62196820D+01:                 *
0.4980   2.01 -0.66151092D+01:           *
0.5000   2.00 -0.74662279D+01: *
```

ORIGINAL PAGE IS
OF POOR QUALITY